Systematics, Gill Raker Morphology, and Pharyngeal Arch Development of Suckers (Cypriniformes: Catostomidae)

A Dissertation
SUBMITTED TO THE FACULTY OF
UNIVERSITY OF MINNESOTA
BY

Michael Vincent Hirt

IN PARTIAL FULFILLMENT OF THE REQUIREMENTS
FOR THE DEGREE OF
DOCTOR OF PHILOSOPHY

Andrew M. Simons, Advisor

June 2015

Acknowledgements

I thank my advisor, Andrew Simons, for his support and guidance throughout my graduate career. His wisdom and advice were invaluable. I am very fortunate to have had a mentor as insightful and supportive as he has been. I am eternally grateful for all he has done to help me and I would not be where I am today without his guidance and support. I thank him for his continued friendship and encouragement and look forward to future collaborations. I would also like to thank my other committee members Sharon Jansa, Susan Weller, and David Fox for their useful comments and guidance.

I thank Miles Coburn for first giving me a chance and starting me on my academic journey. His patience and wisdom put me on the right path and gave me a good start to my career. Although his advice and kind words are deeply missed, he is not forgotten.

I thank Peter Hundt, Brett Young, Brett Nagle, Andrew Simons, Tim Adams, Dominik Halas, Peter Cullen, Konrad Schmidt, Daemin Kim, Pamela Weisenhorn, Ben Lowe, and Mark Hove for their help collecting suckers. Peter Hundt and Brett Young, in particular, were indispensable in the field. I would also like to thank Mark Hove for his help and advice on aquaculture techniques. This research would not have been possible without the hard work and generosity of each of these individuals.

I thank Pamela Weisenhorn for teaching me R, helping me design statistical analyses, and troubleshooting scripts. I would also like to thank her for her continued love, support, and encouragement throughout this process. She was often my inspiration and served as a patient and insightful sounding board for my thoughts and ideas.

Finally, I thank my family for encouraging me to pursue my dream and supporting me each step of the way. I especially want to thank my parents for stressing the importance of education throughout my life and providing the support, guidance, and encouragement I needed.

Abstract

Morphological diversity is shaped by past evolutionary history, function, and ontogeny. Evolutionary history plays an important role in shaping morphological diversity and morphology itself can affect the future evolutionary trajectory of taxa. Morphology is shaped by function through selection and function can be constrained by morphology. Differences among taxa in their morphology arise due to changes in the pattern of development in those taxa. Therefore, a full understanding of morphological diversity requires knowledge about evolutionary history, morphological function, and ontogeny. Suckers, family Catostomidae, are a group of freshwater fish with interesting trophic morphology and feeding habits. I used molecular sequence data and fossil calibrations to reconstruct the phylogeny and divergence times of the families of Cypriniformes, including Catostomidae. I found evidence that gene choice, base compositional heterogeneity, and rate heterogeneity provide challenges to reconstructing the evolutionary history of the order and I found that body size is correlated with the rate of molecular evolution not only in Cypriniformes but in many groups of fishes. Suckers, like most fish, have gill rakers which are complex, repetitive, finger-like projections in the interior of the branchial arches that are important in feeding and vary among species. I quantified and compared gill raker morphology among sucker species and found that multiple aspects of gill raker morphology interact to predict function. Gill rakers are just one component of the complex trophic apparatus of suckers. I described and compared the sequence of chondrification and ossification of the paired elements of the pharyngeal arches and the histological development of the palatal organ, chewing pad, and

pharyngeal teeth in five species of suckers and found several examples where heterochrony has shaped the trophic morphology of suckers.

Table of Contents

List of Tables

List of Figures

Introduction

The great diversity of physical forms (morphology) in the biological world is the result of interactions among evolutionary forces, demands on efficient functioning of biological structures, and the patterns of development that give rise to those structures. The past evolutionary history of a lineage has a great effect on morphological diversity because it can constrain the future direction of evolution and it has a strong influence on the pool of available phenotypic diversity available on which selection can act. In many cases, morphology directly determines function in terms of what task a particular biological structure does and how well it performs that task. Selection on the specific form of the structure can be strong especially for structures that serve vital roles in an organism. Morphological structures can serve multiple functions and there can be trade-offs among those multiple functions with different selection pressures pushing the morphology in different directions. Rarely do fully functioning biological structures appear instantaneously but, instead, reach their final shape and size by changing through time. Changes in the pattern of development can constrain the range of potential morphologies possible but ontological changes can also open up new pathways that lead to novel morphologies. These three factors; ontogeny, function, and past evolutionary history interact to create morphological diversity in biological systems. The research presented here illustrates how these three factors have shaped gill raker morphology in catostomid fishes.

Chapter 1

The Effects of Gene Choice, Base Composition, and Rate Heterogeneity on Phylogenetic Inference and Estimates of Divergence Times in Cypriniformes

Summary

Gene choice, base compositional heterogeneity, and rate heterogeneity are known to influence phylogenetic reconstruction but are often overlooked. Here I investigate the impact of these factors in reconstructing the phylogenetic relationships and divergence times of cypriniform fishes. I compile a multilocus data set of newly sequenced and previously published nuclear protein-coding genes from species from all major lineages of Cypriniformes. I collect data on the oldest known cypriniform fossils and gather body size information. I demonstrate that body size correlates with rates of molecular evolution and contributes to rate heterogeneity not only in Cypriniformes but also in a number of other fish lineages. I find that miniaturized cypriniforms show exceptionally high rates of molecular evolution that may lead to improper phylogenetic placement of these taxa due to issues associated with long-branch attraction. I identify, and correct for base compositional heterogeneity, and find that this has a marked impact on topology and a corresponding impact on estimation of divergence times within Cypriniformes. Using gene sequences, fossil calibrations, and two different methods I show that Catostomidae

is sister to all other cypriniform families and the major clades of cypriniform fishes diverged long before their fossil record indicates.

Introduction

The estimation of divergence times has become a common side product of phylogeny reconstruction and provides valuable information on the ages of clades. It is well established that estimation of divergence times may be biased by a number of factors that include errors in phylogeny reconstruction, choice of loci for phylogeny reconstruction, and misinterpretations of the fossil record. Divergence time estimates may also be biased by other factors, including rate heterogeneity and base compositional heterogeneity, as these impact both tree topology and branch lengths. These issues may be particularly problematic for large, old taxa that contain both species rich and species depauperate clades. Here I investigate the impact of gene choice, base composition, and rate heterogeneity in the Cypriniformes. This is a large clade of ray-finned fishes containing clades of vastly different sizes, including species with a wide range of body sizes. I demonstrate that body size correlates with rates of molecular evolution and contributes to rate heterogeneity. I identify, and correct for base compositional heterogeneity, and find that this has a marked impact on topology and a corresponding impact on estimation of divergence times.

Recently there have been a number of studies that have estimated divergence times of ray-finned fishes. Several of these have included Cypriniformes (Broughton *et al*., 2013; Chen *et al*., 2013, Nakatani *et al,* 2011, Near *et al*., 2012) but only one (Saitoh

et al., 2011) attempted to estimate divergence times of cypriniform families. Saitoh *et al*. (2011) only used mitochondrial sequences from only thirty-seven cypriniforms. Estimates for the age of the split of Cypriniformes from the other otophysans range from the Triassic to the Late Cretaceous. Studies using only mitochondrial sequences estimate older ages than studies using nuclear loci. In all cases, the estimated ages are much older than the fossil record. Fossils are known for only four families of Cypriniformes and many of these fossils are fragmentary (Conway *et al*., 2010). The oldest cypriniform fossil, an *Amyzon* catostomid, dates to the early Paleocene (Wilson, 1980) but is known from only one bone. Few other cypriniform fossils are older than the Eocene (Conway *et al*., 2010). Because the fossil record is so sparse and there is disagreement in the basal relationships of cypriniform families, I collected sequences from six nuclear protein-coding genes from 154 species and fossil information to resolve the family-level relationships within Cypriniformes and estimate divergence times.

With over 320 genera and more than 3,200 species, Cypriniformes is the world's most diverse clade of freshwater fishes (Nelson, 2006). Cypriniformes, along with Characiformes, Gonorynchiformes, Gymnotiformes, and Siluriformes, compose the superorder Ostariophysi (Fink and Fink, 1981) which accounts for 28% of all known fish species and 68% of all freshwater fish species (Nelson, 2006). Cypriniformes has long been divided into two superfamilies; Cyprinoidea and Cobitoidea based on morphology (Siebert, 1987).

Traditionally, Cyprinoidea has been composed of one or two families; Cyprinidae and Psilorhynchidae. The genus *Psilorhynchus* was recognized as belonging to its own

family, Psilorhynchidae, by Hora (1925) but its relationship to other taxa was debated for a long time (reviewed in Conway and Mayden, 2007). Recent phylogenetic studies of osteology and DNA sequences show strong evidence that Psilorhynchidae is a cyprinoid and sister to Cyprinidae (Chen and Mayden, 2009; Conway, 2011; Tang *et al*., 2010). Cyprinidae is the largest cypriniform family, the largest family of freshwater fishes, and possibly even the largest family of vertebrates in the world (Nelson, 2006). Recently, some authors have advocated breaking Cyprinidae into several families (Chen *et al*., 2013; Chen and Mayden, 2009; Mayden and Chen, 2010). That debate is outside the scope of this paper so to avoid confusion, I will simply refer to this clade plus *Psilorhynchus* as Cyprinoidea for the purposes of this paper.

The other superfamily, Cobitoidea, contains the remaining families. Šlechtová *et al*. (2007) recognized seven cobitoid families; Balitoridae, Botiidae, Catostomidae, Cobitidae, Gyrinocheilidae, Nemacheilidae, and Vaillantellidae (Fig. 1.1) based on RAG1 sequences from seventy-two species. Saitoh *et al*. (2006) used whole mitogenome sequences from 59 species and recovered the same clades, although the names were different, and recovered Catostomidae sister to Gyrinocheilidae. Mayden *et al*. (2008) expanded Saitoh et al.'s (2006) taxon sampling to 107 species and sequenced the nuclear protein-coding gene RAG1. They recovered the same relationships within Cobitoidea with one major difference. They recovered Catostomidae as the sister to all other cypriniforms. Mayden and Chen (2010) provided the first multilocus phylogeny based on sequences from six nuclear loci, including RAG1, from eighty-five species. They recovered the miniaturized genera *Paedocypris* sister to all other cypriniforms with

Catostomidae sister to the other cobitoids. This was the first time *Paedocypris* had been found in this phylogenetic position.

A recent morphological study found evidence that *Paedocypris* is a cyprinid and is sister to *Danionella* (Britz and Conway, 2009) but evaluating the morphology in a phylogenetic context is difficult because its development is highly truncated. Mature *Paedocypris* adults only reach 7.9-11.5mm standard length and are likely the smallest known vertebrates (Britz and Kottelat, 2008; Kottelat *et al*., 2006). All previous molecular phylogenies except Mayden and Chen (2010) recovered *Paedocypris* within the cyprinid subfamily Danioninae (Fang *et al*., 2010; Mayden *et al*., 2007; Rüber *et al*., 2007; Tang *et al*., 2010). In addition to their molecular evidence, Mayden and Chen (2010) reevaluated the morphological characters of Britz and Conway (2009) and argue that the morphology supports *Paedocypris* as the sister to all other cypriniforms but their reinterpretation has been criticized (Britz and Conway, 2011).

Materials and methods

Data Collection

Sequences from six nuclear protein-coding genes (EGR1, EGR2b, EGR3, IRBP, RAG1, and Rh) used in Mayden and Chen (2010) were obtained from GenBank. These sequences came from eighty-one cypriniform and four outgroup species. EGR2b, IRBP, and RAG1 sequences from sixty-six cypriniform and three outgroup species (Table 1.1) were obtained from GenBank or amplified and sequenced for this study following Chen *et al*. (2008) for EGR2b and IRBP and López *et al*. (2004) for RAG1. Species were

targeted to improve overall sampling, improve sampling of non-cyprinid cypriniforms, aid in rooting, and to facilitate fossil calibrations. This data set represents increases from Mayden and Chen (2010) of 81% for all cypriniform species, 83% for cyprinoids, and 78% for cobitoids cypriniforms.

Sampling included one specimen per species so analyses of concatenated sequences were chosen over species tree analyses. The concatenated data matrix included 5,867 bp and was partitioned by gene and codon position. Amino acid translations for all gene sequences were determined using MacClade (Maddison and Maddison, 2005) and visually inspected for stop codons. Base compositional heterogeneity was assessed for each partition with a Chi-square goodness-of-fit test using PAUP* (Swofford, 2003). Partitioning schemes and models of molecular evolution were determined using the Bayesian Information Criterion (BIC) as implemented in PartitionFinder v1.1.1 (Lanfear *et al*., 2012).

Phylogenetic Analyses

Phylogenetic analyses were carried out using Maximum Likelihood (ML) as implemented in RAxML v8.0.0 (Stamatakis, 2014) through the CIPRES Science Gateway (Miller *et al*., 2010) and Bayesian methods using BEAST v1.7.5 (Drummond and Rambaut, 2007), using the partitioning schemes determined by PartitionFinder. Nodal support for the ML analysis was assessed using the fast bootstrapping algorithm of RAxML and was allowed to halt automatically. Because there was significant base compositional heterogeneity in the data, two approaches to eliminate the effects of that

heterogeneity and better assess the phylogenetic position of *Paedocypris* were attempted. First, the two partitions with significant heterogeneity (third codon positions of EGR3 and Rh) were removed and second, all gene sequences were translated to amino acids.

BEAST was used to infer the phylogeny and estimate divergence times simultaneously in a Bayesian framework. The data matrix was initially converted to an XML file, as required by BEAST, using BEAUTI v1.4.8 then edited by hand. Six independent runs of 20,000,000 generations each were run with trees saved every 1,000 generations. Convergence of the runs was assessed by visually using Tracer v1.5 (Rambaut and Drummond, 2007). Once convergence was confirmed, the first 20% of trees were removed as burn-in and the remaining trees from all six runs were combined using LogCombiner v1.7.5 (Rambaut and Drummond, 2007) after resampling every 8,000 generations. The combined trees were summarized using TreeAnnotator v1.7.5 with a posterior probability limit of 0.5, a maximum clade credibility target tree, and median node heights.

To test whether these nuclear loci have evolved significantly faster in some species than in others, the distance from each tip in the ML tree to the root (path length) was calculated and plotted as a histogram in R v3.0.2 (R Core Team, 2013). Any tip that was outside two standard deviations from the mean was considered a significant outlier. Outliers were removed from final phylogenetic and divergent time inference.

Body Size and Evolutionary Rate

Maximum standard lengths (MSL) were collected from the online database FishBase (Froese and Pauly, 2013) for nearly all cypriniform species in the dataset. The specific identity of five specimens was unknown and body length data was unavailable in FishBase for seven other species leaving 135 cypriniform species in the analysis. MSL for each species was log transformed prior to analysis. Phylogenetic Independent Contrasts (PIC) were calculated for path lengths and log MSL using the R package "ape" (Paradis *et al*., 2004) to remove any effect of phylogeny on those variables. Regressions using a general linear model were used to test for a relationship between the contrasts for path length and MSL.

To test whether the relationship between path length and body size is a common phenomenon in fish, I collected ML phylogenies from a variety of recently published studies. I chose studies of Osteichthyes fish that included at least one hundred species, had easily accessible maximum likelihood trees, and that covered a range of taxonomic groups ranging from family to class. Data were analyzed using the methods described above for cypriniforms.

Divergence Times

A total of eight fossil-based calibrations were used to estimate divergence times. Three were the oldest known fossils from each of the three cobitoid families with a fossil record; Catostomidae, Cobitidae, and Nemacheilidae. The fossils included *Amyzon* sp. (Catostomidae) from the early Paleocene (61.7 MYA) of Canada (Wilson, 1980); *Cobitis centrochir* (Cobitidae) from the middle Miocene (13.6 MYA) of Germany (Frickhinger,

1994); and *Triplophysa opinata* (Nemacheilidae) from the Middle to Late Miocene (11.6 MYA) of Kyrgyzstan (Prokofiev, 2007; Yakowlew, 1959). One fossil was the oldest known cyprinoid, *Parabarbus* sp. (Cyprinidae) from the Early-Middle Eocene (48.6 MYA) of Kazakhstan (Systchevskaya, 1986). Because Cyprinoidea is the largest cypriniform clade, has the most taxa in this analysis, and has the greatest number of known fossils, three additional cyprinoid fossils were used. These were the gobionin *Protothymallus elongatus* from the Early Oligocene (30.2 MYA) of Czech Republic (Böhme, 2007) which was used to date the split of Gobioninae and Leuciscinae; *Ecocarpia ningmingensis* from the Miocene (23.0 MYA) of China (Chen *et al*., 2005), used to date the split of the clades containing *Chandoichthys flavipinnis* and *Zacco sieboldii*; and *Cyprinus carpio* from the Middle Miocene (13.6 MYA) of China (Zhou, 1990), used to date the split of *Cyprinus* and *Carassius*. Finally, a gonorynchiform from family Chanidae, *Rubiesichthys gregalis*, from the Early Cretaceous (130 MYA) of Spain (Poyato-Ariza, 1994, 1996) was included as a calibration for the root of the tree.

The combined nucleotide data set was tested for a molecular clock using the maximum likelihood based molecular clock test implemented in PAUP* 4.0b10 (Swofford, 2003). I was able to reject a molecular clock for this data set so two relaxed clock methods were used to estimate divergence times, a Bayesian relaxed clock method implemented in BEAST v1.7.5 (Drummond and Rambaut, 2007) and a method proposed by Marshall (2008).

The Bayesian relaxed clock method as implemented in BEAST estimates tree topology, branch lengths, and divergence times simultaneously with a Markov chain

Monte Carlo. Marshall (2008) developed a method, referred to here as the Marshall Scaling Method (MSM), which provides a systematic way to find the fossil calibration that best matches its lineage's true age, and provides a simple way to bracket divergence times with a confidence interval using only information about the number of fossil calibrations present.

Fossil calibrations in the Bayesian analysis were set as lognormal priors offset by the age of the fossil so that the age of each of the fossils acted as a hard minimum age for its corresponding node. The means of the lognormal priors were adjusted so that 95% of the area under the curve was equal to or younger than the minimum age of the most recent ancestral node containing a date calibration. It is expected that the true age of a node is somewhat older than its fossil record and less likely to be either much older or the same age as its fossil record. The lognormal distribution was chosen over alternatives because it best matches these predictions and is often the most appropriate distribution for paleontological data (Ho and Phillips, 2009).

Divergence dates were estimated on the ML tree by implementing MSM. The ML tree was converted to an ultrametric tree using nonparametric rate smoothing and a penalized likelihood relaxed molecular clock as implemented in r8s v1.8 (Sanderson, 2003). The age of the root was fixed at 1.0 so that branch lengths would represent relative time. Empirical scaling factors (s_i) were calculated for each of the nodes with a fossil calibration point, as the age of the fossil divided by its lineage's node to tip length. Node to tip lengths are equal to a lineage's relative age on an ultrametric tree. The node with the largest s_i is the one with the fossil that covers the highest proportion of its lineage's true

age and is deemed the calibration lineage. The age of this fossil was used as the minimum age for its node and the minimum ages of all the other nodes in the tree were calculated from this date. A maximum age bracket was calculated for the calibration lineage using a 95% confidence interval and taking the conservative approach of assuming that only one fossil is known from each lineage with a fossil record. This yields a relatively large range between the minimum and maximum age estimates but increases the probability that the true age is captured within the range. The maximum age of the calibration lineage was used to calculate the maximum ages of all other nodes.

Results

Molecular Data

The alignment of six nuclear protein-coding genes from 157 species contains 5,867 characters, 2,647 of which are parsimony-informative. Codon position three of EGR3 and Rh were found to have significant base compositional heterogeneity (Table 1.2, Fig. 1.2). After removing path length outliers, the dataset was reduced to 147 species. Only the third codon position of Rh was found to be significantly heterogeneous in this reduced data set. Removing this partition reduced the data set to 5,590 characters, 2,321 of which are parsimony-informative.

Phylogenetic Analyses

ML analysis of all 154 species recovered a monophyletic Cypriniformes with the two *Paedocypris* specimens being sister to the other cypriniforms (Fig. 1.3A, Fig. 1.4A).

Two major cyprinoid lineages were recovered that correspond to the subfamilies Cyprininae and Leuciscinae of Cavender and Coburn (1992). *Psilorhynchus*, which was not included in Cavender and Coburn (1992), was recovered as the sister to Cyprininae with strong support, congruent with the results of Chen and Mayden (2009) and Mayden and Chen (2010). The non-*Paedocypris* cyprinoids were recovered as sister to Cobitoidea. Within Cobitoidea, the seven cobitoid families recognized by Šlechtová *et al*. (2007) were recovered with Catostomidae sister to the other families.

After eliminating the heterogeneous sites, I recovered Catostomidae as sister to all other cypriniforms with strong support and *Paedocypris* as sister to all other cyprinoids (Fig. 1.4B). The amino acid translations also recovered this same phylogeny but with reduced support (Fig. 1.4C). Because the branch leading to the two specimens of *Paedocypris* was estimated to be very long it was suspected that long-branch attraction may be leading to incorrect phylogenetic reconstruction.

Body Size and Evolutionary Rate

I calculated path lengths of all ingroup species and tested whether any species had a path length greater than or less than two standard deviations from the mean. I found seven significant outliers, including the two *Paedocypris* specimens (Fig. 1.5), all of which were small fish (less than 12cm MSL) and most of which were miniaturized species (less than 2.5cm MSL). The average MSL for outlier species was 4.8cm while it was 8.3cm for species with path lengths greater than the mean but less than one standard

deviation from the mean and 33.7cm for species with path lengths less than the mean (Fig. 1.5).

I found a statistically significant negative relationship between phylogenetic path length and MSL within several groups of fishes including Cypriniformes and Cyprinoidea (Table 1.3, Fig. 1.6). A significant relationship was found in fifteen of the twenty groups tested. Three of the six subfamilies and families (including Cyprinoidea) tested showed a significant relationship. Four of the six orders showed a significant relationship and all eight of the groups above the level of order showed a significant relationship. Two groups of fishes, Acanthomorpha and Characiformes, were tested twice using phylogenic data from different studies and significant relationships were found in both cases.

Divergence Times

Geologic ages follow Gradstein *et al*. (2012). Divergence times estimated with the MSM and Bayesian method are mostly congruent (Table 1.4, Fig. 1.7). Both produced age ranges that are similar in magnitude but MSM tended to estimate minimums and maximums that are older than the ones from the Bayesian method. These differences tended to be greater closer to the root of the tree and the two methods estimated divergence times that do not overlap for the split of Cypriniformes from the other otophysans. The MSM estimated this split to have occurred as early as the late Permian and as late as the Early Jurassic (255.1-175.4 MYA) whereas the Bayesian method

estimated the split to have occurred later, between the Middle Jurassic and Early Cretaceous (173.8-117.3 MYA).

Both methods estimated that Catostomidae (MSM = 130.0-89.4 MYA, Bayesian = 104.9-71.8 MYA) and Cyprinoidea (MSM = 122.5-84.2 MYA, Bayesian = 97.6-67.1 MYA) arose before the K/T mass extinction event (66.0 MYA) and MSM estimated that Gyrinocheilidae did as well (115.0-79.1 MYA). The Bayesian results suggest that Gyrinocheilidae (91.3-61.8 MYA) likely arose before the K/T boundary but cannot falsify a post-K/T origin. The other cobitoid families likely arose around or just after the K/T boundary with all recognized families arising before the Oligocene. Botiidae was estimated to arise in the Late Cretaceous to early Paleogene (MSM = 86.7-59.6 MYA, Bayesian = 74.8-50.9 MYA). Vaillantellidae arose slightly later (MSM = 80.5-55.4 MYA, Bayesian = 68.4-46.1 MYA). The Bayesian results show that Cobitidae originated after the K/T boundary at 60.4-40.0 MYA but the age estimates from MSM (73.0-50.2 MYA) include the Late Cretaceous. Likewise, the MSM estimate for the split of Balitoridae and Nemacheilidae (68.2-46.9 MYA) includes the Late Cretaceous but the Bayesian method does not (55.8-36.7 MYA).

The two major clades of cyprinoids, Cyprininae and Leuciscinae, were estimated to have split around the K/T boundary (MSM = 90.3-62.1 MYA, Bayesian = 73.3-51.5 MYA). *Psilorhynchus*, sister to Cyprininae, also likely arose around or just after the K/T boundary (MSM = 82.0-56.4 MYA, Bayesian = 65.4-42.8 MYA). *Protothymallus* was determined to be the MSM calibration lineage (43.9-30.2 MYA) and also had a very narrow 95% HPD for its Bayesian estimated age (34.8-30.4 MYA).

Discussion

Accurate estimates of divergence times are dependent on a number of factors. Some of these, such as errors in phylogeny reconstruction, choice of loci, and fossil calibrations, are well known but others, such as rate heterogeneity and base compositional heterogeneity, are often overlooked. Base compositional heterogeneity can effect phylogenetic reconstruction and improper fossil calibrations can alter estimated divergence times but the choice of loci and effects of rate heterogeneity can strongly influence both the underlying phylogenetic reconstruction and estimates of divergence times. By correcting for these factors, it is possible to improve phylogenetic hypotheses of the relationships among taxa and estimates of divergence times.

Phylogenetic Analysis

The results from the dataset containing all partitions from all 154 taxa are congruent with the novel results from Mayden and Chen (2010) where *Paedocypris* was recovered as sister to all other cypriniforms. This is in contrast to a morphological study (Britz and Conway, 2009) and all other molecular phylogenetic studies involving *Paedocypris* (Rüber *et al*., 2007; Mayden *et al*., 2007; Fang *et al*., 2009, Tang *et al*., 2010). Morphology suggests that Paedocypris is sister to *Danionella* and nested within Cyprinoidea. All previous molecular phylogenetic studies except Mayden and Chen (2010) recovered *Paedocypris* sister to *Sundadanio* within the cyprinid subfamily Danioninae. Mayden and Chen (2010) and my study were the only molecular studies that did not incorporate any mitochondrial loci.

Mayden and Chen (2010) found base composition heterogeneity in the third position of four genes (EGR2b, EGR3, RAG1, and Rh) and to compensate they recoded the nucleotides in these four partitions as purines and pyrimidines. Even after this partial RY-coding, they still recovered the same general topology. I found base compositional heterogeneity in the third codon positions of only two genes (EGR2b and Rh) in my expanded taxonomic sampling suggesting that increasing taxonomic sampling might be one method to reduce the effects of base compositional heterogeneity. I used two methods which are more aggressive than partial RY-coding to deal with base compositional heterogeneity; complete removal of heterogeneous partitions, and complete translation of nucleotides to amino acids. Both methods recovered Catostomidae sister to all other cypriniforms and *Paedocypris* as sister to all other cyprinoids. After removing taxa with significantly long path lengths, including *Paedocypris*, and removing heterogeneous partitions, Catostomidae was again recovered as sister to all other cypriniforms. The placement of Catostomidae at the root of Cypriniformes is unusual but not unprecedented as Mayden *et al*. (2008) found a similar result.

Although the effects of uneven base composition are well documented (Barrowclough *et al*., 2006; Foster and Hickey, 1999; Hasegawa and Hashimoto, 1993; Jeffroy *et al*., 2006; Lake, 1994; Lockhart *et al*., 1994; Loomis and Smith, 1990; Mooers and Holmes, 2000; Tarrío *et al*., 2001), most studies do not test nor attempt to correct for this form of bias. My results show that base composition bias has likely lead to incorrect

phylogenetic reconstructions of cypriniform fishes and I suspect that it has similarly effected other phylogenetic studies.

My results suggest that inferences of the phylogenetic position of miniaturized taxa such as *Paedocypris* may be compromised by an increased rate of molecular evolution in the nuclear loci I sampled. Of the seven species with significantly long path lengths, four have maximum body lengths less than 2.5 cm and the average maximum body length for all seven was 4.8 cm. There is also a statistically significant correlation between path length (a proxy for rate of molecular evolution) and body size within Cypriniformes and Cyprinoidea. Three of the loci sampled are Early Growth Response genes (EGR1, EGR2b, and EGR3) that may have been under strong selection during miniaturization. Regardless of the cause of the increase in molecular evolution in at least some miniaturized taxa, the resulting long branches could have an effect of pulling those branches closer to the root in phylogenetic studies than they truly are.

Unfortunately, it appears that my data are insufficient to resolve the position of *Paedocypris* or the other taxa with significantly long path lengths. Given the likelihood of long-branch effects and results from other studies (Britz and Conway, 2009; Fang *et al*., 2009; Mayden *et al*., 2007; Rüber *et al*., 2007; Tang *et al*., 2010), it seems unlikely that *Paedocypris* is sister to all other cypriniforms and likely that it is a cyprinoid.

Body Size and Evolutionary Rate

Increased rates of molecular evolution in small sized fish seems to be a common phenomenon throughout fish evolution. I found a correlation between path length and

maximum body size in a number of recently published studies examining a variety of taxonomic groups. In the data I analyzed, the relationship is very common in higher level taxonomic groups but less common at the family level and below. The data are noisy in general which is not surprising given the variation that exists in fish body size and even though I selected studies with large sampling, some of the studies examined may not have had sufficient sampling to overcome this noise. My results indicate that the increased rate of evolution in small bodied fish compared to larger bodied fish has a significant impact on the reconstruction of phylogenetic relationships within Cypriniformes but the extent and magnitude of this rate heterogeneity due to body size heterogeneity on other phylogenetic studies is yet unknown.

Divergence Times

My estimates of divergence times are substantially older than indicated by the fossil record. The Bayesian median ages are, on average, two times older than the fossil calibrations. The MSM minimum age estimates are two times older and the maximum ages are three times older than the fossils on average. The age estimates from the two methods are not completely congruent and the MSM age ranges are typically older than the Bayesian age ranges. This incongruence is likely because the MSM ages are based on the age of one fossil while the Bayesian ages are constrained by multiple fossils spread across the tree. It is unclear which method does a better job of capturing true divergence times.

Several studies investigating divergence times in fishes have included Cypriniformes. The studies that use nuclear loci (Broughton *et al*, 2013; Chen *et al*., 2013; Near *et al*., 2012) estimate the split of Cypriniformes from the other otophysans to have occurred more recently than the studies using whole mitogenomes (Nakatani *et al*., 2011; Saitoh *et al*., 2012). My MSM estimates for this split are consistent with the estimates from the whole mitogenome studies and my Bayesian estimates are consistent with the nuclear studies. Mitochondrial loci evolve at a faster rate than nuclear loci and can lead to overestimation of divergence times, especially in old groups, as a result of saturation (Zheng *et al*., 2011) so it is possible that my Bayesian age estimates for nodes close to the root may be better than my MSM estimates.

Only one previous study (Saitoh *et al*., 2011) has estimated divergence times within Cypriniformes using molecular phylogenetics and fossil calibrations and it estimated divergence times about twice as old as my Bayesian estimates. That study suffers from three issues; the use of mitochondrial DNA to assess relationships and divergence times, the use of a relatively simple model of nucleotide evolution for their divergence time estimations, and the choice for some of their fossil calibrations.

The problem with using mitochondrial loci to estimate divergence times was discussed above. Saitoh *et al*. (2011) used an F84 model when estimating their divergence times even though a GTR model was determined to be the best model for their initial phylogenetic reconstruction. The simpler F84 model may not have done a good job at properly estimating branch lengths. I feel that several of their fossil calibrations are problematic. They constrain the age of the North American leuciscines to

31.1 MYA but no cyprinoids have been found from the site they reference, the Lower John Day Formation (Cavender, 1991). The age of the oldest known Asian catostomid fossil is actually 48.6 MYA (Liu and Chang, 2009) not 35 MYA. The oldest catostomid fossil should be dated to 61.7 MYA (Gradstein *et al*., 2012; Wilson, 1980) instead of 60 MYA which seems to be a date from a secondary source (Cavender, 1986). *Cobitis longipectoralis* is from the late early Miocene about 15.97 MYA (Chen *et al*., 2010; Zhou, 1992) not 5.3 MYA. Finally, one of their outgroups, the oldest known chanid, should be dated at 130 MYA (Poyato-Ariza, 1994; 1996) instead of 145 MYA which appears to be a misinterpretation of Grande (1999) and not based on specific specimens. Most of Saitoh *et al*.'s (2011) fossil calibrations only included constraints on minimum ages without any constraint on maximum ages and the few maximum constraints were on distant outgroups. This could have led to their analyses overestimating divergence times within Cypriniformes. These improper calibrations, the use of a simplified model, and the use of only mitochondrial DNA may have all contributed to an overestimation of divergence times.

Chapter 2

Many-to-one Mapping of Gill Raker Morphology to Diet in Suckers (Teleostei: Catostomidae)

Summary

The relationship between morphology and function is not always easy to determine especially for morphological traits that are composed of multiple parts and for morphological traits that serve more than one function. For morphological traits with more than two components, different combinations of component parts can lead to convergent functions and the effects on function from changing one component may be dependent on the morphology of the other components. Gill rakers, repetitive, finger-like or arborescent projections that extend from the surface of the branchial arches of most bony fish, are an example of this type of complex morphological trait. Gill rakers are important in separating food from inedible particles during feeding and function by trapping particles against the palatal organ which sits opposite the gill rakers on the roof of the buccal cavity and by one of several mechanical straining processes. The number, shape, size, and position of gill rakers vary among species and play important roles in determining what kinds of particles can be retained and swallowed. In this study, I quantify and compare multiple gill raker traits in a family of freshwater fishes, the suckers, to test for differences among species and to determine which aspects of gill raker morphology are most important in determining diet. I found that no single trait is

predictive of diet but several traits interact in specific ways to determine diet. I show evidence that gill rakers in suckers are an example of many-to-one mapping of morphology to function.

Introduction

The gill rakers of ray-finned fishes are complex, morphological structures, the structure and function of which are poorly understood. Gill rakers are rostro-medial projections from the branchial arches and are clearly associated with feeding, as their length and spacing correlates with diet. They have long been presumed to act as filters, retaining food in the bucco-pharyngeal cavity, and directing it towards the esophagus. How they do this is unclear, particularly as retained food items may be smaller than the spaces between the gill rakers. Recent work has demonstrated that gill rakers may function as simple, dead-end filters (Hoogenboezem *et al.*, 1991), mucosal traps (Drenner *et al.*, 1987), cross-flow filters (Sanderson *et al.*, 2001), or some combination of the three. However, for the vast majority of ray-finned fishes, the filtering mechanism is unknown and there are few, if any, studies examining gill raker morphology and diet across a clade of fishes.

The freshwater fish Family Catostomidae, the suckers, is a monophyletic group that exhibits variation in both gill raker morphology and diet. Catostomidae contains 72 species that occur almost exclusively in North America (Nelson, 2006). Suckers are ecologically important because of their abundance, large size, and diets, which often include primary producers and consumers (Becker, 1983; Jenkins & Burkhead, 1993).

Suckers are named for their subterminal, fleshy-lipped mouths that are used in benthic feeding. All species have a subterminal mouth except for *Ictiobus cyprinellus*, the Bigmouth Buffalo, which is an open water planktivore. The diet of suckers is often species-specific that can include algae, detritus, zooplankton, macroinvertebrates, mollusks, and fish larvae. Accompanying this diversity in diet is substantial variation in gill raker morphology (Smith, 1992) covering a range of morphologies from numerous long, thin rakers (Fig. 2.1A) to few short, bulbous rakers (Fig. 2.1B).

Suckers are members of the order Cypriniformes and are related to the Family Cyprinidae, which contains the often studied Common Carp, *Cyprinus carpio*, and the Zebrafish, *Danio rerio*. In cypriniform fishes, the anterior pharynx contains four paired branchial arches that line the ventral and lateral surfaces and a tongue-like structure, the palatal organ, which opposes the arches and covers the dorsal surface (Sibbing *et al.*, 1986; Doosey & Bart, 2011). The posterior pharynx contains a fifth branchial arch that is highly modified in cypriniform fishes and contains one to three rows of teeth (with the exception of the three gyrinocheilid species). The four branchial arches in the anterior pharynx support the gills on their posterior surfaces and gill rakers on their interior surfaces. Both the gill rakers and the palatal organs contain an abundance of taste buds (Iwai, 1964; Eastman, 1977; Sibbing *et al.*, 1986) (Fig. 2.2).

The pharyngeal anatomy of freshwater suckers resembles that of the Common Carp although there are differences in branchial arch and gill raker structure and the arrangement and size of the teeth on the fifth branchial arch. The mechanics of feeding has not been well studied in suckers but has been in Common Carp. In Common Carp the

palatal organ protrudes, acting against the gill rakers, and retains edible food items while non-edible material is flushed from the pharynx (Sibbing *et al.*, 1986). The gill rakers may also act as a cross-flow filter, enabling feeding on smaller food items (Sanderson *et al.*, 2001). I assume that the feeding mechanisms in Common Carp and suckers are similar based on the similarities in morphology of the posterior pharynx.

Mapping form to function is straight-forward in simple morphological systems because morphological state maps directly to function. Redundant mapping of morphology to function may occur in complex morphological systems with multiple parts, where multiple combinations of morphological traits give rise to identical functions. This many-to-one mapping of morphology to function (Wainwright *et al.*, 2005) is observed in a wide range of systems ranging from genotype affecting RNA secondary structure (Fontana & Schuster, 1998; Schuster, 2000) to *Anolis* hind limb morphology affecting jumping ability (Torro *et al.*, 2004). Many-to-one mapping also allows for the simultaneous optimization of multiple functions carried out by a complex morphological system. Because gill rakers are complex morphological systems that have a direct effect on feeding performance and because they serve two different functions during feeding, they may be another example of many-to-one mapping of morphology to function.

To explore the relationship between gill raker morphology and diet I examined both diet and gill raker morphology in twenty-one species of freshwater suckers, chosen to represent the full range of diet and gill raker morphology in the group. I summarized diet and classified species based on size of food consumed. I quantified nine gill raker

traits from each of the first two pharyngeal arches to test for differences within and among species and to determine whether and how gill raker morphology is predictive of diet.

Materials and Methods

Diet Data

Diet information for twenty-one species of suckers was collected from the literature (Table 2.1). Discrepancies in the methods and means of reporting results of different diet studies required results of those studies to be summarized for the subsequent analyses. Prey items were divided into eight categories based on approximate size. From smallest to largest, these categories are detritus, algae, copepods, cladocerans, insect larvae, crustaceans, mollusks, and fish fry. Each sucker species was given a score of 0 to 3 for each of the nine categories where a score of 0 meant the prey item was never found in diet studies for that species, 1 meant the prey was rare (making up 1-10% of its total diet), 2 meant the prey was common (11-50%), and 3 meant the prey was abundant (51-100%).

A discrete diet score was given to each species by determining which size class of prey was most common in their diet. Detritus and algae were considered small-sized prey, copepods and cladocerans were considered medium-sized prey, insect larvae and crustaceans were considered large-sized prey, and mollusks and fish fry were considered extra-large-sized prey. The discrete diet score was determined by finding the size class of prey with the largest sum of prey categories for each species. Ties were decided by

rounding down to the smaller size class under the assumption that smaller sized prey are more difficult to filter than larger sized prey. A discrete diet score of 1 represents a diet dominated by small prey, a score of 2 represents a diet dominated by medium-sized prey, a score of 3 represents a diet of larger prey, and a score of 4 represents very large prey. The discrete diet score also classifies feeding guild where species with a score of 1 are primarily algivores, species with a score of 2 are primarily zooplanktivores, species with a score of 3 are primarily macroinvertivores, and species with a score of 4 are primarily molluskivores.

This discrete score is an estimate of the size of prey most commonly found in each species' diet but does not take into account the size of other prey that may also be consumed by each species. To account for this variation in diet, a continuous diet score was calculated for each species using the scores from each prey category and the following weighted average equation:

(1),

$$1\times\left(\frac{algae+detritus}{A_i}\right)+2\times\left(\frac{copepods+cladocerans}{A_i}\right)+3\times\left(\frac{crustaceans+insect\ larvae}{A_i}\right)+4\times\left(\frac{fishfry+mollusks}{A_i}\right)$$

where *A* is equal to the sum of all prey category scores (*algae* + *detritus* + *copepods* + *cladocerans* + *crustaceans* + *insects larvae* + *fish fry* + *mollusks*) for sucker species *i* and differs among species depending on the total number of different prey items consumed.

Gill Raker Measurements

Three individuals, each approximately 10 cm SL, from twenty-one catostomid species were obtained from the Bell Museum of Natural History Fish Collection (Table

2.2). Each specimen was measured then dissected. The pharyngeal apparatus was removed whole, the palatal organ was removed, and branchial arches were photographed and measured. The rakers on the first pharyngeal arch are different from the rakers on the other arches in the specimens examined and it has been observed that gill rakers on arch 1 of the Common Carp are larger and farther apart than rakers on the other arches (Sibbing *et al.*, 1986), therefore measurements were taken from the first two pharyngeal arches to quantify and test for differences among the two arches. The arches are paired structures and all measurements were taken from the left arch. The total number of rakers on each arch was counted. Branchial arches are highly curved and measuring distances on a curved surface from a 2-dimensional photograph is problematic, therefore arch length was measured by placing a piece of sewing thread along the dorsal surface of each arch, marking each end of the arch on the thread, and measuring the distance between the marks on the straightened thread with digital calipers. The density of rakers on each arch was calculated as the total number of rakers divided by arch length. Width, length, and inter-raker space of the twenty ventral-most gill rakers (Fig. 2.2) were measured using images captured from a digital camera mounted on a dissecting scope. Branchial arches were pinned so that the dorsal surface was parallel with the imaging sensor. Depending on the severity of the curvature of the arch, one to three images were taken for each specimen to keep the gill rakers of interest parallel to the imaging sensor. Images were auto-corrected for white balance and sharpened slightly to enhance edge contrast as needed before being measured. Image manipulation and measurements were taken using GIMP v2.8 software (Kimball & Mattis, 2012). The area of each raker was calculated by

multiplying the width and length of the raker. The total raker surface area of each arch was calculated as the average surface area of each raker multiplied by the total number of rakers on the arch. The total space was calculated as the average space between rakers multiplied by the total number of rakers on the arch. The ratio of surface area to space (SA:Space) was calculated as the total surface area divided by the total space on each arch.

Four additional specimens of White Sucker (*Catostomus commersonii*) were dissected and combined with the original three to test whether gill raker measurements increase with fish size and to test for differences between arch 1 and 2. Linear regression analysis showed that gill raker space, width, and length all increase with fish size but dividing these measures by SL removes this effect in almost all cases. Therefore, these three measures and gill raker area were corrected for fish length by dividing each measurement by SL for all subsequent analyses. To test the hypothesis that the gill rakers on arch 1 and 2 are different, t-tests were used to test for differences in gill raker space, width, length, and area between arch 1 and 2 using all *C. commersonii* specimens. Morphological traits were log-transformed and two-dimensional traits (surface area and total surface area) were divided by 2 to facilitate comparisons with single-dimensional length measurements.

Phylogenetic Analysis

Mitochondrial ND4 and ND5 sequences and the three intervening tRNA sequences from fifty-nine ingroup and the outgroup taxa *Barbatula toni*, *Chalceus*

macrolepidotus, *Cobitis striata*, *Cyprinus carpio*, *Gobio gobio*, *Gyrinocheilus aymonieri*, *Homaloptera leonardi*, and *Pseudobagrus tokiensis*, used in Doosey *et al.* (2010) were downloaded from GenBank (Doosey *et al*., 2010 Table 2.2). Sequences were aligned with MUSCLE (Edgar, 2004) and then verified and edited by eye resulting in 3,439 total sites. ND4 and ND5 were partitioned by codon position and each tRNA was given its own partition. The optimal partitioning and best fitting model of nucleotide substitution for each partition was determined using PartitionFinder v1.1.1 (Lanfear *et al*., 2012). ND4 codon position 1, ND5 codon partition 2, and all three tRNA's were grouped into one partition; ND4 codon position 2 and ND5 codon position 3 were grouped into a second partition; and ND4 codon position 3 and ND5 codon position 1 were grouped into a third partition. GTR+I+G was determined to be the best model for all three partitions. A Bayesian phylogeny was estimated in BEAST v1.8.0 (Drummond *et al.*, 2012) on the CIPRES Science Gateway (Miller *et al*., 2010). Four independent runs of 20 million generations each were run under a lognormal relaxed clock model and assuming a Yule process of speciation. Trees were sampled every 1,000 generations. During exploratory runs, the transversion rate between Cytosine and Guanine in the first partition and the transversion rate between Guanine and Thymine in the second partition each approached zero and runs had difficulty reaching convergence, thus these rates were excluded in the final analysis. Convergence was assessed by comparing the sampled distribution of parameter estimates and ESS's of each parameter for each run in Tracer v1.6 (Rambaut and Drummond, 2007). Trees were combined using LogCombiner v1.8.0 (Drummond *et al.*, 2012) from all four runs after discarding 50% of generations as burnin and

resampling every 4,000 generations. A maximum clade credibility tree was calculated from the combined trees using TreeAnnotator v1.8.0 (Drummond *et al.*, 2012).

Statistical Analyses

To test whether there was significant phylogenetic signal in the species means of the log-transformed morphological traits and in both diet measurements, Blomberg *et al*.'s *K* (2003) and Pagel's λ (1999) were calculated using the Bayesian phylogeny and tested to see if they were significantly different from zero using the "phytools" package (Revell, 2012) in R v3.1.2 (R Core Team, 2014). To test for differences in gill raker traits among species, analysis of variance (ANOVA) was run on each log-transformed gill raker trait in R. To investigate interspecific patterns in morphological traits, principal components analysis (PCA) was run on the species means of the log-transformed morphological traits using the "prcomp" command in R. Continuous diet score showed significant phylogenetic signal so phylogenetic generalized least squares (PGLS) as implemented in the "caper" package of R was used to test for a significant relationship between diet and principal components 1 and 2 while accounting for shared evolutionary history among species. Linear techniques such as PCA are prone to curvilinear distortion (Minchin, 1987) so a different ordination analysis that is less prone to that type of distortion, non-metric multidimensional scaling (NMDS), was also used to investigate interspecific patterns in morphological space and to determine which specific aspects of gill raker morphology are important in determining diet. The NMDS analysis was run in R using the package "vegan" with each morphological trait as a factor and grouping

species by discrete diet score. A plot of *k*-value by stress value was used to pick an appropriate *k*-value for the NMDS ($k = 2$ was found to be best for these data). Significant factors were determined with the vegan "envfit" command after Bonferroni corrections. Ninety-five percent confidence intervals for feeding guild were drawn around point scores based on standard errors with the vegan "ordiellipse" command.

Results

Diet

The calculated continuous diet scores for the twenty-one catostomid species examined ranged from 1.286 to 3.750 with a mean of 2.283±0.606 (Table 2.1). The species with the lowest continuous diet scores, the ones estimated to feed on the smallest sized prey, are *Thoburnia rhothoeca*, *Carpiodes carpio*, *Catostomus discobolus*, *Carpiodes cyprinus*, *Catostomus latipinnis*, and *Carpiodes velifer*. Each has a continuous diet score less than 2.0, a discrete diet score equal to 1, and are classified as algivores as they all feed primarily on algae and detritus. At the other extreme is the mollusk specialist *Moxostoma carinatum* that has a continuous diet score of 3.750 and is the only species with a discrete score of 4. *Hypentelium nigricans* and *Moxostoma valenciennesi* are the only other species with a continuous diet score ≥3.000 but they have a discrete diet score of 3. All other species have a continuous diet score greater than or equal to 2.000 and less than 3.000.

Gill Arch 1 vs Arch 2

Linear regression analyses show that gill raker space, width, and length show positive relationships with fish body size in *Catostomus commersonii*. I found that by dividing each trait value by the standard length (SL) of the fish, this relationship is removed in all but one case. The exception is the length of gill rakers on arch 2 where correcting for fish size does not eliminate the relationship between fish body size and gill raker length but does reduce the magnitude of the relationship ($slope_{before} = 0.1259$, $R^2_{before} = 0.9909$, $slope_{after} = 0.0030$, $R^2_{after} = 0.8162$). I corrected for body size by dividing each measure (gill raker space, width, length, and area) by SL for all subsequent analyses.

The hypothesis that the gill rakers on arch 1 and 2 have the same morphology can be rejected. Student t-tests show that gill raker space, width, length, and area are all significantly different between arch 1and 2 (Fig. 2.3). The gill rakers on arch 1 are further apart and larger than the gill rakers on arch 2. For this reason, I considered arch 1 and 2 to be independent for all subsequent analyses.

Phylogenetic Analysis

The recovered Bayesian phylogeny (Fig. 2.4) was highly similar to the phylogeny of Doosey *et al*. (2010). Within Catostomidae, the subfamily Catostominae was recovered as sister to the other subfamilies. I recovered Myxocyprininae as sister to Cycleptinae plus Ictiobinae with strong support [posterior probability (PP) = 1.0] whereas Doosey *et al*. recovered Cycleptinae as sister to Myxocyprininae plus Ictiobinae with weak support [PP = 0.76, bootstrap (BP) < 70%]. Within Catostominae, I recovered

Erimyzonini sister to the other tribes and Catostomini as sister to Moxostomatini plus Thoburnini but with fairly weak support (PP = 0.73). Within the two largest tribes, Catostomini and Moxostomatini, I recovered clades A, B, C, D, and E of Doosey *et al*. with nearly the same composition as in that study. Four *Catostomus* species (*C. ardens*, *C. columbianus*, *C. commersonii*, and *C. macrocheilus*) that Doosey *et al.* excluded from lettered clades were recovered as members of clade C in this study. A few of the species-level relationships in my phylogeny are slightly different from the relationships recovered by Doosey *et al*. Most differences have no bearing my other analyses except for two sets of species. I recovered *C. cyprinellus* as sister to *C. carpio* plus *C. velifer* with strong support (PP = 1.0) while Doosey *et al*. recovered *C. velifer* as sister to *C. carpio* plus *C. cyprinus* with weaker support (PP = 0.95, BP = 90%). Doosey *et al*. recovered *M. erythrurum* and *M. cervinum* as sister species but my phylogeny indicates that *M. erythrurum* shares a more recent common ancestor with *M. anisurum* than with *M. cervinum*. Likewise, my phylogeny indicates that *M. anisurum*, *M. erythrurum*, and *M. carinatum* share a more recent common ancestor than any share with *M. cervinum* but the phylogeny of Doosey *et al*. indicates that *M. anisurum*, *M. erythrurum*, and *M. cervinum* share a more common ancestor than any share with *M. carinatum*. Considering the relatively short branch lengths connecting these species, the differences in the two studies probably have little impact on my morphological analyses.

Statistical Analyses

No log-transformed morphological trait has phylogenetic signal significantly different from zero using Blomberg *et al.*'s *K* or Pagel's λ. Discrete diet score is also not significantly different from zero. The only trait examined that shows significant phylogenetic signal is continuous diet score but only using Blomberg *et al.*'s *K* (K = 0.3430, p = 0.019). It was not statistically different from zero using Pagel's λ (λ = 0.2543, p = 0.2383).

There are statistically significant differences among species in all morphological traits after Bonferroni correction ($p < 0.001$). In most cases there is relatively little variation within species but there is quite a bit of variation among species (Figs. 2.5, 2.6) and most of the measurements show a four-fold difference between the species with the smallest measurements and the species with the largest. There are few natural breaks in the data and some traits appear to vary nearly linearly across species (i.e. space and total surface area) but others do not (i.e. number, density, SA:Space). Species do not appear to group with feeding guild in consistent ways across multiple morphological traits and the relationship between morphology and diet is difficult to elucidate using ANOVA.

In the principal components analysis of log-transformed morphological traits, the first two principal components account for 72.79% of the variation among species. PC1 was most strongly correlated with length, area, total SA, and SA:Space on arch 1 and length and total SA on arch 2. All of which were negatively correlated with PC1. PC2 was most strongly correlated with density and space on arch 1 and density, space, and area on arch 2 (Fig. 2.7). Density on arch 1 and 2 was positively correlated and the other

traits were negatively correlated with PC2. No significant phylogenetic signal was found in PC1 or PC2 using Blomberg *et al*.'s *K* or Pagel's λ.

Neither PC1 nor PC2 was significantly correlated with continuous diet score in the PGLS analysis but the interaction term between them was ($p = 0.0188$) which indicates that neither PC1 nor PC2 can predict diet alone but they interact in a complex way to determine diet (Fig. 2.8). A plot of PC2 by the marginal effect of PC1 (Fig. 2.9) shows that when PC2 is negative the relationship between PC1 and diet is positive but when PC2 is positive the relationship between PC1 and diet is negative. It should be noted that the curve defining the relationship between PC2 and the marginal effect of PC1 is not a perfectly straight line with a slope of -1 and the absolute value of PC2 must be larger when PC2 is positive to get an equal magnitude relationship between diet and PC1 than when PC2 is negative.

The NMDS analysis roughly grouped sucker species by discrete diet score (Fig. 2.10). The 95% confidence ellipse for zooplanktivores was completely separate from the ellipses for the algivores and macroinvertivores. The macroinvertivore ellipse is intermediate to, and largely overlapping with, the algivore ellipse and the feeding guilds are separated primarily along NMDS2. The statistically significant predictors of diet after Bonferroni correction are number, density, space, width, surface area, and SA:Space on both arch 1 and 2. The predictors having vertical components of their slopes greater than 0.75 are those that are most strongly aligned with NMDS2, the axis that best separates the feeding guilds. Those predictors are area on arch 1 and 2 and width and SA:Space on arch 2 (Fig. 2.11).

Discussion

I found positive relationships between body size and gill raker length, width, and space in White Sucker (*C. commersonii*) showing that gill raker morphology is not static throughout a sucker's lifetime. Speigel *et al.* (2011) found a similar relationship in adults of seven different species of suckers indicating that this is a common phenomenon and that fish size must be considered when examining traits such as gill raker morphology. All eight of these species show linear relationships between body size and gill raker morphological measures and I found that I could account for this relationship by simply dividing each trait by the standard length of the fish making it possible to make comparisons among different sized fish. Growth of gill rakers is probably not linear throughout an individual's lifetime but appears to be linear or at least nearly linear in sub-adult and adult suckers.

Gill rakers are important trophic structures but the specific ways in which they determine feeding performance are complex. There are significant differences in the morphology of gill rakers on arch 1 versus arch 2, which suggests possible differences in function of rakers on different arches. Gill rakers of *C. commersonii* on arch 1 are significantly larger and farther apart than rakers on arch 2. This is also the case in the Common Carp where it has been observed that the gill rakers on the first arch are larger and farther apart than the gill rakers on the other arches and that much of the small inorganic particles such as sand grains and small gravel taken into the buccopharyngeal cavity during feeding exits via the slit formed by the first branchial arch (Sibbing *et al.*, 1986). It is highly likely that the same thing occurs in suckers and other cypriniform

fishes. It has been shown that large inorganic particles such as gravel are spit out of the mouth of Common Carp while food particles are held in place between projections of the palatal organ and the ceratobranchials of arches 2-4 (arch 1 is never involved in this pinning) (Callan & Sanderson, 2003) which also points to a differentiation of function between the gill rakers on arch 1 and those on the other three branchial arches.

In Common Carp, gill rakers function to separate food from inedible particles through cross-flow filtration and by working in concert with the palatal organ to trap particles in the anterior pharynx. When Common Carp feed on a mixture of small-sized food particles and inedible particles, most of the food particles travel posteriorly without contacting the pharyngeal surface and are concentrated in the posterior pharynx. Small, inedible particles travel ventrally through the branchial arches (primarily arch 1) and are expelled out the opercular slits. Large inedible particles are tasted and pinned by ventral protrusions of the palatal organ and the dorsal surface of gill rakers on arches 2-4 while food is concentrated in the posterior pharynx. When Common Carp feed on large-sized food particles and inedible particles, food particles are tasted and trapped by the palatal organ and the gill rakers before being transported posteriorly by undulations of the palatal organ. Small, inedible particles pass ventrally through the arches and large inedible particles are tasted and spit out the mouth (Callan & Sanderson, 2003). This suggests that gill rakers play two important roles in feeding in Common Carp; they serve as the filtering apparatus for cross-flow filtration and they, in conjunction with the palatal organ, are important in tasting and trapping large particles. It is likely that the same

functions also occur in suckers because Common Carp and suckers share similar general buccopharyngeal morphologies and have fairly similar diets.

My multivariate analyses illustrate that the relationship between gill raker morphology and diet is not a simple, direct one. The PCA analysis showed that gill raker morphology can be summarized by two complex characters. PC1 is most highly correlated with measures of surface area like gill raker length, area, total surface area, and SA:Space while PC2 is most highly correlated with gill raker density and spacing. PGLS analysis shows that neither PC1 nor PC2 is predictive of diet by itself but the interaction of the two is. Most of the traits that were found to be important in the PCA analysis were also found to be important in the NMDS analysis. The significant predictors of diet in the NMDS analysis were gill raker width, area, SA:Space, number, density, and space.

Gill rakers in suckers appear to be an example of many-to-one mapping of morphology to function. Wainwright *et al.* (2005) coined the phrase to describe how different morphological systems with more than two components can arrive at the same functional solution by varying different components. This many-to-one mapping allows for greater functional diversity than a strictly one-to-one system and also allows for the maximization of several different functions simultaneously (e.g. cross-flow filtering and tasting/pinning). My PCA and PGLS analyses illustrate this many-to-one mapping in gill rakers of suckers (Fig. 2.8). When PC1 has a large value (most strongly correlated with characters that lead to low surface area) and PC2 has a large value (most strongly correlated high density and low spacing) then species are predicted to feed on very small-sized prey. When PC1 has a large value and PC2 has a low value then species are

predicted to feed on very large-sized prey. The model also predicts a diet of very small prey when PC1 and PC2 have extremely low values and predicts a diet of very large prey when PC1 has an extremely low value and PC2 has an extremely high value but none of the species in this study occupy those regions of morphospace. It remains to be seen whether other species fill these areas of morphospace or whether these areas are even physically possible due to other limitations on morphology.

Most species of suckers do not feed exclusively on very small- or very large-sized prey and the model is most interesting when predicting these intermediate diets as any specific diet score is predicted by several combinations of values for PC1 and PC2. This many-to-one mapping would allow for changes in diet to occur rather quickly in evolutionary time because there are multiple morphological changes that could lead to a change in diet. As new resources open up in an environment, populations are able to quickly adapt to that change because there are multiple potential pathways of morphological change that would allow efficient feeding on the new resources. Because many-to-one mapping allows for quick evolutionary changes in morphology it might be the reason why I found no significant phylogenetic signal in any morphological trait. Catostomidae is an old family of Cypriniformes with a long fossil record (Conway *et al*., 2010) and the lack of phylogenetic signal in gill raker morphology may be due to this long history combined with a fast rate of morphological evolution made possible by many-to-one mapping of gill raker morphology to diet.

Chapter 3

Heterochrony in the Paired Cartilages and Bones of the Pharyngeal Arches and Associated Structures in Five Species of Catostomidae

Summary

Knowing the sequence of developmental events is vital in understanding how heterochrony shapes morphological diversity evolution but it is often difficult to get the developmental series from closely related, non-model organisms that are required for such studies. The goal of this study is to describe and compare the sequence of chondrification and ossification of the paired elements of the pharyngeal arches and the histological development of the palatal organ, chewing pad, and pharyngeal teeth in 5 species of catostomid fishes and compare these results to previous studies of other cypriniform fishes to understand the role heterochrony has played in shaping catostomid trophic morphology. The paired elements of the pharyngeal arches and associated structures are extremely important ecologically for bony fishes because they are the primary structures used in prey capture and processing and are also important in respiration. In this study, cleared and double-stained specimens and histologically sectioned specimens were photographed, measured, and described from developmental series of five species of Catostomidae. I found evidence that the sequence of development is mostly conserved across Catostomidae and Cyprinidae but in some cases there is

evidence that shifts in the timing and rate of development has led to heterochrony in the trophic apparatus of catostomid fishes.

Introduction

Heterochrony, changes in timing or rate of development of morphological traits, has long been recognized as being an important driver of morphological evolution and can have profound impacts on adult morphology (de Beer, 1930; de Beer, 1940; Gould, 1977; McNamera, 1988, Hall, 1992). To study heterochrony, the ontogenetic pattern of a morphological trait must be known from an ancestor and a descendent. Differences in these patterns can be caused by alterations of three parameters; the onset time, the offset time, and the rate of development (Alberch *et al*., 1979; Fink, 1982, 1988). The onset time of a trait is the beginning of ontogeny or the beginning of any period of change of that trait during ontogeny and the offset time is the point when the size or shape of a trait stops changing during ontogeny (Reilly, 1997). By comparing these three parameters between two taxa, it is possible to identify the type of change needed to shift between the two and if one taxon is an ancestor of the other, it is possible to infer the direction of change that occurred (Reilley, 1997).

Altering the three parameters results in six heterochronic processes; acceleration, deceleration, hypermorphosis, hypomorphosis, pre-displacement, and post-displacement (Reilly, 1997). Altering these parameters results in truncated development (paedomorphosis), extended development (peramorphosis), or no net change (isomorphosis) which is possible if more than more is altered. Changes in the rate of

development result in rate modifications. Acceleration is an increase in the rate of development and results in extended development. Deceleration, sometimes referred to as neoteny (Alberch *et al*., 1979), is a decrease in the rate of development and results in truncated development. Shifts in onset and offset times are considered timing modifications (Webster & Zelditch, 2005). Shifting the offset time to a later time results in extended development and is called hypermorphosis. Shifting the offset time to an earlier time results in truncated development and is called hypomorphosis or progenesis (Alberch *et al*., 1979). Pre-displacement is a shift in onset time to an earlier time and results in extended development. Post-displacement is a shift in onset time to a later time and results in truncated development.

One challenge to comparisons of developmental patterns among taxa is standardization of the time axis. Size and stage, based on morphological landmarks, are often used as a proxy for age (developmental time) but they can be problematic both theoretically and practically (Hall and Miyake, 1995). One solution, especially useful when comparing distantly related species or species that differ greatly in size or life history, is to use the sequence of developmental events as the measure of time. This approach has been called sequence heterochrony and when using the sequence of events as a proxy for time the definition of heterochrony is slightly altered to a change in the sequence position of one event relative to other developmental events (Smith, 2002). This avoids many of the problems associated with using other measures of time that may not be directly comparable among taxa (Smith, 2002).

In this study I document the sequence of development of oral and pharyngeal structures in catostomid fishes and compare those sequences to studies of related taxa to determine the impact of heterochrony on trophic morphology. The pharyngeal arches are ecologically and phylogenetically significant in cypriniform fishes (Siebert, 1987) and several studies have demonstrated their morphological diversity (Conway and Mayden, 2007; Sawada, 1981; Siebert, 1987); however, only a few studies have documented the timing of chondrification and ossification of pharyngeal arch structures through ontogeny. The development of the pharyngeal arches has been well documented in only four species belonging to two of the eight cypriniform families. These include the cyprinids *Barbus barbus* (Vandewalle *et al.*, 1992), *Danio rerio* (Cubbage & Mabee, 1996), and *Puntius semifasciolatus* (Block & Mabee, 2012) and the catostomid *Catostomus commersonii* (Engeman *et al.*, 2009). To understand fully how changes in developmental timing can drive morphological evolution, differences in developmental timing need to be documented in more species and in species that are more closely related than the ones studied to date.

Cypriniformes is a species rich order of primary freshwater fishes containing more than 3,200 species (Nelson, 2006). The morphology of the feeding and respiratory structures plays an important role in cypriniform classification. Eight of nine cypriniform synapomorphies are characters associated with the pharyngeal arches (Conway *et al*., 2010). One cypriniform family with particularly interesting trophic morphology is the family Catostomidae, the suckers. All sucker larvae have terminal mouths and feed on zooplankton but during development the orientation of the mouth undergoes a

transformation and become subterminal in orientation. Only *I. cyprinellus* retains a terminal mouth orientation.

Most living jawed vertebrates, gnathostomes, including cypriniforms have seven pharyngeal arches (Javier, 2004). The anterior-most arch, the mandibular arch, along with several associated bones of dermal origin make up the oral jaws. The primary cartilages of the mandibular arch are the palatoquadrate and Meckel's cartilage. Several endochondral bones ossify from these cartilages including the angulo-articular, autopalatine, metapterygoid, quadrate, and retroarticular. Several bones of dermal origin ossify around the mandibular arch including the coronomeckelian, dentary, ectopterygoid, and entopterygoid. In teleosts, there is a protrusible upper jaw anterior to the mandibular arch that is composed of the maxilla and premaxilla and in cypriniforms there is an unpaired kinethmoid (Conway *et al*., 2010). The maxilla and premaxilla are dermal bones. Unlike endochondral bones that ossify from cartilaginous precursors, dermal bones ossify within condensations of mesenchymal tissue without a cartilage model.

The second pharyngeal arch, the hyoid arch, supports the lower jaw and connects it to the skull. It is composed of two main cartilages, the hyosymplectic and ceratohyal cartilages, several ossifications around those cartilages including the anterior ceratohyal, dorsal hypohyal, hyomandibula, interhyal, posterior ceratohyal, symplectic, and ventral hypohyal, and the branchiostegal rays which are dermal in origin.

The remaining five pharyngeal arches are the five branchial arches. The first four occupy the ventral and lateral surfaces of the anterior pharynx and support gill filaments

on their exterior surfaces and gill rakers on their interior surfaces. Dorsal to these four branchial arches is the palatal organ that is composed of soft tissues (Sibbing *et al*., 1986; Doosey & Bart, 2011). Directly posterior to the palatal organ lies the basioccipital pad which covers the ventral surface of the basioccipital process, a posterior-ventral extension of the basioccipital bone. Posterior to the first four branchial arches and ventral to the basioccipital pad lies the fifth branchial arch which is highly modified in Cypriniformes and in all families except Gyrinocheilidae, contains one to three rows of teeth.

The aim of this study is to provide a general description of the sequence of chondrification and ossification of the paired elements of the pharyngeal arches and a description of the histological development of the palatal organ, basioccipital pad, and pharyngeal teeth in five species of suckers to answer the following questions about the development of the trophic apparatus of suckers. 1) What morphological changes to the paired cartilages and bones of the trophic apparatus of suckers occur during the transition from a terminal to subterminal orientation of the mouth? 2) Are these changes consistent across Catostomidae or has there been heterochrony? 3) Are differences in the number of gill rakers and teeth and differences in gill raker density in adult suckers due to heterochrony due to rate modifications or timing modifications?

Materials and Methods

Spawning adults of *Catostomus commersonii*, *Hypentelium nigricans*, *Ictiobus cyprinellus*, *Moxostoma anisurum*, and *Moxostoma erythrurum* were collected from rivers in Minnesota in the spring between 2008 and 2011 (Table 3.1). Ripe ova were

gently squeezed from each female and immediately fertilized with sperm collected from 2-3 males. Fertilized eggs were rinsed several times in river water, mixed with Fuller's earth to prevent clumping, and transferred to 10-gallon aquaria. Aquaria were supplied with a continuous flow of fresh well water, heated to match the temperature of the St. Croix River at Stillwater, MN as recorded by USGS streamflow station 05341550. Aquaria were vigorously aerated to keep the eggs slowly rocking to help prevent fungal growth (Nevin Aspinwall, personal communication). After the eggs hatched, aeration was reduced. Newly hatched larvae were fed *Paramecium* (Ward's Scientific, Rochester, NY) and brine shrimp nauplii (Brine Shrimp Direct, Ogden, UT). Golden Pearls Reef & Larval Fish Diet (size range 100 to 800 μm) (Brine Shrimp Direct, Ogden, UT) was added to the diet as larvae grew. Every three days post-hatching, 5 to 10 larva were collected, euthanized in MS-222 (300 mg/L), fixed in 10% formalin for 2 days, transferred to 35% ethanol for 1 day, then stored in 70% ethanol. Specimen body length was measured as either notochord length for preflexion larvae or standard length for larger larvae and juveniles, and measured to the nearest 0.01 mm with calipers. Collection, housing, and euthanasia procedures were approved by the University of Minnesota Institutional Animal Use and Care committee (IACUC 1002A77739).

Observations of paired cartilaginous and bony elements of the branchial, hyoid, and mandibular arches and of dermal bones associated with the mandibular arch were conducted on a developmental series of 12 to 19 larvae (mean = 15.4) from each of the 5 species ranging from newly hatched to juvenile where their general external morphology matched adult morphology and they had the same fin ray counts as adults. These

specimens from the series were enzymatically cleared with trypsin and double stained with Alizarin Red and Alcian Blue following Dingerkus and Uhler (1977) with modifications suggested by Potthoff (1984). The earliest sign of Alcian Blue uptake was recorded as presence of cartilage. The earliest sign of Alizarin Red uptake or the appearance of unstained bone matrix was recorded as presence of bone. Specimens were observed and photographed using a Nikon SMZ-U stereoscope with attached SPOT Insight 4 digital camera.

Gill rakers on the left side of the second branchial arch and teeth on the left side of the fifth branchial arch were counted on the cleared and stained specimens. Gill rakers on the first branchial arch function differently from rakers on the other arches in a related and ecologically similar species, the Common carp (*Cyprinus carpio*) (Sibbing *et al.*, 1986; Callan and Sanderson, 2003), and the number of gill rakers differs between branchial arch 1 and 2 in *C. commersonii* (Chapter 2) so gill rakers were counted from the second branchial arch instead of the first. Gill raker density was calculated as the number of gill rakers divided by the length of the ceratobranchial, epibranchial, and hypobranchial of the left side of the second branchial arch. To prevent bias from excess of zeros, all specimens with either zero gill rakers or zero teeth except the largest specimen with zero gill rakers or zero teeth were not included in the statistical analyses. Number of gill rakers, number of teeth, and gill raker density were regressed against body length to test for differences among species in the rate of accumulation of these characters. A general linear model was used for all regression comparisons and significant differences in the slope and intercept of the models among species were tested

with an analysis of covariance (ANCOVA). Visual inspection of the scatter plots revealed that the rate of accumulation of some structures in some species decrease during ontogeny so quadratic models were tested and compared to the linear models to find the best fitting model for each species for each character. All statistical tests were performed in R (R Core Team, 2014) with significance assessed at $\alpha = 0.05$.

A series of 3 to 9 larval and juvenile heads (mean = 6.2) from each species was prepared for histological examination by paraffin sectioning following Presnell and Schreibman, 1997) with modifications. Specimens were rehydrated from 70% ethanol to 35% ethanol to water over the course of one day then decalcified for 12-72 hours as needed. After decalcification, specimens were rinsed in running tap water for 1 hour, dehydrated through a series of ethanol solutions of 35%, 70%, 95%, 100%, and 100% for 1 hour each, followed by 2 transfers to xylene for 1 hour each. They were then transferred to molten paraffin overnight before being embedded in fresh paraffin the following day. Each block was sectioned transversely from anterior to posterior on a rotary microtome at a thickness of either 7 µm for specimens less than about 13 mm in body length or 10 µm for larger specimens. Sections were mounted on slides and dried. Staining was based on methods modified from Presnell and Schreibman (1997). Sections were stained with Harris hematoxylin (Fisher Scientific SH26-500D) and counterstained with an eosin solution made of 1.0 g eosin Y (Acros 40943-0250), 1000 ml 70% ethanol, and 5.0 ml glacial acetic acid following Presnell and Schreibman (1997). After eosin counterstaining, sections were dipped 5 times in 70% ethanol, 10 times in 95% ethanol, stained in Alcian Blue solution for 20-30 seconds, then fully dehydrated and cleared in

xylene (Sigma-Aldrich 434056). Alcian Blue solution was made from 70 ml absolute ethanol, 30 ml glacial acetic acid (Mallinckrodt Chemicals V193-14), and 20 mg Alcian Blue (Sigma A-5268) following Potthoff (1984). The addition of the Alcian Blue stain was found to act as an acidic de-stain and give cartilage a slight blue tint facilitating observation of cartilaginous and bony structures. Observations of the histological sections focused on the soft tissues associated with the gill rakers, pharyngeal teeth, palatal organ, and basioccipital pad. Stained sections were observed and photographed using a Nikon Eclipse E400 microscope with attached SPOT Insight 4 digital camera.

Results

The sequence of chondrification and ossification of the paired cartilages and bones of the pharyngeal arches is described below in the following order: mandibular arch, hyoid arch, branchial arches followed by descriptions of the palatal organ and basioccipital pad. Within each arch, elements are described in order of first appearance with the exception of mouth orientation which is presented first. Comparisons among species are made based on body length which is either notochord length for preflexion larvae or standard length for larger specimens. The smallest specimen in which an element is first observed is given for each species.

Mandibular Arch and Associated Bones

The mandibular arch is composed of the palatoquadrate and Meckel's cartilages and the endochondral bones that ossify from those cartilages; angulo-articular, autopalatine, metapterygoid, quadrate, and retroarticular. Complementing those bones and cartilages

are a number of dermal bones that form around the mandibular arch or mandibular arch cartilages including the coronomeckelian, dentary, ectopterygoid, and entopterygoid. There is also a protrusible upper jaw anterior to the mandibular arch composed of the paired dermal maxilla and premaxilla and the unpaired sesamoid kinethmoid (Conway *et al*., 2010).

The mouths of newly hatched suckers have a terminal orientation and are supported by the palatoquadrate cartilage and Meckel's cartilage (Fig. 3.1A), prior to the ossification of the premaxilla and maxilla. During ontogeny the orientation becomes subterminal except in *Ictiobus cyprinellus* which retains a terminal mouth throughout its life. In the other four species examined, the transition in mouth orientation takes place as the bones of the upper and lower jaws ossify. The premaxilla seems to play a critical role during the transition because it supports the fleshy upper lip. During the transition, the premaxilla elongates and moves slightly ventrally pushing the upper lip ventrally (Fig. 3.1B) until the mouth has a fully subterminal orientation and becomes supported by the premaxilla and maxilla instead of the palatoquadrate cartilage and Meckel's cartilage (Fig. 3.1C). The transition begins earliest in *Hypentelium nigricans* (body length = 12.80 mm) and *Moxostoma anisurum* (12.75 mm) and slightly later for *Catostomus commersonii* (14.09 mm) and *Moxostoma erythrurum* (14.05 mm) (Fig. 3.2) although no *M. erythrurum* specimens of approximately 13 mm were examined. The transition in *M. erythrurum* was quick as specimens of 10.85 mm have a terminal mouth and by the next collecting event at 14.05 mm the transition to a subterminal mouth had started and been

completed. The transition was complete by 14.95 mm for *C. commersonii*, and 15.05 mm for *H. nigricans* and *M. anisurum*.

The palatoquadrate cartilage and Meckel's cartilage were present in the smallest specimens examined of all 5 species (Fig. 3.2). The smallest specimens of *C. commersonii*, *H. nigricans*, *M. anisurum*, and *M. erythrurum* were approximately 10 mm but *I. cyprinellus* specimens were much smaller (3.50 mm), as this species hatches at a smaller size. At this early stage in all 5 species, the palatoquadrate cartilage consists of 2 parts; a denser rod-shaped ventral portion that curves dorsally from anterior to posterior and a less dense, triangular sheet that extends anterio-dorsally and slightly medially from the rod-shaped ventral portion (Fig. 3.3A). Over time the triangular portion becomes slightly denser and dorsal tip elongates slightly and becomes noticeably denser just prior to ossification of the entopterygoid while the ventral rod-shaped portion thins slightly except for the anterior tip where the quadrate will articulate with the angulo-articular (Fig. 3.3B, C).

In all species examined the dermal maxilla is generally the first bone to ossify in the anterior head (Fig. 3.2). It starts as a thin sliver of bone anterior to the ethmoid plate (Fig. 3.3B). When the mouth is closed, the maxilla slopes ventrally from anterior to posterior. The dorsal portion ossifies faster than the ventral portion and forms a flat sheet that extends medially and is flat when viewed rostrally. The lateral portion expands and is flat when viewed laterally (Fig. 3.3C). The maxilla begins to ossify later in *H. nigricans* (12.35 mm) than it does in the other 4 species where it forms at nearly the same time (*I.*

cyprinellus = 10.30 mm, *M. erythrurum* = 10.45 mm *C. commersonii* = 11.20 mm, *M. anisurum* = 11.35 mm).

The premaxilla is also dermal in origin and ossifies anterior and medial to the dorsal end of the maxilla. It begins to form as a thin, sliver of bone near the midline of the anterior-most point of the head (Fig. 3.3B). It broadens laterally as it ossifies ventrally to form a triangular bone that is widest at its ventral edge which forms the bony support of the upper lip (Fig. 3.3C). The premaxilla begins to form slightly after the maxilla except in *H. nigricans* where it ossifies at the same time (12.35 mm) (Fig. 3.2). The ossification of the premaxilla occurs at the same time as the transition from a terminal to subterminal mouth orientation in the 4 species that undergo such a transformation. Early in its development, the premaxilla is situated so that its dorsal-most point is dorsal to the dorsal-most point of the maxilla when the mouth is closed and is less than half the length of the maxilla in lateral view. By the time the mouth has switched orientation, the dorsal tip of the premaxilla has moved so that it is ventral to the dorsal-most tip of the maxilla and elongates to be at least half as long as the maxilla. In *I. cyprinellus,* which does not undergo a change in mouth orientation, the premaxilla begins to ossify much earlier (10.70 mm) than it does in other species (*H. nigricans* = 12.35 mm, *M. anisurum* = 12.75 mm, *M. erythrurum* = 14.05 mm, *C. commersonii* = 14.09 mm) and does not move relative to the maxilla, remaining relatively short.

The dermal entopterygoid is the first bone associated with the palatoquadrate to ossify (Fig. 3.2) and does so sooner in *I. cyprinellus* (10.30 mm) and *C. commersonii* (11.20 mm) than it does in *H. nigricans* (12.35 mm), *M. anisurum* (12.75 mm), and *M.*

erythrurum (14.05 mm). The entopterygoid ossifies as a thin sliver of bone on the concave, dorsal edge of the palatoquadrate (Fig. 3.3B). This sliver thickens to form a ridge while a thinner sheet ossifies medially and dorsally and cups about 2/3 to 3/4 of the anterior portion of the ventral part of the eye (Fig. 3.3C). The entopterygoid ossifies before the switch in mouth position in *C. commersonii* but at the same time as the transformation in *H. nigricans*, *M. anisurum*, and *M. erythrurum*.

The quadrate ossifies just after or at nearly the same time as the entopterygoid and does so earlier in *I. cyprinellus* (10.70 mm) than the other 4 species (mean = 12.93 mm) (Fig. 3.2). It forms from two parts; a membranous ossification that lies just ventral to the palatoquadrate and an endochondral ossification of the antero-ventral portion of the palatoquadrate (Fig. 3.3B). The endochondral ossification begins near the articular knob and spreads over the knob and then dorsally and posteriorly. The membranous portion ossifies earlier than the endochondral portion and fuses with the endochondral portion at the articular knob (Fig. 3.3C). The quadrate ossifies before the change in mouth position in *C. commersonii* but at the same time as the transformation in *H. nigricans*, *M. anisurum*, and *M. erythrurum*.

The ectopterygoid is a dermal ossification that forms along the anterior edge of the dorsal, triangular portion of the palatoquadrate (Fig. 3.3B). It begins to ossify at approximately 13.5 mm in *C. commersonii*, *H. nigricans*, and *M. erythrurum* (Fig. 3.2). The ectopterygoid ossifies earlier in *I. cyprinellus* (10.70 mm) than is does in the other four species (*H. nigricans* = 12.35 mm, *C. commersonii* = 12.57 mm, *M. anisurum* = 12.75 mm, *M. erythrurum* = 14.05 mm) and forms at the same time as the quadrate. The

ectopterygoid ossifies anteriorly from the original sliver along the palatoquadrate to form a thin sheet connected to a slightly thicker ridge along the anterior edge of the palatoquadrate (Fig. 3.3C).

The metapterygoid ossifies in the concave dorso-posterior portion of the palatoquadrate (Fig. 3.3B). It ossifies at the same time as the ectopterygoid in *H. nigricans* (12.35 mm) and the 2 *Moxostoma* species (12.75 mm and 14.05 mm) but later in *I. cyprinellus* (13.85 mm) and *C. commersonii* (14.35 mm) (Fig. 3.2). As it ossifies it spreads ventrally and anteriorly and connects with the entopterygoid anteriorly, the quadrate antero-ventrally, and the symplectic ventrally (Fig. 3.3C). The metapterygoid ossifies at the same time as the switch in mouth position in *C. commersonii, H. nigricans, M. anisurum,* and *M. erythrurum*.

The autopalatine is a perichondral ossification of the rounded antero-dorsal process of the palatoquadrate. It begins to form at about the same time as the metapterygoid in *C. commersonii* (14.35 mm), *H. nigricans* (12.80 mm), *M. anisurum* (12.90 mm), and *M. erythrurum* (14.05 mm) but ossifies noticeably later in *I. cyprinellus* (16.10 mm) (Fig. 3.2). The autopalatine begins to ossify in the middle of the rounded, thickened antero-dorsal process and the ossification spreads anteriorly and posteriorly from the central portion. The autopalatine ossifies at approximately the same time as the switch in mouth position in *C. commersonii, H. nigricans, M. anisurum,* and *M. erythrurum*.

Meckel's cartilage forms anterior to the palatoquadrate cartilage and is present in the smallest specimens examined (Fig. 3.2). The paired Meckel's cartilages meet at the anterior midline of the head and angle laterally going anterior to posterior. The posterior

end of Meckel's cartilage sits medially to the antero-ventral portion of the palatoquadrate cartilage (Fig. 3A). The bones of the lower jaw; the dentary, angulo-articular, and retroarticular, ossify around Meckel's cartilage. In the larger specimens of *H. nigricans* examined, Meckel's cartilage expands dorsally near its posterior end to become more triangular in shape than in the other 4 species.

The dermal dentary is the first lower jaw bone to ossify (Fig. 3.2). It begins to ossify at the anterior end of Meckel's cartilage (Fig. 3.3B). It begins to spread posteriorly along the exterior face of the cartilage slightly before spreading along the interior face. As it spreads anteriorly along the exterior face of Meckel's cartilage, it spreads dorsally to form a triangular sheet whose dorsal tip sits medial to the maxilla (Fig. 3.3C). Ossification of the dentary precedes the switch in mouth position except in *H. nigricans* and *M. erythrurum* where they occur at the same time.

The retroarticular begins to form after the dentary and ossifies on the ventral portion of the posterior end of Meckel's cartilage (Fig. 3.3B). Unlike the dentary, it ossifies later in *I. cyprinellus* (13.85 mm) than it does in *C. commersonii* (12.57 mm), *H. nigricans* (12.35 mm), and *M. anisurum* (12.75 mm) (Fig. 3.2). The retroarticular ends up forming a small triangular bone ventral to the angulo-articular (Fig. 3.3C). Ossification of the retroarticular occurs before the switch in mouth position in *C. commersonii* but at about the same time in *H. nigricans, M. anisurum*, and *M. erythrurum*.

The angulo-articular forms at the posterior end of Meckel's cartilage (Fig. 3.3B) and begins to ossify slightly after or at about the same time as the retroarticular in all species

examined except for *I. cyprinellus* where it begins to ossify much earlier (10.70 mm for the angulo-articular compared to 13.85 mm for the retroarticular) (Fig. 3.2). It first ossifies along the edge of the cavity where the palatoquadrate articulates. It ossifies posteriorly and cups the cavity and also spreads anteriorly along the lateral edge of Meckel's cartilage. It ends up ossifying most of the posterior end of Meckel's cartilage except for the ventral portion with is ossified by the retroarticular (Fig. 3.3C). Ossification of the angulo-articular occurs during the switch in mouth position in the four species examined that undergo the transformation.

The coronomeckelian is a small, triangular bone at about the midpoint of the dorsal surface of Meckel's cartilage (Fig. 3.3C). It begins to ossify at about the same time as or slightly after the angulo-articular except in *I. cyprinellus* where it ossifies noticeably later (10.70 mm for the angulo-articular and 13.85 mm for the coronomeckelian) (Fig. 3.2). As the angulo-articular ossifies most of the posterior portion of Meckel's cartilage, the coronomeckelian remains a small bump on the dorsal edge of the angulo-articular. Ossification of the coronomeckelian occurs during the switch in mouth position in the four species examined that undergo the transformation.

Hyoid Arch

The hyosymplectic, ceratohyal, and interhyal cartilages are present in the smallest specimens of each species examined except *M. erythrurum*. In *M. erythrurum* the interhyal cartilage was not observed in the smallest specimen examined but was present by 10.25 mm (Fig. 3.4). In the smallest specimens examined for each species, except for the very smallest *I. cyprinellus*, the hyosymplectic cartilage consists of a ventral rod-

shaped portion that sits ventral to the posterior portion of the palatoquadrate cartilage (Fig. 3.5A, B). This rod-shaped portion angles dorsally from anterior to posterior and widens into a triangular cartilage that sits posterior to the palatoquadrate cartilage. The dorsal, triangular portion contains a central foramen for cranial nerve VII and the anterior lateral line nerve. In the smallest *I. cyprinellus* (3.50 mm), the dorsal portion is diffuse and rod-like with very little widening but by 4.70 mm the dorsal portion has begun to widen and by 7.00 mm is fully triangular. The dorsal portion of the cartilage is replaced by the hyomandibula (Fig. 3.5C) and the ventral portion is replaced by the symplectic (Fig. 3.5E) but remnants of cartilage remain at the articulations even in the largest specimens examined.

The hyomandibula begins ossifying around the foramen of the hyosymplectic cartilage and continues ossifying dorsally and ventrally (Fig. 3.5C). As the dorsal portion of the hyosymplectic cartilage ossifies it thins and elongates in the central portion but remains wider at its dorsal extreme forming a “T”-shape. In the larger specimens examined, a sheet of bone forms on the anterior side of the “T” that cups the ventral half of the posterior side of the eye while the entopterygoid cups the ventral half of the anterior side of the eye (Fig. 3.5E). The hyomandibula begins to ossify before the transition in mouth position in *C. commersonii* (11.20 mm), *H. nigricans* (12.35 mm), and *M. anisurum* (12.75 mm) and begins to ossify earlier in those three species than in *I. cyprinellus* (13.85 mm) (Fig. 3.4).

The symplectic ossifies from the ventral rod-shaped portion of the hyosymplectic cartilage. The ventral edge ossifies faster than the dorsal edge and it remains rod-shaped

until an additional process ossifies on the dorsal edge later in ontogeny (Fig. 3.5E). The symplectic begins to ossify at the same time as the hyomandibula in *I. cyprinellus*, *H. nigricans*, *M. anisurum*, and *M. erythrurum* but ossifies just after the hyomandibula in *C. commersonii* (12.57 mm) but in all cases, the symplectic begins to ossify just prior to the beginning of the transition to a subterminal mouth (Fig. 3.4).

The ceratohyal cartilage forms the precursor for the anterior ceratohyal, posterior ceratohyal, dorsal hypohyal, and ventral hypohyal (Fig. 3.5A, B). It first appears as a rod-shaped cartilage that angles dorsally and laterally from anterior to posterior and it sits posterio-dorsal to the hyosymplectic cartilage. As it forms it broadens dorso-ventrally and the antero-medial end becomes somewhat bulbous. Most of the ceratohyal cartilage gets replaced by bone and the only remaining cartilage in the largest specimens examined is at the anterior and posterior ends (Fig. 3.5E, F).

The anterior ceratohyal and ventral hypohyal are the first ceratohyal bones to ossify (Fig. 3.4). The anterior ceratohyal begins to ossify in the middle of the ceratohyal cartilage and continues anteriorly and posteriorly (Fig. 3.5D, F). It begins to ossify before the transition in mouth orientation in *C. commersonii* (12.57 mm), *H. nigricans* (12.35 mm), and *M. anisurum* (12.75 mm). It forms earlier in these species than in *I. cyprinellus* (13.85 mm) (Fig. 3.4).

The ventral hypohyal is an endochondral ossification of the ventral edge of the anterior, bulbous end of the ceratohyal cartilage (Fig. 3.5D, F). It first appears at the same time as the anterior ceratohyal in all 5 species examined (Fig. 3.4). It begins to ossify at the ventral tip and proceeds a short distance dorsally.

The dorsal hypohyal ossifies on the anterior end of the ceratohyal cartilage dorsal to the ventral hypohyal (Fig. 3.5E). It first appears at the same time as the ventral hypohyal in *H. nigricans* (12.35 mm), *M. anisurum* (12.75 mm), and *M. erythrurum* (14.05 mm) but first appears after the ventral hypohyal in *I. cyprinellus* (16.10 mm) and *C. commersonii* (14.35 mm) (Fig. 3.4). In *C. commersonii*, it ossifies during the transformation in mouth position but in *H. nigricans* and *M. erythrurum* it ossifies before the transformation.

The posterior ceratohyal is an ossification of the posterior end of the ceratohyal cartilage. It begins to ossify near the interhyal and proceeds anteriorly (Fig. 3.5E, F). The posterior ceratohyal ossifies at the same time as the dorsal hypohyal in all 5 species examined (Fig. 3.4).

The interhyal cartilage is a short rod-shaped cartilage that sits between the posterior end of the ceratohyal cartilage and the ventral edge of the hyosymplectic cartilage (Fig. 3.5A, E). It is present in the smallest specimens examined except for in *M. erythrurum* where it first appears at 10.25 mm (Fig. 3.4). It remains a short rod-shaped cartilage until it begins to ossify at its ventral end and proceeds dorsally (Fig. 3.5E). It ossifies at about the same time in *C. commersonii* (14.95 mm), *H. nigricans* (15.05 mm), and *M. erythrurum* (15.60 mm). It ossifies later in *M. anisurum* (17.60 mm) than in the previous 3 species and ossification was never observed in *I. cyprinellus* even in the largest specimen examined (25.05 mm SL) (Fig. 3.4).

The 3 branchiostegal rays are membranous ossifications of the branchiostegal membrane and insert in the ceratohyal cartilage (Fig. 3.5E). They first appear as thin

slivers of bone before enlarging. Branchiostegal rays 2 and 3 ossify together in all 5 species examined, appearing first in *I. cyprinellus* (10.30 mm) followed closely by *M. erythrurum* (14.05 mm) then *C. commersonii* (11.20 mm), *H. nigricans* (11.85 mm), and *M. anisurum* (12.75 mm) (Fig. 3.4). Branchiostegal ray 1 forms at the same time as rays 2 and 3 in *I. cyprinellus*, *M. anisurum*, and *M. erythrurum* but appears after rays 2 and 3 in *C. commersonii* (14.35 mm) and *H. nigricans* (12.35 mm). The first appearance of branchiostegal ray 1 precedes the switch in mouth position in *H. nigricans* and *M. anisurum* but occurs at the same time with the transformation in *C. commersonii* and *M. erythrurum*. The branchiostegal rays often appear first as unstained bone matrix before taking up Alizarin Red.

Branchial Arches

Ceratobranchial 1-5 cartilages are all present in the smallest specimens examined (Fig. 3.6). They first appear as rod-shaped cartilages that angle slightly posteriorly ventral to dorsal (Fig. 3.7A, B). They are curved such that the middle is lateral to both the ventral and dorsal ends. The general pattern of ossification is ossification of ceratobranchial 5 followed by 4, 3, 2, and 1. In *I. cyprinellus* ceratobranchial 5 ossifies first (8.35 mm) followed by 2, 3, and 4 (13.85 mm) and finally 1 (16.10 mm). Ossification of ceratobranchial 5 occurs much earlier in *I. cyprinellus* than the other species but ossification of ceratobranchial 1 occurs much later in *I. cyprinellus* than the other species. In *C. commersonii* they ossify at the same time (12.57 mm) although a smaller specimen (11.20 mm) may show the very beginnings of ossification in ceratobranchial 5 but is it unclear. In *H. nigricans* ceratobranchial 5 ossifies first (11.00 mm) followed by 3 and 4

(12.35 mm) and finally 1 and 2 (12.80 mm). In *M. anisurum* all 5 ceratobranchials ossify at about the same time (12.75 mm). In *M. erythrurum* ceratobranchial 5 ossifies first (10.45 mm). Unstained bone matrix appears at the same time (14.05 mm) in the remaining ceratobranchials but ceratobranchials 3 and 4 (14.55 mm) take up Alizarin Red before 1 and 2 (15.60 mm). Each ceratobranchial begins to ossify near the middle and ossification proceeds dorsally and ventrally simultaneously (Fig. 3.7C, D). The ceratobranchials thin and flatten as they ossify. Ceratobranchials 1-4 appear very similar but ceratobranchial 5 undergoes further morphogenesis. It becomes noticeably larger and more robust than the other ceratobranchials (Fig. 3.7C). Ceratobranchial 5 develops a single row of teeth while the other ceratobranchials support the gill filaments. Ossification of all 5 ceratobranchials begins before the transformation in mouth position in the species that develop a subterminal mouth.

There are 4 hypobranchial cartilages but only hypobranchial 1 and 2 ossify. The hypobranchials form between the basibranchial and the ventral ends of ceratobranchial 1-4 (Fig. 3.7D). Hypobranchial 1 and 2 are present in the smallest specimens examined in all species except *M. erythrurum* where they first appear at 10.25 mm (Fig. 3.6). They first appear as small, square-shaped cartilages (Fig. 3.7D) that elongate through development (Fig. 3.7F). By the time they begin to ossify, hypobranchial 2 is approximately three-quarters as long as hypobranchial 1. Ossification begins in the middle of each cartilage and proceeds medially and laterally toward each end. Ossification occurs later in *I. cyprinellus* (16.10 mm) than in the other species where ossification begins during the transition to a subterminal mouth (Fig. 3.6). Hypobranchial

3 and 4 are much shorter than hypobranchial 1 and 2 and they do not undergo significant elongation and remain square-shaped or ball-like (Fig. 7F). Hypobranchial 3 is present in the smallest specimens of *I. cyprinellus*, *C. commersonii*, and *H. nigricans* but not *M. anisurum* and *M. erythrurum* where it is first observed at 10.75 mm and 10.25 mm respectively. Hypobranchial 4 is observed in the smallest *H. nigricans*. It first appears slightly after hypobranchial 3 in *I. cyprinellus* (7.00 mm) and *C. commersonii* (9.86 mm) and at the same time as hypobranchial 3 in *M. anisurum* and *M. erythrurum*. Hypobranchial 4 never ossifies but it does fuse with ceratobranchial 4 later in development (Fig. 3.6, 3.7F) except in *I. cyprinellus* where hypobranchial 4 was observed as a separate cartilage even in the largest specimen examined. In the other 4 species, fusion occurs after the transition to a subterminal mouth and occurred earliest in *M. anisurum* (15.05 mm), followed by *C. commersonii* (16.88 mm), *M. erythrurum* (19.75 mm), and *H. nigricans* (21.80 mm).

Five epibranchial cartilages form at the dorsal ends of ceratobranchials 1-4. Epibranchials 1-4 appear at the same time. They appear first in *I. cyprinellus* (9.10 mm) followed by *M. erythrurum* (10.30 mm), *H. nigricans* (10.52 mm), *C. commersonii* (11.20 mm), and *M. anisurum* (11.40 mm). At first, they are short rod-shaped cartilages that chondrify ventro-medially toward the ceratobranchials and curve dorsally. The dorsal portion of each epibranchial expands and an uncinated process forms on each (Fig. 3.7C, E). Epibranchial 1-4 ossify at about the same time and they ossify during the transition to a subterminal mouth except in *I. cyprinellus* where they ossify after the other species (16.10 mm) (Fig. 3.6). Epibranchial 5 forms at the same time as epibranchial 4 or slightly

later. It forms at the dorsal end of ceratobranchial 4 (Fig. 3.7C, E) and unlike the other epibranchials, it never ossifies and remains smaller and thinner.

The 4 pharyngobranchial cartilages are dorso-ventrally flat cartilages with irregular shapes that form on the dorso-medial ends of the epibranchials at the roof of the buccal cavity. The 4 pharyngobranchial cartilages first appear at the same time in *I. cyprinellus* (10.30 mm), *C. commersonii* (12.57 mm), and *H. nigricans* (11.25 mm). In *M. anisurum* and *M. erythrurum*, pharyngobranchial 2 and 3 appear slightly before (11.40 mm, 10.40 mm) pharyngobranchial 1 and 4 (12.75 mm, 10.45 mm) (Fig. 3.6). Pharyngobranchial 2 and 3 ossify while 1 and 4 do not. Pharyngobranchial 3 ossifies before pharyngobranchial 2 in *H. nigricans* (12.90 mm, 16.35 mm) and *M. anisurum* (12.90 mm, 16.30 mm) but at the same time in *I. cyprinellus* (25.05 mm), *C. commersonii* (14.45 mm), and *M. erythrurum* (15.60 mm). Ossification occurs during the switch in mouth orientation in *C. commersonii*, *H. nigricans*, and *M. anisurum* but occurs after in *M. erythrurum*. Ossification occurs much later in *I. cyprinellus* than in the 4 species that undergo a mouth position transformation.

Suckers have a single row of teeth on ceratobranchial 5. These pharyngeal teeth first appear early in ontogeny and are some of the first structures to take up Alizarin Red (Fig. 3.6). Teeth are present in the smallest specimens examined of *C. commersonii*, *M. anisurum*, and *M. erythrurum*. They are first observed in *I. cyprinellus* at 4.70 mm and *H. nigricans* at 10.35 mm. The first teeth that form are triangular and project posteriorly off ceratobranchial 5 (Fig. 3.7B). They are longer than they are wide at their bases. Teeth first begin to form in epithelial tissue surrounding ceratobranchial 5 and grow anteriorly

toward ceratobranchial 5 where they ankylose. Through ontogeny, the teeth become larger and curve medially (Fig. 3.7D, F). Ventral teeth tend to be larger than ones near the dorsal end of ceratobranchial 5.

Ceratobranchial 5 is covered by a layer of striated muscle and irregular connective tissue which in turn is covered by stratified cuboidal or columnar epithelium (Fig. 3.8). Tooth caps first appear in indentions of the epithelium. The caps elongate ventrally toward ceratobranchial 5 and eventually ankylose to the bone. The teeth remain surrounded by a thin layer of epithelium until their dorsal tips pierce through the epithelium layer and become exposed. The ventral portion of each tooth remains covered in a thin layer of epithelium and that is embedded in the muscle and connective tissue layer above ceratobranchial 5. Even though the tip of each tooth becomes exposed to the buccal cavity, they do not extend out of the surrounding soft tissue but remain in invaginations of the epithelial layer (Fig. 3.8).

Gill rakers first appear as small, rounded pyramids of bone on the medial face of the ceratobranchials (Fig. 3.7C). They appear first in *I. cyprinellus* (8.60 mm) followed by *C. commersonii* (9.86 mm), *M. erythrurum* (10.30 mm), *H. nigricans* (10.52 mm), and *H. anisurum* (11.35 mm) (Fig. 3.6). Through ontogeny they increase in number and spread along the ceratobranchials and eventually onto the epibranchials and hypobranchials. After starting as round pyramids, their bases become wider and shallow while the tops elongate and eventually become comb- or fan-shaped (Fig. 3.7E).

The underlying bone of a gill raker ossifies in a layer of dense connective tissue that surrounds each of the first 4 ceratobranchials (Fig. 3.9). This connective tissue layer also

surrounds the gill raker bones as they grow. Adipose cells are also present in the connective tissue layer but are rare, especially in small specimens. Stratified cuboidal epithelium covers the connective tissue (Fig. 3.9) and through ontogeny the epithelial cells become more columnar in shape. There is a high density of taste buds in the epithelium covering gill rakers but none are present in the epithelium between gill rakers (Fig. 3.9). A thin strand of muscle connects the base of each gill raker on a ceratobranchial (Fig. 3.9). This strand of muscle is very thin in small specimens but becomes thicker as the gill rakers become larger.

Palatal Organ and Chewing Pad

The palatal organ is ventral to the basioccipital and forms the dorsal roof of the posterior portion of the buccal cavity. It sits dorsal to the branchial arches and is composed of a thick pad of striated muscle and irregular connective tissue (Fig. 3.10). Some adipose cells are also present and are most highly concentrated in the central portion of the organ (Fig. 3.10). On the ventral surface, covering the striated muscle and adipose cells, is thick stratified columnar epithelium that contains a high density of taste buds (Fig. 3.10). Posterior to the palatal organ and opposing the pharyngeal teeth is a chewing pad. The subepithelium of the chewing pad is continuous with the subepithelium of the palatal organ but is thinner. The epithelium of the chewing pad is heavily keratinized stratified cuboidal epithelium that lacks taste buds (Fig. 3.11). The palatal organ and chewing pad are present in the smallest specimens sectioned and their cellular composition does not change much through ontogeny except that adipose becomes more prevalent in larger specimens. The histology of these two organs does not differ

significantly except that adipose tissue appears to be more abundant in *I. cyprinellus* than in the other species.

Statistical Tests

The slopes of the linear regressions of number of number of gill rakers over body length were not significantly different among the 5 species examined [Pr(>F) = 0.673953] but the intercepts of those regressions were significantly different [Pr(>F) = 0.000556] indicating that gill rakers accumulate at similar rates among these species but gill rakers begin forming at different times in each species (Table 3.2, Fig 3.12). For *I. cyprinellus*, a linear model was the best fit to the data but quadratic models were better for the other species. These quadratic models indicate some slowing in the rate of accumulation in these four species with *C. commersonii* showing the least reduction in accumulation of gill rakers.

The slopes of the linear regressions of branchial arch length over body length were significantly different among species [Pr(>F) = 0.0233] and so were the intercepts [Pr(>F) = 9.15e-16] (Table 3.3, Fig 3.13). This significant difference in slopes indicates that the branchial arches grow at different rates among the five species examined. The slope was greatest for *M. anisurum* (0.1976) followed by *I. cyprinellus* (0.1859), *C. commersonii* (0.1729), *M. erythrurum* (0.1677), and *H. nigricans* (0.1629). Quadratic models were not significantly better than linear models (Table 3.3).

The slopes of the linear regressions of gill raker density over body length were not significantly different from zero for any of the 5 species examined (Table 3.4) but there seems to be a trend in *H. nigricans*, *M. anisurum*, and *M. erythrurum* for raker density to

increase at first then slowly decrease (Fig. 3.14). The maximum raker density occurs at a body length of 12.35 mm for *H. nigricans*, 13.20 mm for *M. anisurum*, and 14.05 mm for *M. erythrurum* which is also very close to the body sizes in these species where the transformation to a subterminal mouth orientation occurs.

The slopes of the linear regressions of number of pharyngeal teeth over body size were significantly different among species [Pr(>F) = 1.26e-05] as were the intercepts of the regressions (2.25e-08) indicating that these 5 species accumulate teeth at different rates and start forming teeth at different sizes (Fig. 3.15). Linear models were better than quadratic models for *I. cyprinellus* and *C. commersonii* (Table 3.5) and the slope for *I. cyprinellus* (0.9273) was greater than the slope for *C. commersonii* (0.8537). Quadratic models were better than linear models for the other 3 species (Table 3.5) and the models show that teeth accumulate more quickly at smaller body sizes in these species than they accumulate later in ontogeny.

Discussion

Changes in the timing of appearance and development of trophic characters account for observed differences in trophic morphology of adult catostomids. These changes impact gill raker number and density, tooth number, and the transformation of the mouth from a terminal to subterminal position and therefore have a significant impact on feeding performance and adult ecology (Alexander 1967; Iwai 1964; Nicolsky 1963; Yasuda 1960). The results of this study document a consensus of the sequence of development among species, with just a few exceptions. More importantly, the results

document examples of heterochrony in the development of the paired elements of the pharyngeal arches and associated structures.

This study is not the first to document the sequence of ossification and chondrification in the pharyngeal arches and associated structures of cypriniform fishes but it is the first to tackle multiple species at the same time and only the second study of any catostomid species. The first study of a catostomid investigated *Catostomus commersonii* (Engeman *et al*., 2009). All other similar studies of cypriniforms looked at species of Cyprinidae. These include studies of the zebrafish, *Danio rerio*, (Cubbage and Mabee, 1996) which is commonly used as a model organism in developmental biology, *Barbus barbus* (Vandewalle *et al*., 1992), and most recently, *Puntius semifasciolatus* (Block and Mabee, 2012). By comparing the sequence of ossification in catostomid species to these outgroup taxa, it is possible to discover examples of heterochrony in the pharyngeal arches and associated structures.

The first example of heterochrony in the pharyngeal arches of catostomid fishes involves the timing of the ossification of the premaxilla relative to the anterior ceratohyal. Premaxilla development is very important in catostomid development because the elongation of the premaxilla drives the transformation from a terminal mouth orientation to a subterminal orientation. The premaxilla ossifies before the anterior ceratohyal in the cyprinid *P. semifasciolatus* (Block and Mabee, 2012) and two catostomids; *C. commersonii* from Engeman *et al.* (2009) and *I. cyprinellus* from this study but the premaxilla ossifies after the anterior ceratohyal in the cyprinid *D. rerio* (Cubbage and Mabee, 1996) and the catostomid *C. commersonii*. In the other species examined to date;

the cyprinid *B. barbus* (Vandewalle *et al*., 1992) and the catostomids *H. nigricans, M. anisurum,* and *M. erythrurum* the premaxilla appears to ossifies at the same time as the anterior ceratohyal. It should be noted that it can be very difficult to differentiate between simultaneous ossification and ossifications that occur in very quick succession without very large sample sizes so reports of simultaneous ossification of two structures should not be taken as evidence disproving that one structure ossifies before another unless the study investigated a large number of individuals from genetically diverse populations. Species with subterminal mouths have longer premaxilla than species with terminal mouths and this difference in premaxilla size is either the result of heterochrony caused by an earlier onset time (pre-displacement), a later offset time (hypermorphosis), or an increase in rate of development (acceleration). Given the results of these studies, there is no evidence for pre-displacement in catostomids. Hypermorphosis seems unlikely because the premaxilla forms in approximately the same amount of time in all catostomid species examined. Although there isn't comparable data from cyprinids, the difference in premaxilla length is likely due to an increase in the rate of change where an ancestor of all extant catostomids accelerated the development of the premaxilla and *I. cyprinellus* reverted back to the slower ancestral condition.

The timing of the ossification of the dorsal hypohyal and the ventral hypohyal is different among cypriniforms. The ventral hypohyal ossifies before the dorsal hypohyal in the cyprinids *B. barbus* (Vandewalle *et al*., 1992), *D. rerio* (Cubbage and Mabee, 1996), and *P. semifasciolatus* (Block and Mabee, 2012) and the catostomids *C. commersonii* (Engeman *et al.*, 2009; this study) and *I. cyprinellus*. The dorsal hypohyal

and ventral hypohyal appear to ossify at the same time in *H. nigricans*, *M. anisurum*, and *M. erythrurum*. The ventral hypohyal ossifies at the same time as the anterior hypohyal in all species, including *H. nigricans*, *M. anisurum*, and *M. erythrurum*, except in *P. semifasciolatus* where it ossifies right after the anterior hypohyal. *H. nigricans*, *M. anisurum*, and *M. erythrurum* are more closely related to one another than any is to any other species examined (Chapter 2) so the simplest explanation for this potential heterochrony is that there was pre-displacement of the dorsal hypohyal in the lineage leading to these species.

The relative timing of ossification of pharyngobranchials 2 and 3 varies among species. Pharyngobranchial 3 ossifies before pharyngobranchials 2 in the cyprinids *D. rerio* (Cubbage and Mabee, 1996), and *P. semifasciolatus* (Block and Mabee, 2012) and in the catostomids *C. commersonii* (Engeman *et al.*, 2009), *H. nigricans*, and *M. anisurum*. Pharyngobranchials 2 and 3 ossify at the same time *I. cyprinellus*, *M. erythrurum*, and *C. commersonii* from this study. This apparent difference in ossification rate could indicate pre-displacement of pharyngobranchial 2 but is more likely an artifact of sampling for several reasons. The pharyngobranchials are small bones that ossify in quick succession and it can be difficult to differentiate between pharyngobranchial 3 ossifying first or at the same time as pharyngobranchial 2. *Ictiobus cyprinellus*, *M. erythrurum*, and *C. commersonii* are not very closely related and belong to three different tribes of Catostomidae (Chapter 2). Pharyngobranchial 2 and 3 have the same function so it seems unlikely for there to be selection in those three species for a heterochronic shift. That doesn't mean there hasn't been a shift in onset time due to stochastic reasons like

genetic drift but it makes it less likely especially considering it would have to have occurred at least three independent times within Catostomidae.

The angulo-articular and retroarticular ossify simultaneously and ossify before the metapterygoid in the three cyprinids; *B. barbus* (Vandewalle *et al*., 1992), *D. rerio* (Cubbage and Mabee, 1996), and *P. semifasciolatus* (Block and Mabee, 2012). The sequence of ossification of these three bones is more variable in catostomids than in cyprinids. In *I. cyprinellus*, the angulo-articular ossifies before; the retroarticular and metapterygoid which ossify simultaneously. Engeman *et al*. (2009) showed that in *C. commersonii* the metapterygoid ossifies first followed by the angulo-articular and retroarticular which ossify simultaneously. This is the same pattern as seen in the three cyprinids. The results presented in this study show that in *C. commersonii* the retroarticular ossified first followed by the angulo-articular and metapterygoid which ossify simultaneously. In *H. nigricans*, *M. anisurum*, and *M. erythrurum*, all three bones appear to ossify simultaneously.

Based on these patterns the sequence appears fixed in Cyprinidae but is highly variable within Catostomidae. This heterochrony may be the result of multiple pre-displacement and post-displacement events within the evolutionary history of Catostomidae but more species need to be sampled to determine the evolutionary history of these processes. The sequence discovered by Engeman *et al*. (2009) in *C. commersonii* is different from the results presented here suggesting that heterochrony may exist within species. Further work needs to be done to quantify this intraspecific heterochrony and to determine whether it is caused by genetic differences or environmental factors.

In two cyprinids, *B. barbus* (Vandewalle *et al*., 1992) and *P. semifasciolatus* (Block and Mabee, 2012), and a single catostomid, *C. commersonii* (Engeman *et al.*, 2009), the dorsal hypohyal ossifies before the symplectic but in one cyprinid, *D. rerio* (Cubbage and Mabee, 1996) and two catostomids, *I. cyprinellus* and *C. commersonii*, the reverse is true. This likely represents heterochrony due to a shift in onset time of one of these bones. It is interesting that two different studies of *C. commersonii* found a different sequence of ossification and, like the heterochrony in the angulo-articular, retroarticular, and metapterygoid, suggests that intraspecific heterochrony may be more common than previously thought and needs to be investigated more thoroughly. The dorsal hypohyal and symplectic appear to ossify simultaneously in *H. nigricans*, *M. anisurum*, and *M. erythrurum* and because they are closely related, may indicate heterochrony by pre-displacement of the symplectic but more sampling is required to verify this.

The dentary ossifies before the entopterygoid in the cyprinids *B. barbus* (Vandewalle *et al*., 1992) and *P. semifasciolatus* (Block and Mabee, 2012) and in the catostomid *M. anisurum* but Engeman *et al*. (2009) found the reverse in *C. commersonii*. In *D. rerio* (Cubbage and Mabee, 1996) and the four other catostomids studied here, the dentary and entopterygoid seem to ossify at the same time. This may represent pre-displacement in these species with an even larger shift in onset time in *C. commersonii*.

Comparisons of gill raker development and pharyngeal teeth development among species are relatively easy as these structures can be counted through ontogeny to study their rates of development. It is possible study heterochrony by timing modifications by investigating when these structures first appear and it is easy to study heterochrony by

rate modification by studying the rate in which they accumulate. Heterochrony due to a change in rate is seen as a difference in the slopes of regression lines of an ancestor and decedent (Webster and Zelditch, 2005). Unfortunately, there is no data on rate of accumulation of gill rakers and pharyngeal teeth in any suitable outgroup of Catostomidae so it is not possible to infer the direction of change but it is still possible to discover heterochrony by comparing developmental rates among related species. If no heterochrony has taken place then all species will have the same rate of development but if one or more species differ then that is evidence that heterochrony has taken place.

The analysis of gill raker accumulation shows that gill rakers accumulate at similar rates among the five catostomid species studied but gill rakers first appear at significantly different times among species (Fig. 3.12). Therefore, there is no evidence of heterochrony due to rate modification but there is evidence of heterochrony due to timing modification. Specifically, the onset time of gill raker initiation has shifted multiple times in Catostomidae. This suggests that onset time is a more important driver in determining gill raker number in adults than rate of accumulation is.

The rate of growth of the branchial arch through ontogeny was significantly different among species as was the length of the arch when it first forms. This suggests that there is heterochrony due to timing modification and rate modification in catostomid fishes. This is not unique as it is not uncommon for heterochrony to be caused by multiple shits in timing and rate (Klingenberg & Spence, 1993).

Gill raker density in adult catostomids has been shown to vary among species and is important in feeding (Chapter 2) but there is no clear pattern in gill raker density through

time in any of the five species examined even though there were significant patterns in number of gill rakers through time and arch length. It appears that gill rakers begin to form at different times in different sucker species but accumulate at similar rates while the branchial arches are growing at constant but different rates among species. These interact in such a way that there is no simple pattern in the rate in which gill raker density changes through time. It should be noted that in three of the five species (*H. nigricans*, *M. anisurum*, and *M. erythrurum*), the three most closely related species, there was a peak in gill raker density at the same time in development when the mouth was transitioning to a subterminal orientation.

Like gill rakers, pharyngeal teeth appear at different times in sucker species but unlike gill rakers, teeth are added at different rates among species. This is evidence that there is heterochrony in pharyngeal teeth development in catostomid fishes due to both timing modification and rate modification. *Ictiobus cyprinellus* and *C. commersonii* accumulate teeth at linear rates while the other three species exhibit a decrease in the rate of accumulation. Quadratic models where rate of accumulation slowed through time were better predictors than linear models in *H. nigricans*, *M. anisurum*, and *M. erythrurum*. Because these three species share a more recent common ancestor than they do with *I. cyprinellus* or *C. commersonii* (Doosey *et al*., 2010), this decrease in rate of tooth accumulation likely evolved in the lineage leading to these taxa.

This investigation of the development of the paired bones and cartilages of the pharyngeal arches and associated structures shows that although the sequence of ossification is largely conserved across Cypriniformes, there are a few differences among

(and within) species. These differences provide evidence of heterochrony in catostomid fishes. The analyses of gill raker and pharyngeal teeth development also provide evidence of heterochrony due to timing modifications and rate modifications in catostomid fishes.

Conclusion

Morphological diversity is both shaped by and shapes past evolutionary history, function, and ontogeny. The results presented here illustrate how these three factors have shaped morphological diversity in catostomid fishes. First, I found evidence that Catostomidae is sister to all other cypriniform families and is older than its fossil record indicates. These results affect interpretations of morphological, functional, and ontological character evolution within Cypriniformes. Second, I showed that an important function of gill rakers, diet, is not dependent on a single gill raker characteristic but is dependent on a complex interaction between groups of characters and this many-to-one mapping of morphology to function may be an evolutionary consequence of gill rakers having multiple functions in catostomid fishes. Third, I discovered that differences among species in adult morphology of gill rakers and other pharyngeal elements are due to heterochrony from both timing modifications and rate modifications. Therefore, diversity in catostomid gill raker morphology is a result of changes in developmental patterns (ontogeny) and diet (function) through evolutionary time.

Table 1.1. GenBank accession numbers for all sequences used in reconstructing the Cypriniformes phylogeny.

Family	Species	EGR1	EGR2b	EGR3	IRBP	RAG1	Rh
Outgroups							
Alestiidae	*Phenacogrammus interruptus*	FJ650423	FJ650439	FJ650455	FJ197123	FJ197124	FJ197073
Bagridae	*Pseudobagrus tokiensis*	FJ650422	FJ650438	FJ650454	---	FJ650410	FJ197075
Callichthyidae	*Corydoras rabauti*	---	---	---	---	FJ197125	---
Chanidae	*Chanos chanos*	---	---	---	---	AY430207	---
Characidae	*Chalceus macrolepidotus*	EU409697	EU409729	EU409761	EU409665	EU409607	EU409633
Clariidae	*Clarias batrachus*	---	---	---	---	DQ492521	---
Gonorynchidae	*Gonorynchus greyi*	EU409696	EU409728	EU409760	EU409664	EU409606	EU409632
Cypriniformes							
Cyprinoidea	*Acheilognathus tabira tabira*	EU409708	EU409740	EU409772	EU409676	EU409617	EU409644
	Acrossocheilus paradoxus	FJ531255	FJ531284	FJ531313	FJ531362	FJ531245	FJ531342
	Alburnus alburnus	---		---	FJ197094		---
	Aphyocypris chinensis	FJ531256	FJ531285	FJ531314	FJ197117	EU292692	FJ197066
	Aspidoparia morar	FJ531257	FJ531286	FJ531315	FJ531363	EU711105	FJ531343
	Barboides gracilis	---		---			---
	Barbonymus gonionotus	FJ531258	FJ531287	FJ531316	FJ531364	FJ531246	FJ531344
	Barbus barbus	---		---	FJ197099	EU711147	---
	Barbus bynni	---		---			---
	Barbus callipterus	FJ531259	FJ531288	FJ531317	FJ531365	FJ531247	FJ531345
	Barilius bakeri	---		---		HM224076	---
	Barilius bendelisis	FJ531260	FJ531289	FJ531318	FJ531366	EU292693	FJ531346
	Biwia zezera	EU409718	EU409750	EU409782	EU409686	EU409626	EU409654
	Blicca bjoerkna	---		---		EU711108	---
	Boraras merah	GQ365229	GQ365238	GQ365247	GQ365256	EF452838	GQ365220
	Carassius gibelio	---	GQ911676	---	GQ911667	GQ911678	---
	Chanodichthys flavipinnis	---		---			---
	Cirrhinus microlepis	---	GQ913555	---	GQ913610	GQ913451	---
	Crossocheilus reticulatus	---	GQ913558	---	GQ913613	GQ913454	---
	Cyclocheilichthys enoplus	---		---			---
	Cyprinus carpio	---		---	FJ197101		---
	Danio albolineatus	EU409725	EU409757	EU409789	EU409693	EU292696	EU409661
	Danio dangila	EU409724	EU409756	EU409788	EU409692	EU292697	EU409660
	Danio margaritatus	GQ365232	GQ365241	GQ365250	GQ365259	EU292695	GQ365223
	Danio rerio	NM 131248	NM_130997	scaffold2320.1	X85957	U71093	L11014
	Danionella mirifica	FJ531261	FJ531290	FJ531319	FJ531367	EU292700	FJ531347
	Devario regina	FJ531262	FJ531291	FJ531320	FJ531368	EU292701	FJ531348
	Epalzeorhynchos kalopterus	---	GQ913562	---	GQ913617	GQ913458	---
	Esomus longimanus	FJ531263	FJ531292	FJ531321	FJ531369	FJ531248	FJ531349
	Garra fasciacauda	---	GQ911673	---	GQ911661	GQ911683	---
	Garra makiensis	---	GQ911675	---	GQ911663	GQ911677	---
	Garra quadrimaculata	---		---			---
	Garra spilota	EU409713	EU409745	EU409777	EU409681	EU409621	EU409649
	Gila orcuttii	---		---			---
	Gobio gobio	FJ531264	FJ531293	FJ531322	FJ197107	EU292689	FJ197056
	Gymnocypris przewalskii	FJ531265	FJ531294	FJ531323	FJ197102	EU711149	FJ197051
	Hampala macrolepidota	EU409715	EU409747	EU409779	EU409683	EU409623	EU409651
	Hemibarbus barbus	FJ531266	FJ531295	FJ531324	FJ197108	EU711154	FJ197057
	Horadandia atukorali	FJ531267	FJ531296	FJ531325	FJ531370	EU292703	FJ531350
	Hypsibarbus malcolmi	---		---			---
	Ischikauia steenackeri	EU409712	EU409744	EU409776	EU409680	EU292687	EU409648
	Labeo boga	---	GQ913577	---	GQ913631	GQ913471	---
	Labeo chrysophekadion	EU409714	EU409746	EU409778	EU409682	EU409622	EU409650
	Labeo cylindricus	---		---			---
	Labeo weeksii	---	GQ911670	---	GQ911665	GQ911680	---
	Laubuca dadiburjori	GQ365230	GQ365239	GQ365248	GQ365257	EU292694	GQ365221
	Leptobarbus hoevenii	FJ531268	FJ531297	FJ531326	FJ531371	FJ531249	FJ531351
	Luciosoma setigerum	FJ531269	FJ531298	FJ531327	FJ531372	EU292704	FJ531352
	Macrochirichthys macrochirus	EU409723	EU409755	EU409787	EU409691	EU409630	EU409659
	Megalobrama amblycephala	EU409711	EU409743	EU409775	EU409679	EU409620	EU409647

	Mekongina erythrospila	---	GQ911674	---	GQ911668	GQ911684	---
	Microdevario kubotai	FJ531270	FJ531299	FJ531328	FJ531373	EU292707	FJ531353
	Microdevario nana	GQ365233	GQ365242	GQ365251	GQ365260	EU292705	GQ365224
	Microrasbora erythromicron	GQ365231	GQ365240	GQ365249	GQ365258	EU292698	GQ365222
	Microrasbora rubescens	GQ365234	GQ365243	GQ365252	GQ365261	EU292706	GQ365225
	Mystacoleucus marginatus	---		---			---
	Notemigonus crysoleucas	---	FJ197113	---			---
	Notropis baileyi	EU409721	EU409753	EU409785	EU409689	EU292691	EU409657
	Opsariichthys uncirostris	FJ531271	FJ531300	FJ531329	FJ197119	FJ197126	FJ197068
	Oreichthys cosuatis	---	GQ913544	---	GQ913600	GQ913441	---
	Osteochilus microcephalus	---	GQ913589	---	GQ913642	GQ913482	---
	Paedocypris sp. 1	GQ365235	GQ365244	GQ365253	GQ365262	GQ365218	GQ365226
	Paedocypris sp. 2	GQ365236	GQ365245	GQ365254	GQ365263	GQ365219	GQ365227
	Parachela williaminae	---		---		HM224063	---
	Paralaubuca typus	EU409710	EU409742	EU409774	EU409678	EU409619	EU409646
	Pelecus cultratus	FJ531272	FJ531301	FJ531330	FJ197095	EU711144	FJ197045
	Phoxinus phoxinus	---		---	FJ197116	EU711161	---
	Pimephales notatus	---		---			---
	Pseudobarbus burchelli	---		---			---
	Pseudorasbora pumila	---		---	FJ197109	EU711155	---
	Puntius cumingii	---		---			---
	Puntius hexazona	---		---			---
	Puntius titteya	FJ531275	FJ531304	FJ531333	FJ531375	EU292685	FJ531356
	Raiamas senegalensis	---		---		HM224093	---
	Rasbora aurotaenia	---		---		HM224096	---
	Rasbora bankanensis	FJ531276	FJ531305	FJ531334	FJ531376	EU292709	FJ531357
	Rasbora rasbora	---		---		HM224121	---
	Rasbora steineri	EU409726	EU409758	EU409790	EU409694	EU409631	EU409662
	Rasbora taeniata	---		---		EU292710	---
	Rasborinus lineatus	---		---		HM224067	---
	Rhodeus atremius	---		---		EU711125	---
	Rhodeus ocellatus kurumeus	FJ531277	FJ531306	FJ531335	FJ197093	EU711142	FJ197043
	Rhynchocypris percnurus	EU409719	EU409751	EU409783	EU409687	EU409627	EU409655
	Romanogobio ciscaucasicus	EU409716	EU409748	EU409780	EU409684	EU409624	EU409652
	Sarcocheilichthys biwaensis	---		---			---
	Sarcocheilichthys parvus	EU409717	EU409749	EU409781	EU409685	EU409625	EU409653
	Scardinius erythrophthalmus	EU409720	EU409752	EU409784	EU409688	EU409628	EU409656
	Schizothorax meridionalis	---		---			---
	Semotilus atromaculatus	EU409722	EU409754	EU409786	EU409690	EU409629	EU409658
	Sikukia gudgeri	---		---			---
	Squalidus chankaensis	FJ531278	FJ531307	FJ531336	FJ531377	FJ531252	FJ531358
	Squalidus japonicus	---		---			---
	Squaliobarbus curriculus	---		---		HM224069	---
	Sundadanio axelrodi	GQ365237	GQ365246	GQ365255	GQ365264	EU292711	GQ365228
	Tanakia himantegus	EU409709	EU409741	EU409773	EU409677	EU409618	EU409645
	Tanichthys albonubes	FJ531279	FJ531308	FJ531337	FJ531378	FJ531253	FJ531359
	Thynnichthys thynnoides	---		---			---
	Tinca tinca	FJ531280	FJ531309	FJ531338	FJ197121	EU711162	FJ197070
	Tribolodon nakamurai	---		---	FJ197114	EU711159	---
	Trigonostigma heteromorpha	FJ531281	FJ531310	FJ531339	FJ531379	EU292712	FJ531360
	Varicorhinus axelrodi	---		---			---
	Yaoshanicus arcus	FJ531282	FJ531311	FJ531340	FJ531380	FJ531254	FJ531361
	Yasuhikotakia sidthimunki	---		---			---
	Zacco sieboldii	FJ531283	FJ531312	FJ531341	FJ197120	EU292713	FJ197069
Psilorhynchidae	*Psilorhynchus homaloptera*	FJ531273	FJ531302	FJ531331	---	FJ531250	FJ531354
	Psilorhynchus sucatio	FJ531274	FJ531303	FJ531332	FJ531374	FJ531251	FJ531355
Cobitoidea							
Balitoridae	*Gastromyzon cranbrooki*	---	---	---			---
	Gastromyzon lepidogaster	---	---	---			---
	Homaloptera leonardi	---	---	---	FJ197076	EU711130	---
	Homaloptera parclitella	EU409700	EU409732	EU409764	EU409668	EU409610	EU409636
	Pseudogastromyzon sp.	---		---			---
	Sewellia lineolata	EU409699	EU409731	EU409763	EU409667	EU409609	EU409635
Botiidae	*Botia dario*	EU409705	EU409737	EU409769	EU409673	EU409614	EU409641
	Botia helodes	---	---	---	EU409673	EU409614	---
	Botia lohachata	---		---			---
	Botia robusta	---	---	---	---		---
	Botia striata	---		---		EU711109	---

	Chromobotia macracanthus	---		---	FJ197086	EU711137	---
	Leptobotia pellegrini	EU409704	EU409736	EU409768	EU409672	EU292683	EU409640
	Leptobotia sp.	---		---			---
	Syncrossus beauforti	FJ650424	FJ650440	FJ650456	FJ650482	FJ650411	FJ650470
	Yasuhikotakia morleti	FJ650425	FJ650441	FJ650457	FJ650483	FJ650412	FJ650471
Catostomidae	*Catostomus commersonii*	EU409702	EU409734	EU409766	EU409670	EU409612	EU409638
	Cycleptus elongatus	EU409703	EU409735	EU409767	EU409671	EU409613	EU409639
	Erimyzon oblongus	---		---		EU711117	---
Cobitidae	*Acantopsis* sp.	FJ650426	FJ650442	FJ650458	FJ650484	FJ650413	FJ650472
	Canthophrys gongota	FJ650428	FJ650444	FJ650460	FJ650485	FJ650414	FJ650473
	Cobitis shikokuensis	---		---			---
	Cobitis striata	---		---			---
	Cobitis takatsuensis	EU409707	EU409739	EU409771	EU409675	EU409616	EU409643
	Kichulchoia multifasciata	EU409706	EU409738	EU409770	EU409674	EU409615	EU409642
	Lepidocephalichthys guntea	---		---	---		---
	Pangio oblonga	FJ650427	FJ650443	FJ650459	FJ197091	EU711141	FJ197041
Gyrinocheilidae	*Gyrinocheilus aymonieri*	EU409727	EU409759	EU409791	FJ197122	EU292682	FJ197071
	Gyrinocheilus pennocki	FJ650429	FJ650445	FJ650461	FJ650486	FJ650415	FJ650474
Nemacheilidae	*Acanthocobitis* sp.	FJ650430	FJ650446	FJ650462	FJ650487	FJ650416	FJ650475
	Barbatula barbatula	FJ650431	FJ650447	FJ650463	FJ650488	EU711107	FJ650476
	Barbatula toni	---		---	FJ197079	EU711133	---
	Lefua costata	EU409698	EU409730	EU409762	EU409666	EU409608	EU409634
	Lefua echigonia	---		---	FJ197077		---
	Lefua nikkonis	---		---			---
	Micronemacheilus pulcher	EU409701	EU409733	EU409765	EU409669	EU409611	EU409637
	Oreonectes platycephalus	FJ650433	FJ650449	FJ650465	FJ650490	FJ650418	FJ650478
	Schistura savona	FJ650434	FJ650450	FJ650466	FJ650491	FJ650419	FJ650479
	Triplophysa gundriseri	FJ650435	FJ650451	FJ650467	FJ650492	FJ650420	FJ650480
Vaillantellidae	*Vaillantella maassi*	FJ650437	FJ650453	FJ650469	FJ197080	EU711132	FJ197031

Table 1.2. Results of Chi-square goodness-of-fit test for base compositional heterogeneity and base composition for each codon position of each gene for the two data sets investigated. Loci with significant heterogeneity are in bold.

		Base Proportions					
	Locus	A	C	G	T	G+C	*p*
Full Dataset	EGR1-1	0.2936	0.3073	0.1794	0.2197	0.4867	1.000
	EGR1-2	0.2574	0.3602	0.1950	0.1874	0.5552	1.000
	EGR1-3	0.1071	0.4934	0.2480	0.1516	0.7414	1.000
	EGR2b-1	0.2262	0.3661	0.2381	0.1695	0.6042	1.000
	EGR2b-2	0.1941	0.3929	0.2642	0.1488	0.6571	1.000
	EGR2b-3	0.2256	0.3855	0.1811	0.2078	0.5666	1.000
	EGR3-1	0.2718	0.3063	0.2291	0.1928	0.5355	1.000
	EGR3-2	0.2835	0.2911	0.2193	0.2060	0.5104	1.000
	EGR3-3	**0.1495**	**0.4492**	**0.2507**	**0.1507**	**0.6999**	**0.002**
	IRBP-1	0.2866	0.2635	0.1570	0.2928	0.4206	1.000
	IRBP-2	0.2092	0.2980	0.2228	0.2700	0.5208	1.000
	IRBP-3	0.3180	0.1756	0.3521	0.1543	0.5277	1.000
	RAG1-1	0.2293	0.2622	0.2628	0.2457	0.5250	1.000
	RAG1-2	0.2547	0.2351	0.3045	0.2057	0.5396	1.000
	RAG1-3	0.2890	0.2187	0.2290	0.2633	0.4477	1.000
	RH-1	0.2452	0.1934	0.3112	0.2502	0.5046	1.000
	RH-2	0.2021	0.2313	0.1833	0.3833	0.4146	1.000
	RH-3	**0.0707**	**0.5216**	**0.2537**	**0.1540**	**0.7753**	**0.000**
With Branch Length Outliers Removed	EGR1-1	0.2936	0.3076	0.1791	0.2198	0.4867	1.000
	EGR1-2	0.2572	0.3605	0.1953	0.1871	0.5557	1.000
	EGR1-3	0.1070	0.4937	0.2475	0.1518	0.7412	1.000
	EGR2b-1	0.2261	0.3662	0.2383	0.1694	0.6045	1.000
	EGR2b-2	0.1941	0.3935	0.2638	0.1487	0.6572	1.000
	EGR2b-3	0.2253	0.3856	0.1813	0.2078	0.5670	1.000
	EGR3-1	0.2725	0.3062	0.2286	0.1927	0.5348	1.000
	EGR3-2	0.2838	0.2909	0.2192	0.2062	0.5101	1.000
	EGR3-3	0.1526	0.4433	0.2505	0.1537	0.6938	1.000
	IRBP-1	0.2864	0.2634	0.1573	0.2930	0.4207	1.000
	IRBP-2	0.2086	0.2991	0.2228	0.2696	0.5219	1.000
	IRBP-3	0.3175	0.1759	0.3524	0.1542	0.5283	1.000
	RAG1-1	0.2292	0.2616	0.2626	0.2466	0.5242	1.000
	RAG1-2	0.2547	0.2351	0.3045	0.2058	0.5395	1.000
	RAG1-3	0.2889	0.2187	0.2290	0.2633	0.4478	1.000
	RH-1	0.2446	0.1933	0.3115	0.2506	0.5049	1.000
	RH-2	0.2023	0.2317	0.1832	0.3828	0.4148	1.000
	RH-3	**0.0715**	**0.5185**	**0.2517**	**0.1584**	**0.7702**	**0.000**

Table 1.3. Divergence time estimates in millions of years from present using the Marshall Scaling Method and a Bayesian method. The Marshall minimum age is a hard minimum based on the age of the fossil of the calibration lineage, found to be *Protothymallus* in this analysis, and the maximum age is the upper bound of the 95% confidence interval. The Bayesian lower and upper HPD ages represent the end points of the 95% posterior probability for the age of each node.

			Marshall Method			Bayesian Method		
Taxon	Node	Fossil	S_i	Min. Age	Max. Age	Lower HPD	Upper HPD	Median
	1	130.0	130.00	199.8	290.5	131.5	180.4	149.2
Cypriniformes				175.4	255.1	117.3	173.8	141.2
Catostomidae	2	61.7	137.90	89.4	130.0	71.8	104.9	87.2
Cyprinoidea	3	48.6	115.28	84.2	122.5	67.1	97.6	80.9
Cyprininae/Leuciscinae				62.1	90.3	51.5	73.3	61.8
Psilorhynchus				56.4	82.0	42.8	65.4	53.7
Protothymallus	4	30.2	**199.79**	30.2	43.9	30.4	34.8	32.0
Ecocarpia	5	23.0	175.30	26.2	38.1	23.5	31.5	26.7
Cyprinus	6	13.6	116.67	23.3	33.9	14.7	29.3	21.5
Gyrinocheilidae				79.1	115.0	61.8	91.3	75.3
Botiidae				59.6	86.7	50.9	74.8	61.3
Vaillentellidae				55.4	80.5	46.1	68.4	56.3
Cobitidae	7	13.6	54.10	50.2	73.0	40.0	60.4	49.9
Balitoridae				46.9	68.2	36.7	55.8	45.5
Nemacheilidae	8	11.6	49.42	46.9	68.2	36.7	55.8	45.5

Table 1.4. Regression analysis using a general linear model of the phylogenetic independent contrasts of path length and maximum standard length for fish species from a number of recently published maximum likelihood-based phylogenetic studies. Significant relationships after Bonferroni correction, if applicable, are indicated in bold.

Study	Taxon	Species Included	Model Fit (R^2)	Significance (p)
This study	Cypriniformes	135	0.4757	**<0.001**
	Cyprinoidea	101	0.5358	**<0.001**
Betancur-R et al., 2013a	Actinopterygii	1350	0.0360	**<0.001**
	Teleostei	1319	0.0365	**<0.001**
	Euteleosteomorpha	1210	0.0310	**<0.001**
	Neoteleostei	1169	0.0299	**<0.001**
	Acanthomorphata	1122	0.0327	**<0.001**
	Percomorphaceae	1040	0.0372	**<0.001**
	Perciformes	670	0.0508	**<0.001**
	Ostariophysi	89	0.1609	**<0.001**
	Characiformes	26	0.3676	**<0.001**
	Siluriformes	32	0.0550	0.196
Betancur-R et al., 2013b	Pleuronectiformes	72	0.0468	0.068
Near et al., 2013	Acanthomorpha	528	0.0326	**<0.001**
Friedman et al., 2013	Cichlidae	84	0.0597	**0.025**
Hundt et al., 2014	Blenniidae	98	0.0112	0.299
Unmack et al., 2013	Melanotaeniidae	61	0.0002	0.971
Near et al., 2011	Etheostomatinae	159	0.0433	**<0.001**
Oliveira et al., 2011	Characiformes	193	0.0477	**<0.001**
	Characidae	117	0.0175	0.156

Table 2.1. Diet scores for twenty-one species of freshwater sucker (Catostomidae). Scores for each of the nine prey categories range from 0 to 3 where a score of 0 means the prey item is never found in the diet of that species, 1 means the prey is rare (making up 1-10% of its total diet), 2 means the prey is common (11-50%), and 3 means the prey is abundant (51-100%). Small-sized prey are generally less than 0.2 mm, medium-sized prey are generally 0.2-5 mm, large-sized prey are generally 5-12 mm, and extra-large prey are greater than 12 mm. The discrete diet score is based on which size class of prey was most common in the diet where 1 represents small-size, 2 represents medium-size, 3 represents large-size, and 4 represents extra-large-size. The continuous diet score was calculated for each species using the scores from each prey category and a weighted average equation. Whereas the discrete score only accounts for the prey size class most common in the diet, the continuous score also considers the total range of prey sizes consumed and their relative abundances.

	Small		*Medium*		*Large*		*Extra-large*		Diet Scores		
Species	**detritus**	**algae**	**copepods**	**cladocerans**	**insect larvae**	**crustaceans**	**mollusks**	**fish fry**	**Discrete**	**Continuous**	**Primary Reference**
Carpiodes carpio	3	3	1	0	2	1	0	0	1	1.700	Becker (1983)
Carpiodes cyprinus	3	2	0	0	1	0	1	0	1	1.714	Becker (1983)
Carpiodes velifer	3	3	2	0	2	0	0	0	1	1.600	Becker (1983)
Catostomus catostomus	0	1	2	2	3	3	1	0	3	2.583	Becker (1983)
Catostomus commersonii	0	2	0	0	2	1	2	1	3	2.875	Becker (1983)
Catostomus discolobus	2	3	0	0	1	0	0	0	1	1.333	Dezzerides and Bestgen (2002)
Catostomus latipinnis	3	1	0	2	2	0	0	0	1	1.750	Rees et al. (2005)
Erimyzon sucetta	0	3	2	2	2	2	0	0	2	2.091	Becker (1983)
Hypentelium nigricans	0	1	0	0	3	1	2	0	3	3.000	Becker (1983)
Hypentelium roanokense	1	1	0	0	3	0	0	0	3	2.200	Jenkins and Burkhead (1993)
Ictiobus bubalus	3	3	3	3	2	0	2	0	1	2.000	Becker (1983)
Ictiobus cyprinellus	0	1	3	3	1	1	1	0	2	2.300	Becker (1983)
Minytrema melanops	0	1	2	3	3	3	0	0	3	2.417	Becker (1983)
Moxostoma anisurum	0	2	0	0	3	1	0	1	3	2.571	Becker (1983)
Moxostoma carinatum	0	0	0	0	1	0	3	0	4	3.750	Becker (1983)
Moxostoma cervinum	1	1	0	0	3	0	0	0	3	2.200	Jenkins and Burkhead (1993)
Moxostoma duquesnei	0	0	2	2	3	0	0	0	2	2.429	Becker (1983)
Moxostoma erythrurum	0	3	1	0	3	0	3	0	3	2.600	Becker (1983)
Moxostoma macrolepidotum	0	2	3	2	3	3	1	1	3	2.533	Becker (1983)
Moxostoma valenciennesi	0	1	0	0	1	3	2	0	3	3.000	Becker (1983)
Thoburnia rhothoeca	3	3	0	0	1	0	0	0	1	1.286	Jenkins and Burkhead (1993)

Table 2.2. Accession numbers and standard lengths of specimens used in investigating gill raker morphology.

Species	Catalog No. (JFBM)	Length (cm)
Carpiodes carpio	21090-01	8.588
Carpiodes carpio	21090-02	8.519
Carpiodes carpio	21090-03	7.609
Carpiodes cyprinus	33250-01	9.115
Carpiodes cyprinus	33250-02	9.175
Carpiodes cyprinus	44851-01	10.382
Carpiodes velifer	43780-01	9.083
Carpiodes velifer	43789-01	7.669
Carpiodes velifer	45700-01	8.408
Catostomus catostomus	17720-01	11.512
Catostomus catostomus	17720-02	10.227
Catostomus catostomus	17720-03	8.958
Catostomus commersonii	30876-01	12.019
Catostomus commersonii	30876-02	10.706
Catostomus commersonii	30876-03	11.526
Catostomus commersonii	40691-01	8.322
Catostomus commersonii	40691-02	7.747
Catostomus commersonii	40691-03	7.767
Catostomus commersonii	40691-05	7.848
Catostomus discolobus	19236-01	10.907
Catostomus discolobus	19236-02	9.265
Catostomus discolobus	19236-03	8.712
Catostomus latipinnis	15091-01	9.769
Catostomus latipinnis	20937-01	10.057
Catostomus latipinnis	20937-02	9.485
Erimyzon sucetta	20050-01	9.705
Erimyzon sucetta	20050-02	9.872
Erimyzon sucetta	20050-03	9.952
Hypentelium nigricans	41899-01	11.190
Hypentelium nigricans	41899-02	11.056
Hypentelium nigricans	41899-03	11.867
Hypentelium roanokense	17115-01	10.073
Hypentelium roanokense	17115-02	8.684
Hypentelium roanokense	17281-01	9.216
Ictiobus bubalus	34780-01	10.356
Ictiobus bubalus	34780-02	8.821
Ictiobus bubalus	34780-03	9.836
Ictiobus cyprinellus	39411-01	7.567
Ictiobus cyprinellus	39703-01	9.526
Ictiobus cyprinellus	40325-01	7.977
Minytrema melanops	44838-01	10.122
Minytrema melanops	44838-02	10.129
Minytrema melanops	44838-03	10.858

Moxostoma anisurum	21601-01	12.250
Moxostoma anisurum	21601-02	11.627
Moxostoma anisurum	21601-03	12.682
Moxostoma carinatum	36454-01	11.632
Moxostoma carinatum	36454-02	10.581
Moxostoma carinatum	36454-03	11.000
Moxostoma cervinum	17070-01	9.636
Moxostoma cervinum	17070-02	11.389
Moxostoma cervinum	17070-03	12.462
Moxostoma duquesnei	43584-01	8.387
Moxostoma duquesnei	43584-02	8.262
Moxostoma duquesnei	43584-03	7.959
Moxostoma erythrurum	36018-01	9.881
Moxostoma erythrurum	36039-01	8.915
Moxostoma erythrurum	39076-01	9.532
Moxostoma macrolepidotum	42071-01	10.502
Moxostoma macrolepidotum	42071-02	9.382
Moxostoma macrolepidotum	42071-03	10.892
Moxostoma valenciennesi	34221-01	10.239
Moxostoma valenciennesi	34221-02	8.803
Moxostoma valenciennesi	44667-01	8.882
Thoburnia rhothoeca	17043-01	10.089
Thoburnia rhothoeca	17043-02	8.787
Thoburnia rhothoeca	17043-03	8.834

Table 3.1. Collection information for adult freshwater suckers used to create developmental series.

Species	Females	Males	Date	Body of Water	State	County
Catostomus commersonii	4	10	May 22, 2008	Mississippi River	MN	Beltrami
Hypentelium nigricans	2	4	May 19, 2011	Root River	MN	Olmstead
Ictiobus cyprinellus	1	3	May 8, 2008	Mississippi River	MN	Wabasha
Moxostoma anisurum	3	7	April 26, 2010	Mississippi River	MN	Ramsey
Moxostoma erythrurum	4	8	May 19, 2011	Root River	MN	Olmstead

Table 3.2. Models used to test for a significant relationship between number of gill rakers on branchial arch 2 and body length in larval freshwater suckers.

	Linear Model			Quadratic Model		
	p	R^2	Equation	Pr(>|t|)	R^2	Equation
Ictiobus cyprinellus	1.45E-05	0.9331	1.3278x-7.0933	0.09788	0.9524	$-0.04091x^2+2.67793x-16.62508$
Catostomus commersonii	1.27E-08	0.9332	1.23064x-7.73754	0.031403	0.9531	$-0.04612x^2+2.65008x-17.82840$
Hypentelium nigricans	1.57E-07	0.8181	1.1497x-8.3874	0.000942	0.9086	$-0.11483x^2+4.75442x-35.18894$
Moxostoma anisurum	1.01E-05	0.7715	1.2482x-9.1739	0.0414	0.8274	$-0.12687x^2+5.36671x-40.75012$
Moxostoma erythrurum	2.42E-06	0.8160	1.0662x-6.2585	0.000673	0.9267	$-0.10832x^2+4.46572x-31.10855$

Table 3.3. Models used to test for a significant relationship between length of branchial arch 2 and body length in larval freshwater suckers.

	Linear Model			Quadratic Model		
	p	R^2	Equation	Pr(>|t|)	R^2	Equation
Ictiobus cyprinellus	2.95E-07	0.9779	0.185913x-1.004604	0.255	0.9796	$0.002361x^2+0.107989x-0.45447$
Catostomus commersonii	2.68E-10	0.9648	0.172927x-1.397132	0.816	0.9618	$0.0005569x^2+0.1557904x-1.12753038$
Hypentelium nigricans	6.51E-14	0.9708	0.162857x-1.204154	0.35047	0.9706	$-0.001999x^2+0.225606x-1.670704$
Moxostoma anisurum	2.81E-12	0.9773	0.197575x-1.599145	0.2789	0.9778	$-0.003212x^2+0.301834x-2.398497$
Moxostoma erythrurum	2.46E-13	0.9844	0.167657x-1.166298	0.128124	0.9862	$-0.002443x^2+0.244328-1.726754$

Table 3.4. Models used to test for a significant relationship between density of gill rakers on branchial arch 2 and body length in larval freshwater suckers.

	Linear Model			Quadratic Model		
	p	R^2	Equation	Pr(>|t|)	R^2	Equation
Ictiobus cyprinellus	0.5724	-0.08835	0.1130x+5.4529	0.165	0.1042	$-0.05417x^2+1.90093x-7.17051$
Catostomus commersonii	0.2802	0.02101	-0.3003x+14.4250	0.496	-0.02182	$-0.04689x^2+1.14263x+4.16694$
Hypentelium nigricans	0.3966	-0.0144	0.1421x+4.9044	0.0158	0.2755	$-0.11339x^2+3.70162x-21.56112$
Moxostoma anisurum	0.6491	-0.05925	0.09132x+5.41575	0.0211	0.2763	$-0.15288x^2+5.05400x-32.63306$
Moxostoma erythrurum	0.8258	-0.07276	0.03406x+6.58015	0.0645	0.1361	$-0.07796x^2+2.48076x-11.30488$

Table 3.5. Models used to test for a significant relationship between number of pharyngeal teeth and body length in larval freshwater suckers.

	Linear Model			Quadratic Model		
	p	R^2	Equation	Pr(>|t|)	R^2	Equation
Ictiobus cyprinellus	1.1200E-11	0.9906	0.92733x-2.84467	0.2052	0.9914	$0.004779x^2+0.792729x-2.092513$
Catostomus commersonii	1.3880E-07	0.8408	0.85369x-3.69629	0.646	0.832	$-0.01073x^2+1.18627x-6.10348$
Hypentelium nigricans	8.3490E-09	0.8402	1.4673x-9.8224	0.000458	0.9195	$-0.13207x^2+5.54443x-39.48224$
Moxostoma anisurum	5.2370E-06	0.7677	1.2354x-7.0223	0.004933	0.8668	$-0.14758x^2+5.95917x-42.57862$
Moxostoma erythrurum	6.3240E-08	0.8944	1.7154x-11.3847	0.04522	0.9192	$-0.08630x^2+4.42390x-31.18333$

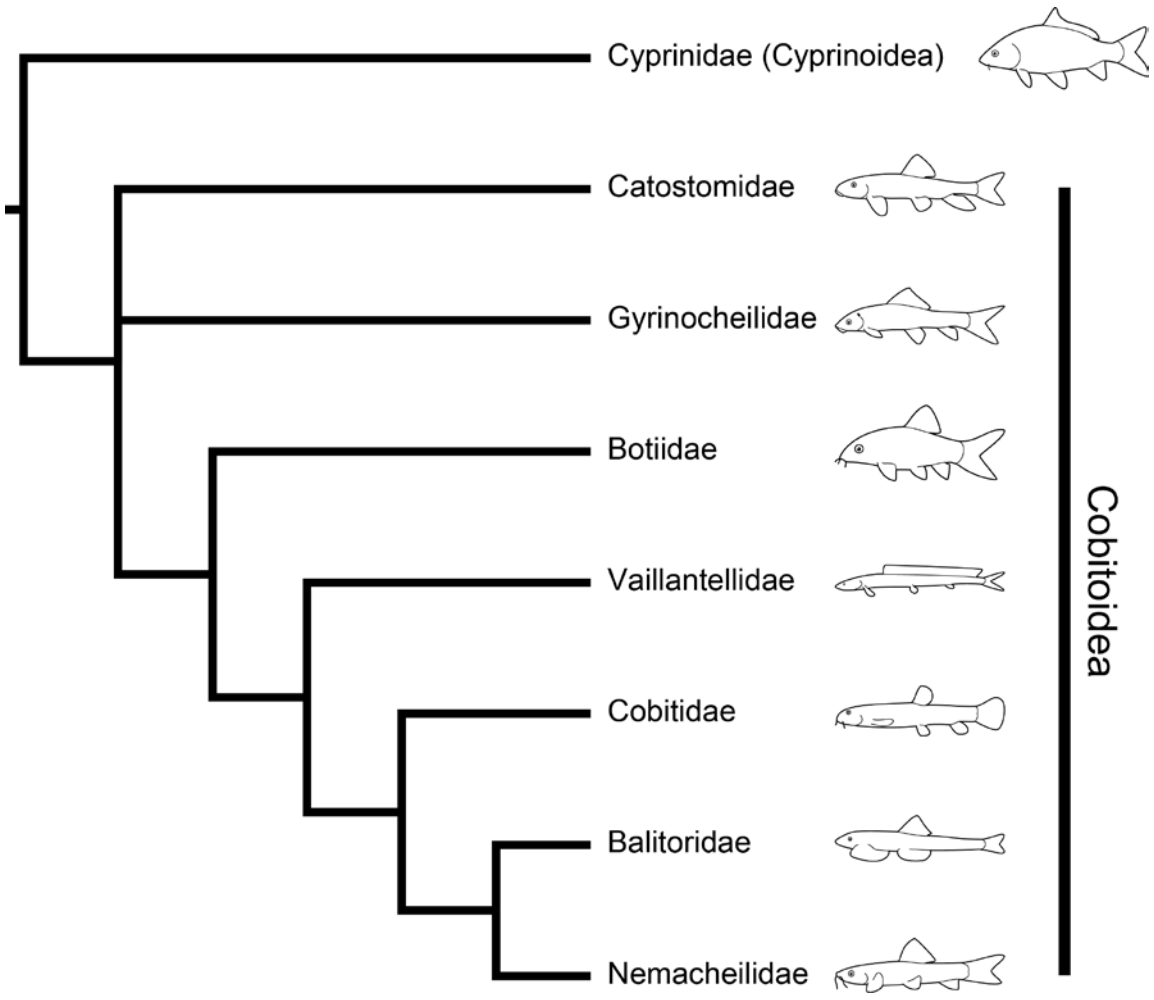

Figure 1.1. Hypothesized relationships among families of Cypriniformes as inferred from sequences of the nuclear protein-coding gene RAG1 from seventy-two species. Redrawn from Šlechtová *et al*. (2007).

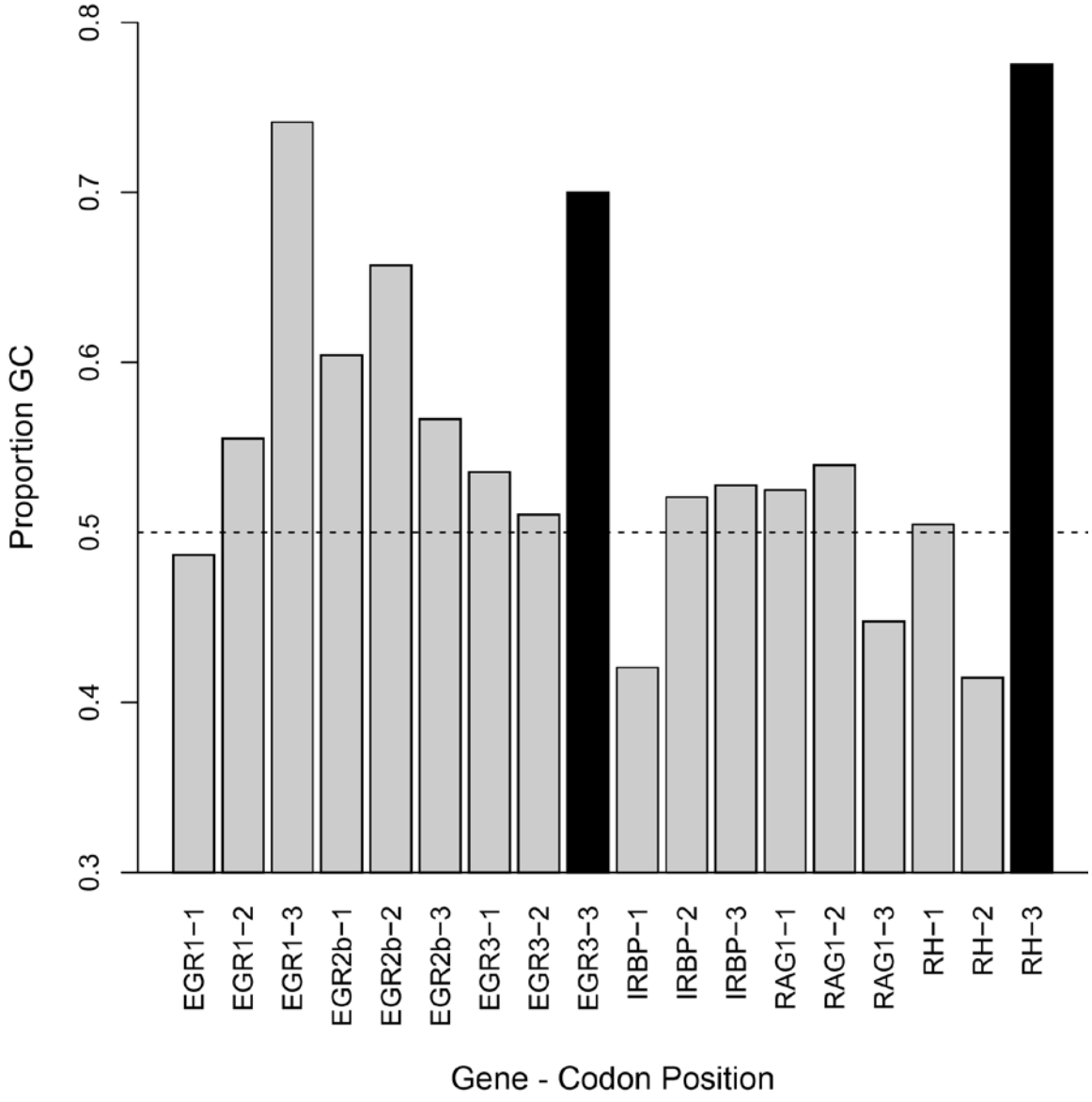

Figure 1.2. Base composition for each codon position for each gene for all 154 species. Third position of EGR3 and Rh (in black) were found to have significant base compositional heterogeneity.

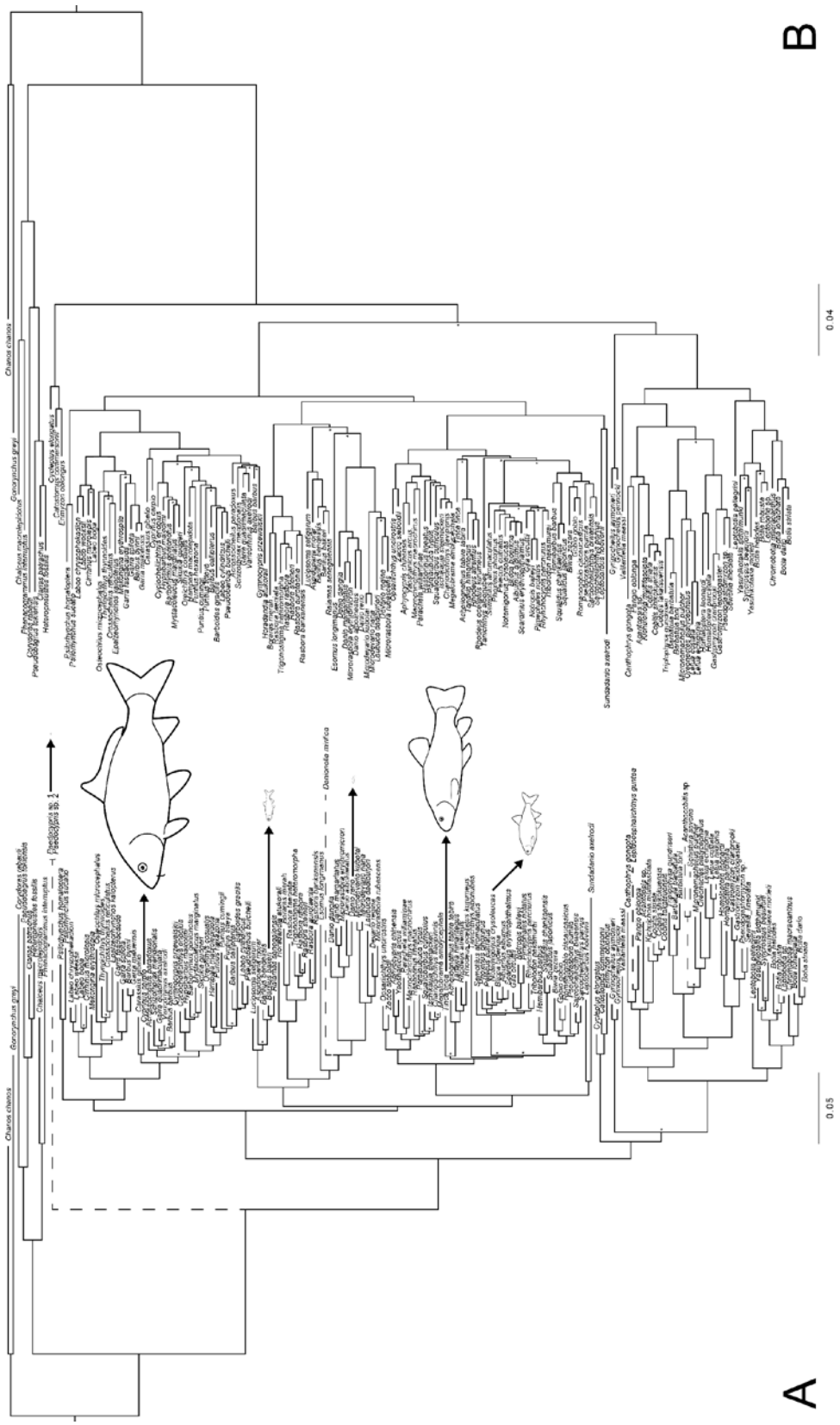
A
B
0.05
0.04

Figure 1.3. Maximum likelihood phylogenies using all 154 species (**A**) and excluding significant path length outliers (**B**). The species excluded from B are shown with dashed branches in A. Nodes with bootstrap support less than 75% are indicated with asterisks. Line drawings of a few cyprinid species are shown scaled to each other to illustrate the extreme variation in body size present within Cypriniformes. [Note that the largest known cyprinid is at least three times larger than the largest cyprinid illustrated (*Cyprinus carpio*)].

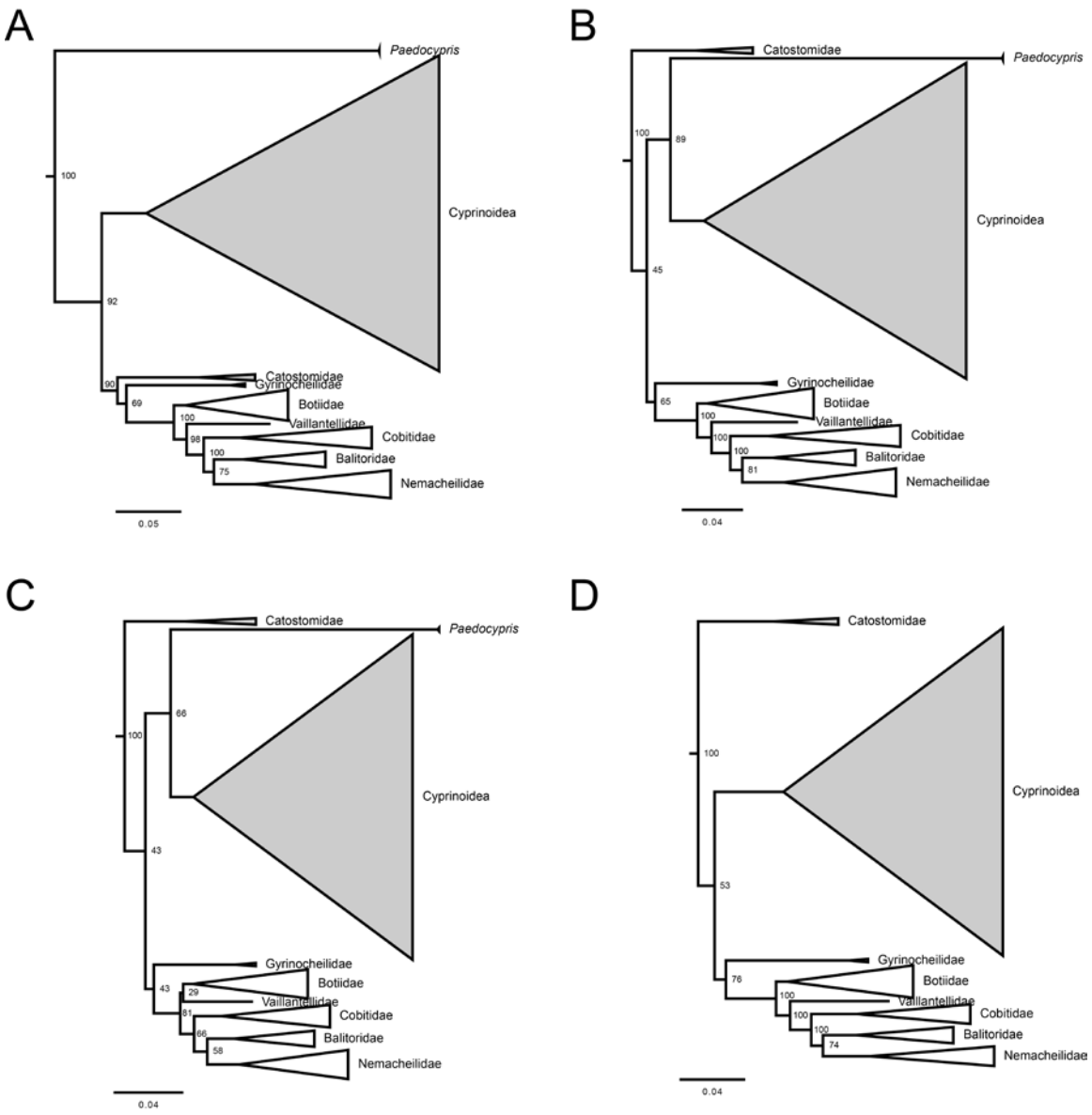

Figure 1.4. Maximum likelihood phylogenies for different subsets of the data. **A**) All partitions for all 154 species included. *Paedocypris* recovered as sister to all other cypriniforms. **B**) Partitions with significant base compositional heterogeneity (third codon position of EGR3 and Rh) excluded. Catostomidae recovered as sister to all other

cypriniforms. *Paedocypris* recovered as sister to Cyprinidae. **C**) Amino acid translations for all partitions. Catostomidae recovered as sister to all other cypriniforms. *Paedocypris* recovered as sister to Cyprinidae. **D**) Species with path lengths which were deemed significant outliers and the heterogeneous partition composed of third codon position of Rh excluded. Catostomidae recovered as sister to all other cypriniforms.

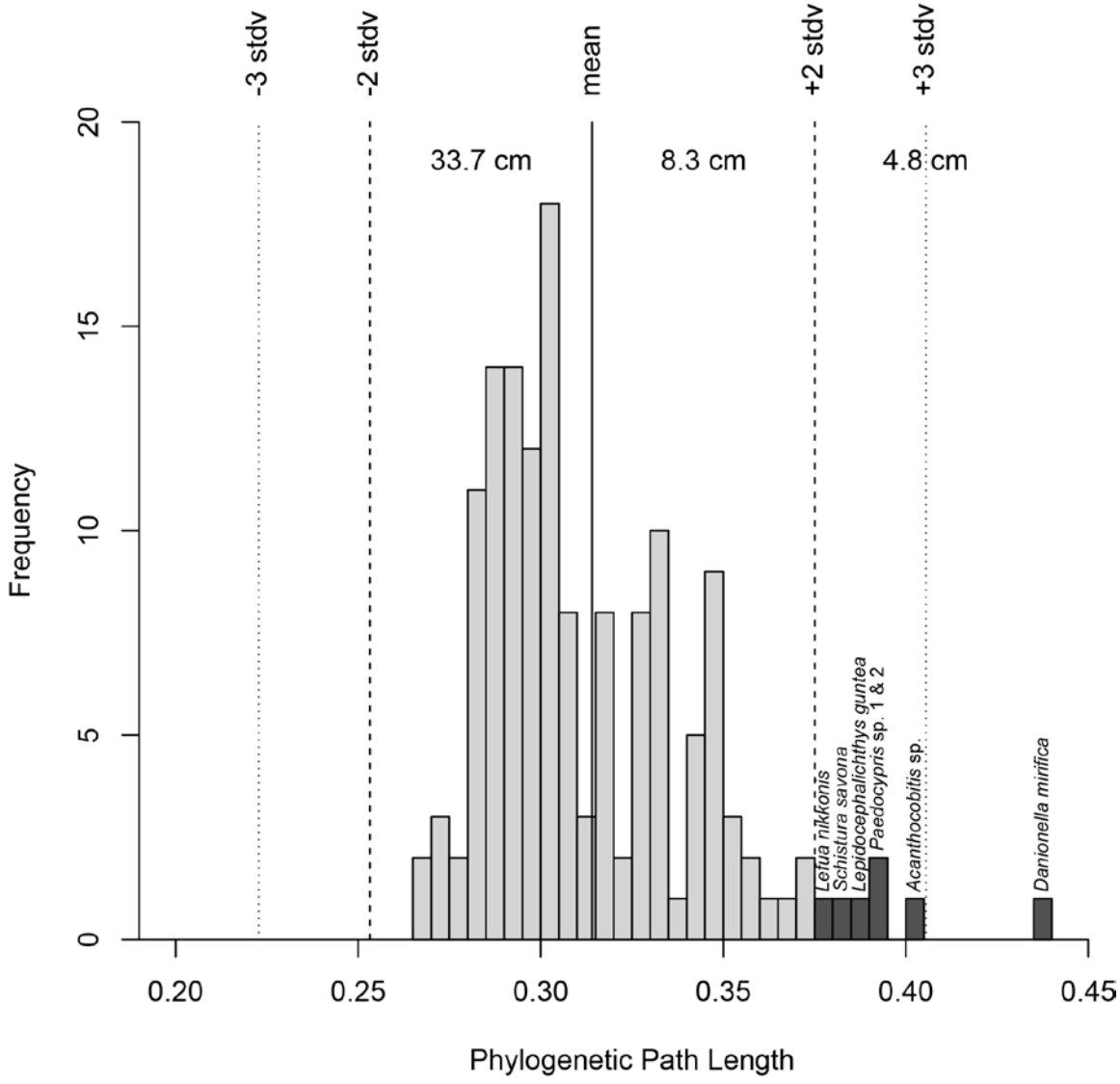

Figure 1.5. Histogram showing the distribution of phylogenetic path lengths for all cypriniform species in this study. The seven species with path lengths greater than two standard deviations from the mean are listed and indicated with dark gray bars. The average maximum standard length for species in three categories (path lengths greater than two standard deviations from the mean, path lengths greater than the mean but less than two standard deviations from the mean, and path lengths less than the mean) are

shown. Species with longer path lengths tend to have smaller body size than species with shorter path lengths.

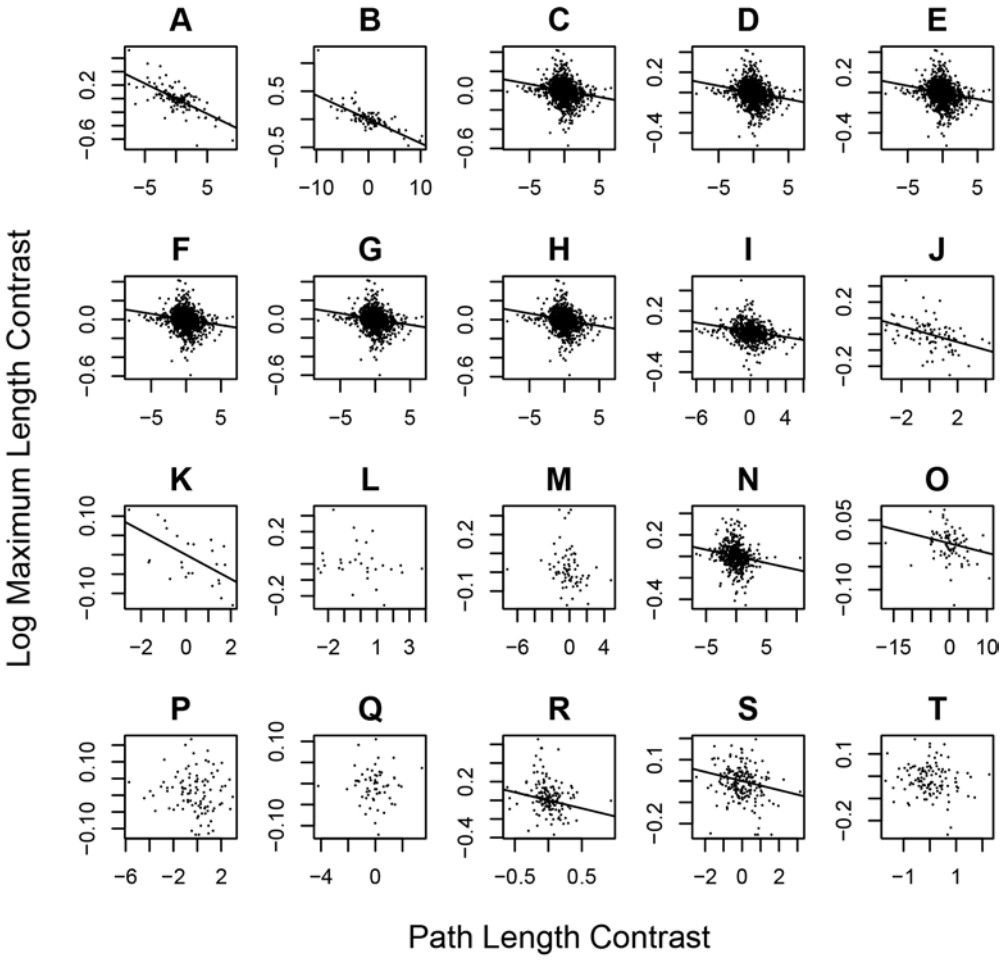

Figure 1.6. Many fish groups show a significant relationship between the phylogenetic independent contrasts for path length on a maximum likelihood phylogeny and log maximum standard length as shown by regressions using a general linear model. The slopes of significant relationships are drawn. The phylogenetic data used are from; **A**-**B**) this study, **C**-**L**) Betancur-R *et al*. (2013a), **M**) Betancur-R *et al*. (2013b), **N**) Near *et al*. (2013), **O**) Friedman *et al*. (2013), **P**) Hundt *et al*. (2014), **Q**) Unmack *et al*. (2013), **R**) Near *et al*. (2011), and **S**-**T**) Oliveira *et al*. (2011). The taxa plotted are **A**) Cypriniformes, **B**) Cyprinidae, **C**) Actinopterygii, **D**) Teleostei, **E**) Euteleostomorpha, **F**) Neoteleostei,

G) Acanthomorpha, **H**) Percomorphaceae, **I**) Perciformes, **J**) Ostariophysi, **K**) Characiformes, **L**) Siluriformes, **M**) Pleuronectiformes, **N**) Acanthomorpha, **O**) Cichlidae, **P**) Blenniidae, **Q**) Melanotaeniidae, **R**) Etheostomatinae, **S**) Characiformes, and **T**) Characidae.

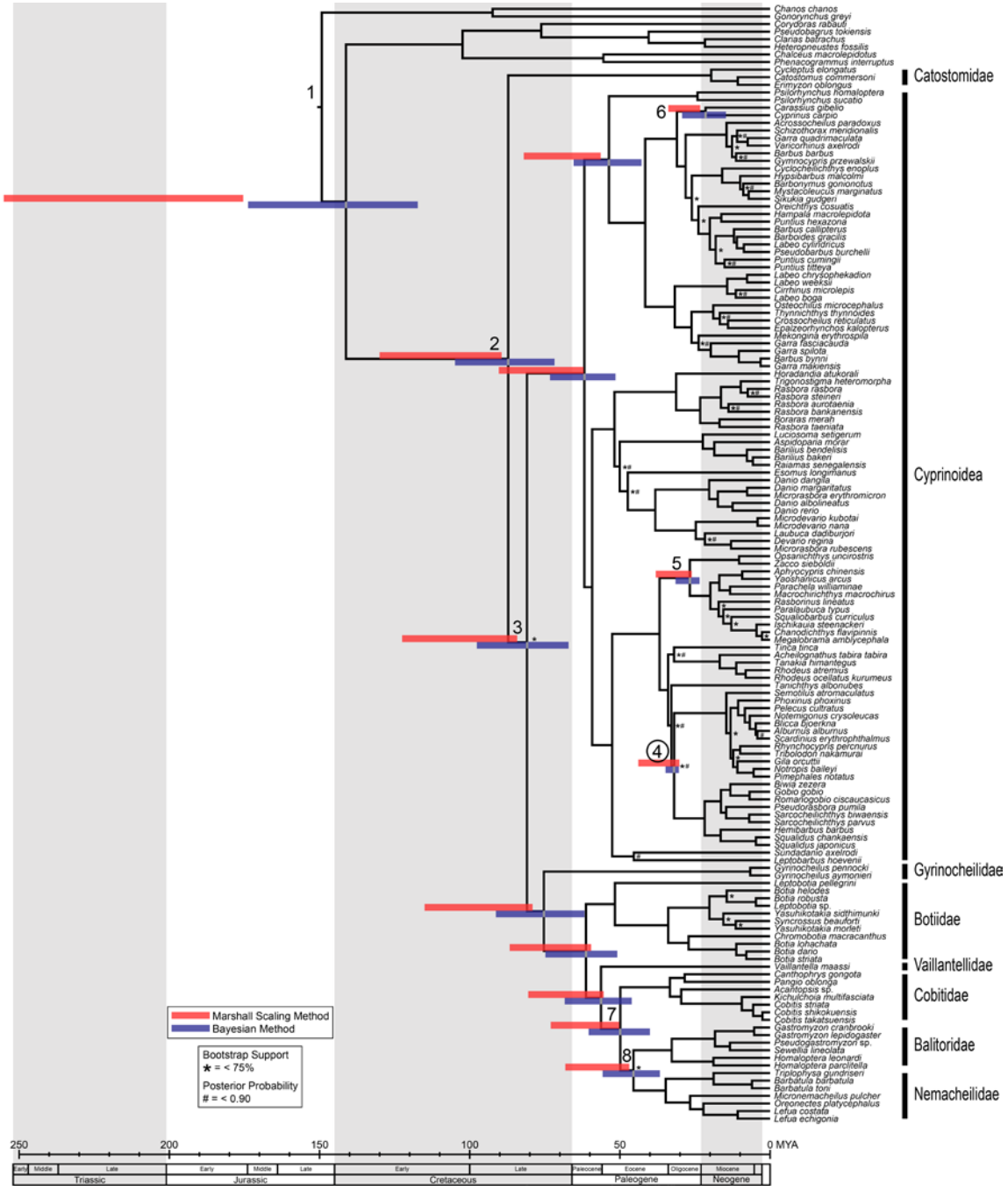
Catostomidae
Cyprinoidea
Gyrinocheilidae
Botiidae
Vaillantellidae
Cobitidae
Balitoridae
Nemacheilidae
1
2
3
4
5
6
7
8
Marshall Scaling Method
Bayesian Method
Bootstrap Support
★ = < 75%
Posterior Probability
= < 0.90
250
200
150
100
50
0 MYA
Triassic
Jurassic
Cretaceous
Paleogene
Neogene

Figure 1.7. Phylogenetic reconstruction of cypriniform fishes inferred from EGR1, EGR2b, EGR3, IRBP, RAG1, and Rh gene sequences using a Bayesian method. Divergence dates of major cypriniform lineages are shown as bars on nodes. Ages were estimated using the Marshall Scaling Method (shown in red) and a Bayesian method (shown in blue). Numbered nodes represent nodes with a fossil calibration. The circled number (node 4) indicates the node determined to be the calibration lineage in the Marshall Scaling Method. Asterisks and pound signs indicate nodes with low support in the maximum likelihood and Bayesian analyses, respectively.

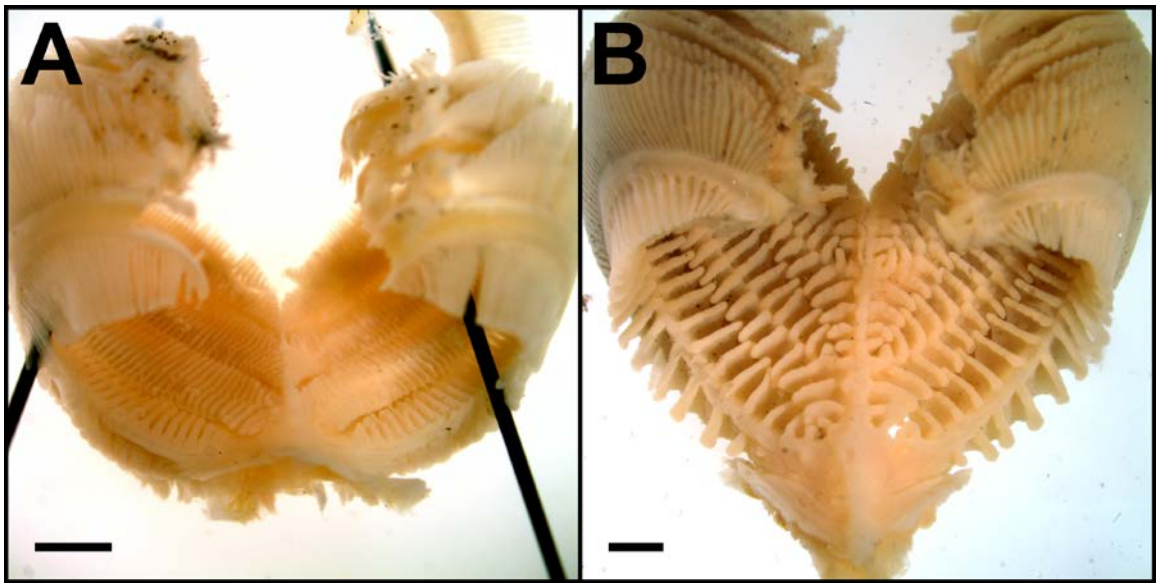

Figure 2.1. Representative gill arches from two species of freshwater sucker illustrating variation in gill raker morphology. **A**) *Carpiodes velifer* has a high number and a high density of gill rakers but there is little space between individual gill rakers and the gill rakers are very thin while **B**) *Moxostoma anisurum* has gill rakers that have high surface area. Scale bars = 2 mm.

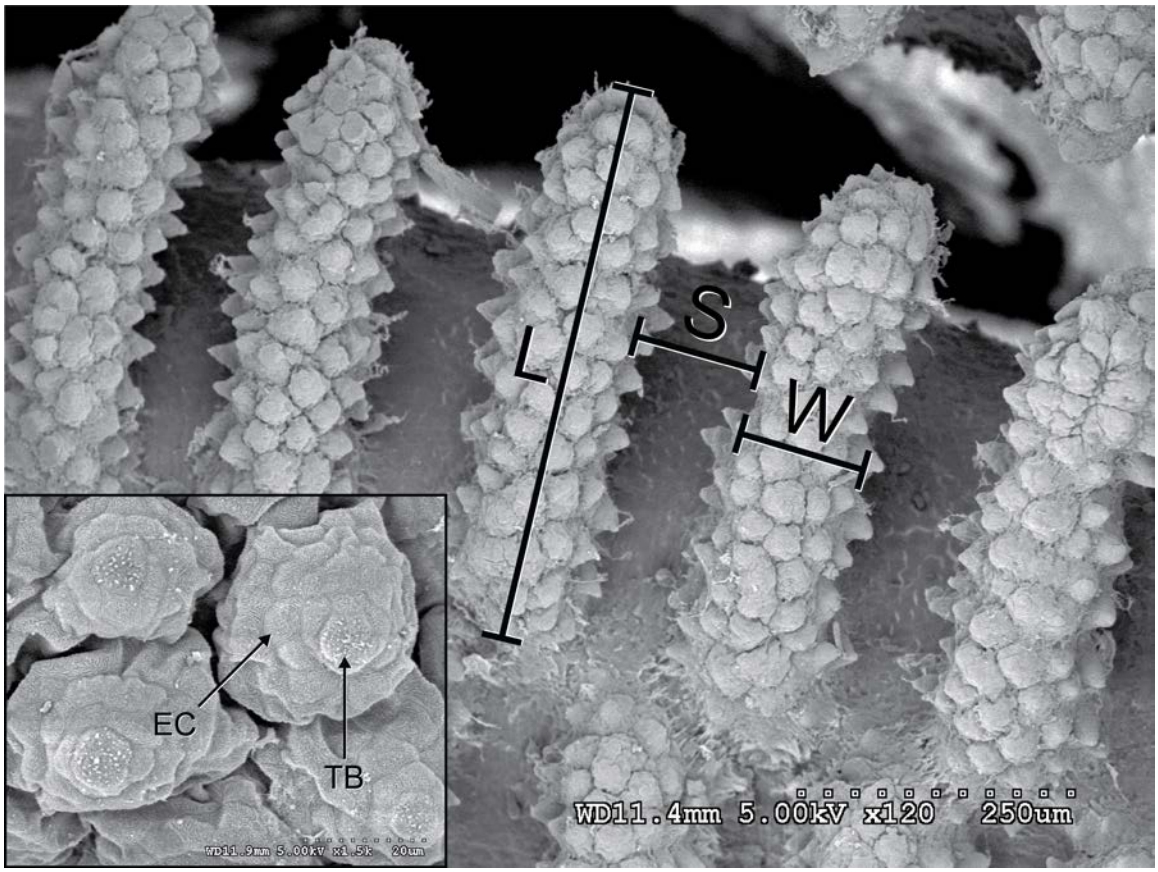

Figure 2.2. Scanning electron micrographs of gill rakers of *Moxostoma macrolepidotum* and magnified view of taste buds on the gill rakers of *Hypentelium nigricans* (insert). Measurements used in this study include the length of individual gill rakers (L), the space between adjacent gill rakers (S), and the width of individual gill rakers (W). The gill rakers are covered in taste buds each consisting of a mound of epithelial cells (EC) with a taste bud cell (TB) at the apex.

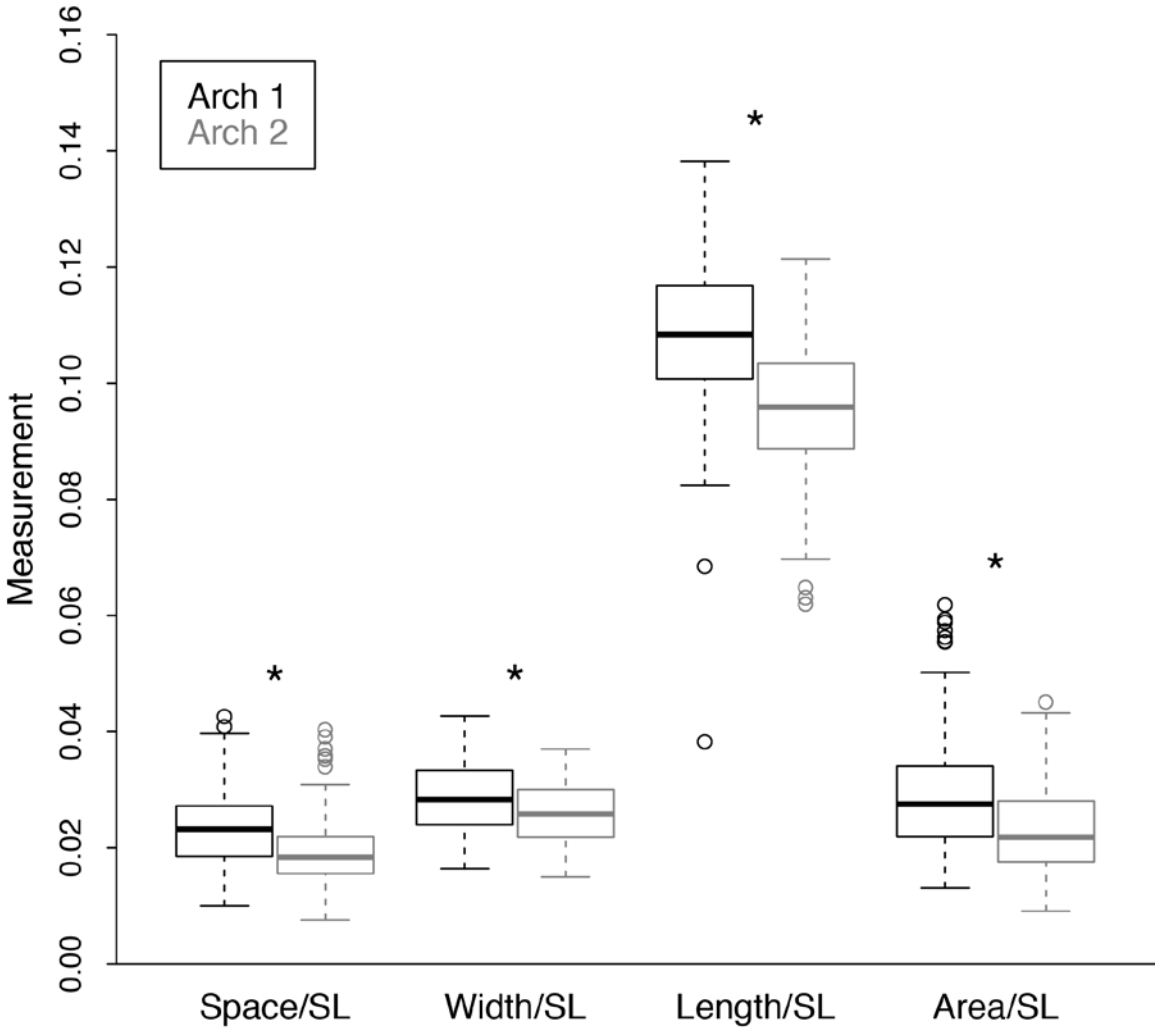

Figure 2.3. Comparison of gill raker measurements between gill arch 1 (black) and gill arch 2 (gray) of *Catostomus commersonii*. Thick, horizontal lines mark characteristic medians, boxes show interquartile ranges, whiskers mark the minimum and maximum values within 1.5 times the interquartile range, and open circles indicate points outside 1.5 times the interquartile range. Asterisks indicate characteristics that are significantly different between arches.

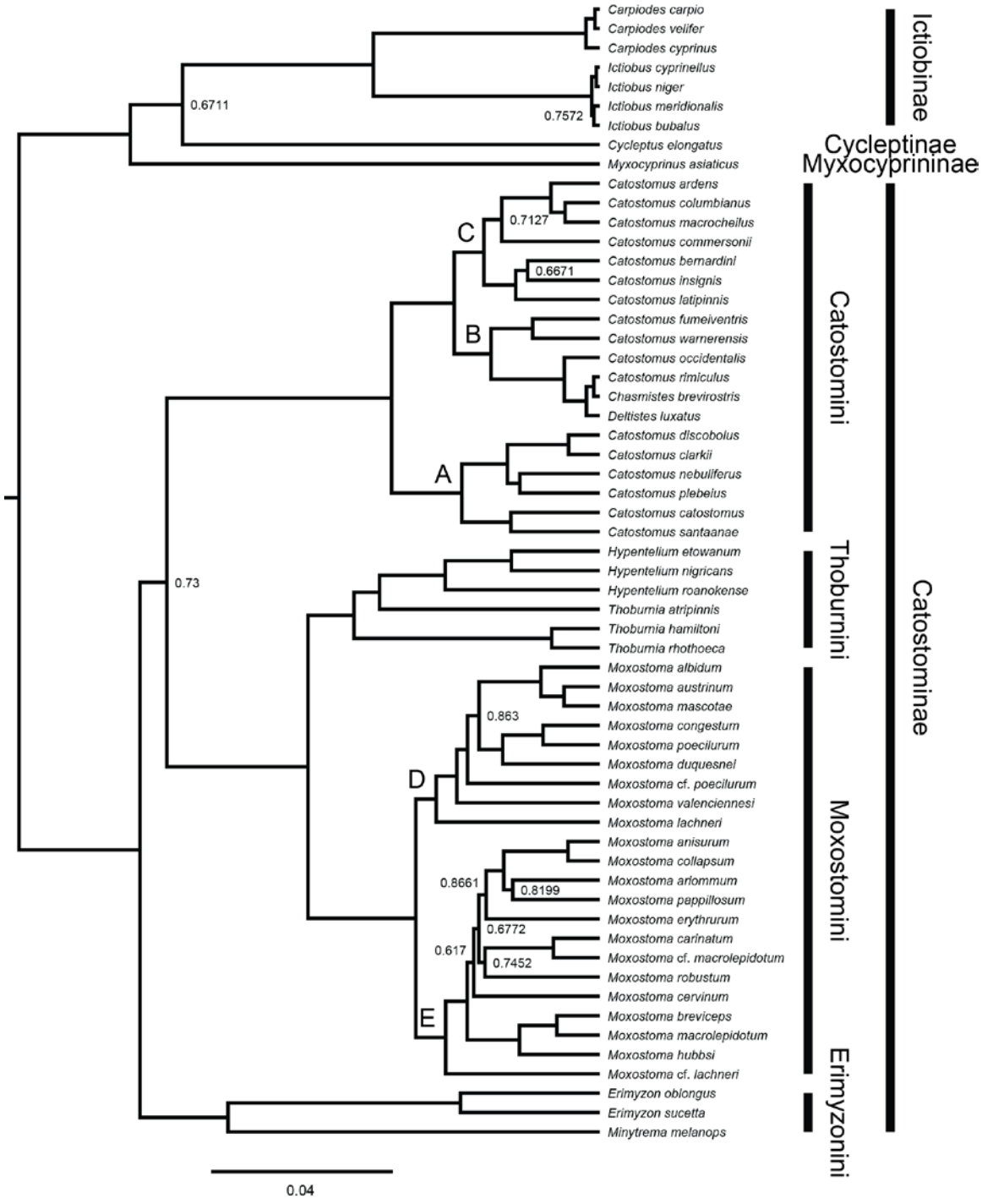
Carpiodes carpio
Carpiodes velifer
Carpiodes cyprinus
Ictiobus cyprinellus
Ictiobus niger
Ictiobus meridionalis
Ictiobus bubalus
Cycleptus elongatus
Myxocyprinus asiaticus
Catostomus ardens
Catostomus columbianus
Catostomus macrocheilus
Catostomus commersonii
Catostomus bernardini
Catostomus insignis
Catostomus latipinnis
Catostomus fumeiventris
Catostomus warnerensis
Catostomus occidentalis
Catostomus rimiculus
Chasmistes brevirostris
Deltistes luxatus
Catostomus discobolus
Catostomus clarkii
Catostomus nebuliferus
Catostomus plebeius
Catostomus catostomus
Catostomus santaanae
Hypentelium etowanum
Hypentelium nigricans
Hypentelium roanokense
Thoburnia atripinnis
Thoburnia hamiltoni
Thoburnia rhothoeca
Moxostoma albidum
Moxostoma austrinum
Moxostoma mascotae
Moxostoma congestum
Moxostoma poecilurum
Moxostoma duquesnei
Moxostoma cf. poecilurum
Moxostoma valenciennesi
Moxostoma lachneri
Moxostoma anisurum
Moxostoma collapsum
Moxostoma arlommum
Moxostoma pappillosum
Moxostoma erythrurum
Moxostoma carinatum
Moxostoma cf. macrolepidotum
Moxostoma robustum
Moxostoma cervinum
Moxostoma breviceps
Moxostoma macrolepidotum
Moxostoma hubbsi
Moxostoma cf. lachneri
Erimyzon oblongus
Erimyzon sucetta
Minytrema melanops
0.6711
0.7572
0.7127
0.6671
0.73
0.863
0.8661
0.8199
0.6772
0.617
0.7452
A
B
C
D
E
0.04
Ictiobinae
Cycleptinae
Myxocyprininae
Catostomini
Thoburnini
Moxostomini
Erimyzonini
Catostominae

Figure 2.4. Bayesian phylogeny of Catostomidae based on ND4, ND5, and three intervening tRNA sequences. Lettered clades are designated with the same letter as used by Doosey *et al*. (2010). Support values are shown for nodes with posterior probabilities less than 0.9.

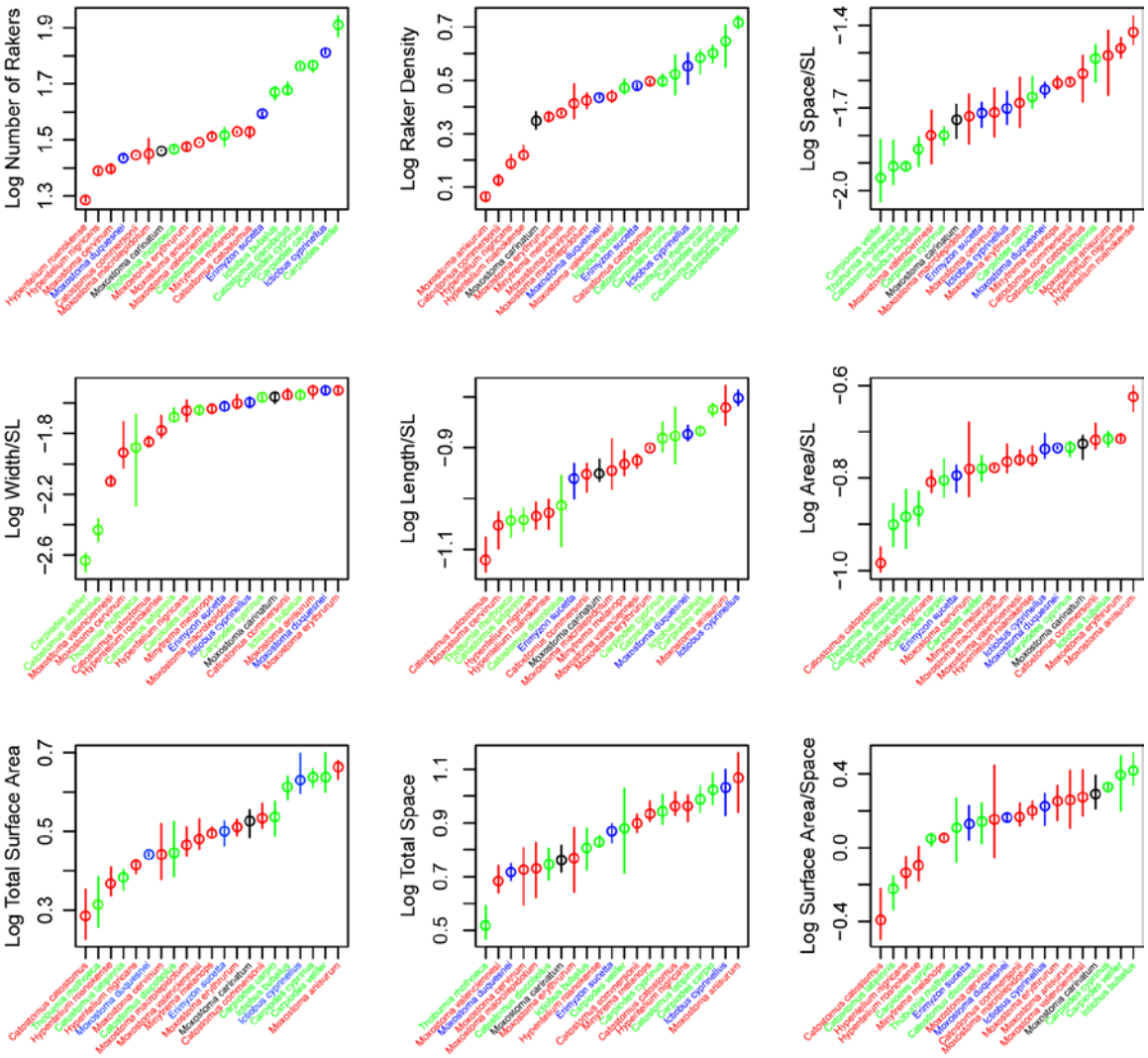

Figure 2.5. Species means for gill raker measures taken from gill arch 1. Analysis of variance tests indicate that there are statistically significant differences among species in all gill raker measures. Vertical lines represent the range of measurements within a species. Species are colored by feeding guild as determined by the discrete diet score; algivores = red, zooplanktonivores = blue, macroinvertivores = red, molluskivores = black.

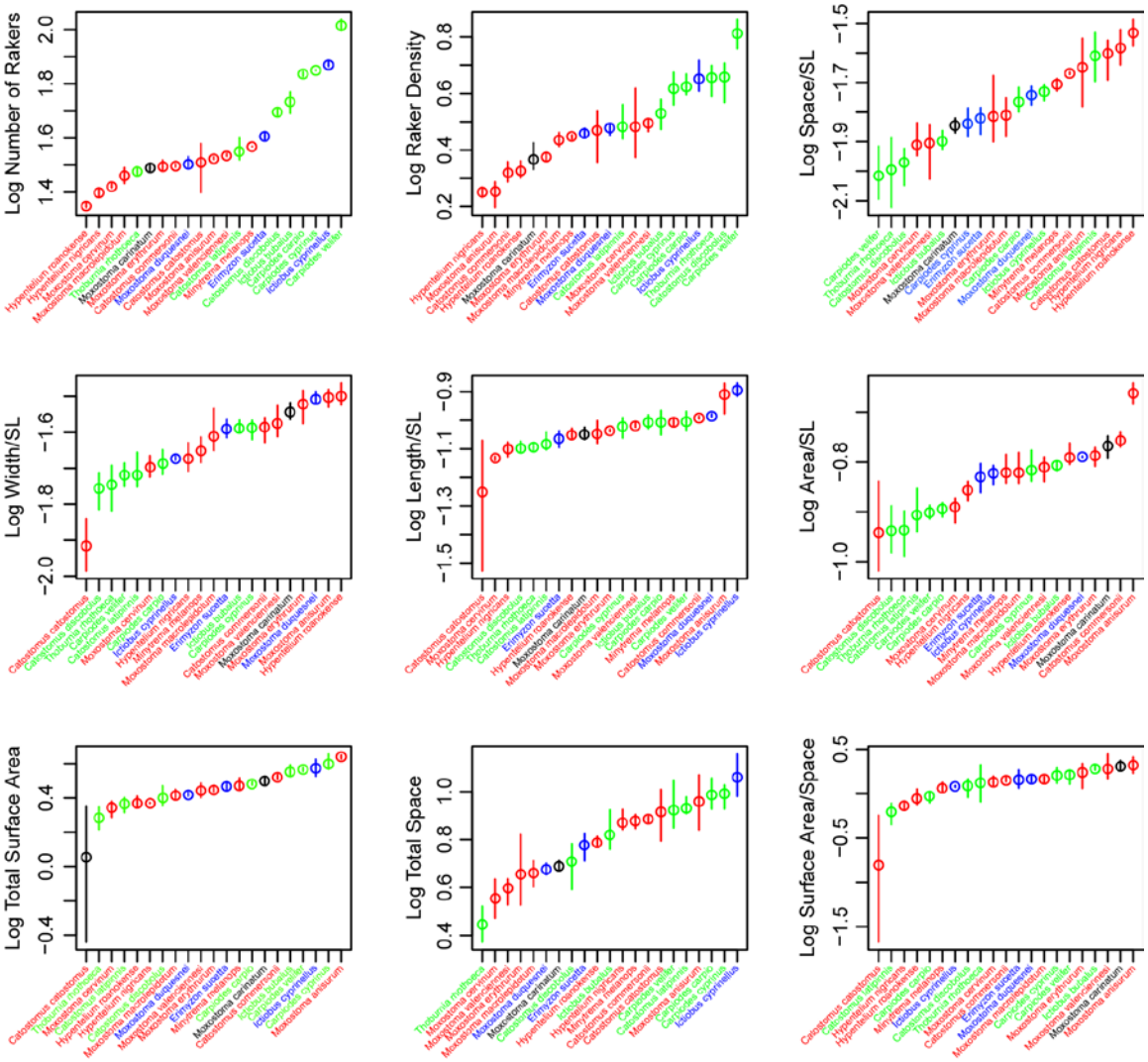

Figure 2.6. Species means for gill raker measures taken from gill arch 2. Analysis of variance tests indicate that there are statistically significant differences among species in all gill raker measures. Vertical lines represent the range of measurements within a species. Species are colored by feeding guild as determined by the discrete diet score; algivores = red, zooplanktonivores = blue, macroinvertivores = red, molluskivores = black.

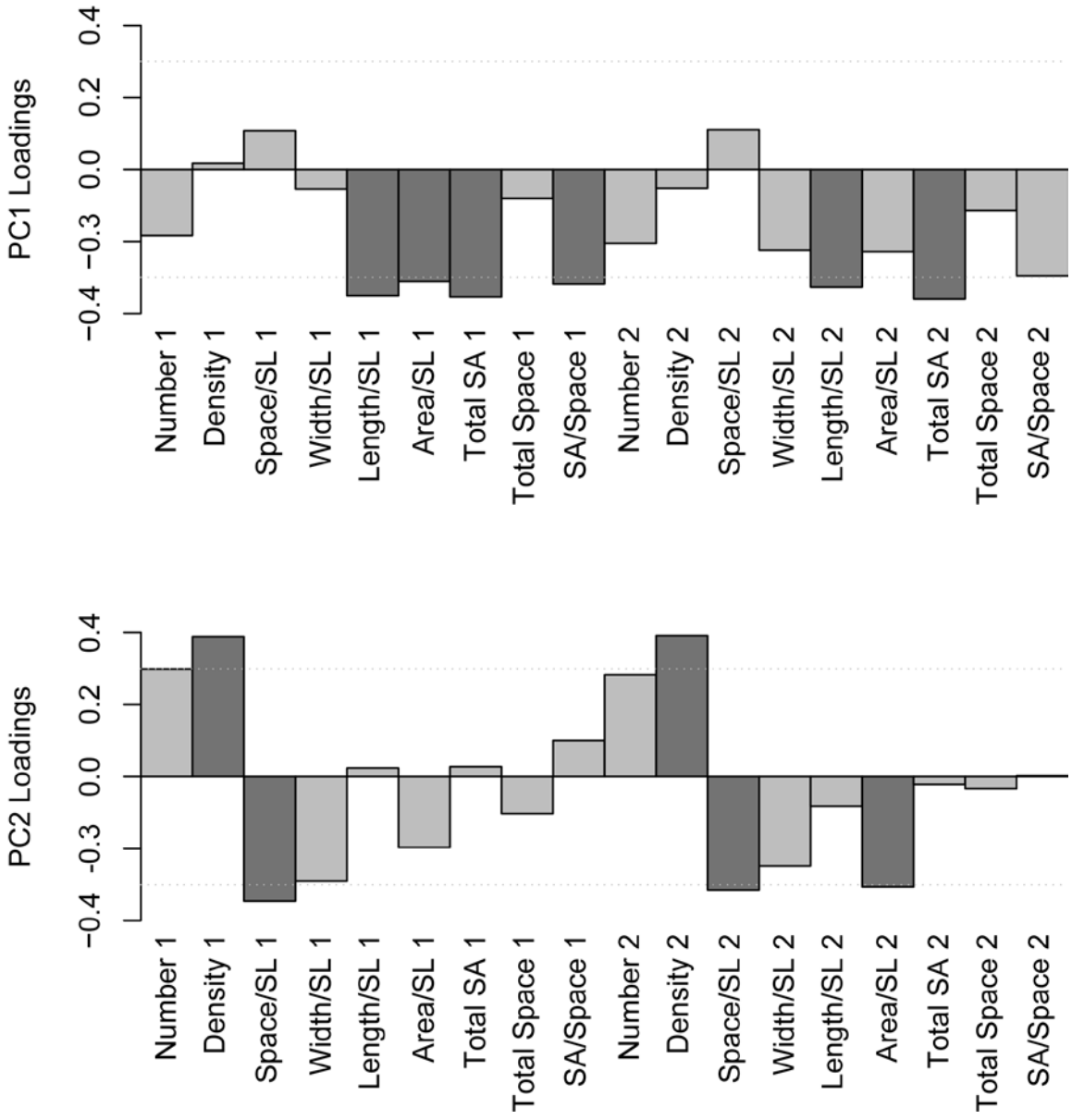

Figure 2.7. PCA loadings for the first two PC axes. The gill raker measures that most strongly contribute to each axis are colored in dark gray.

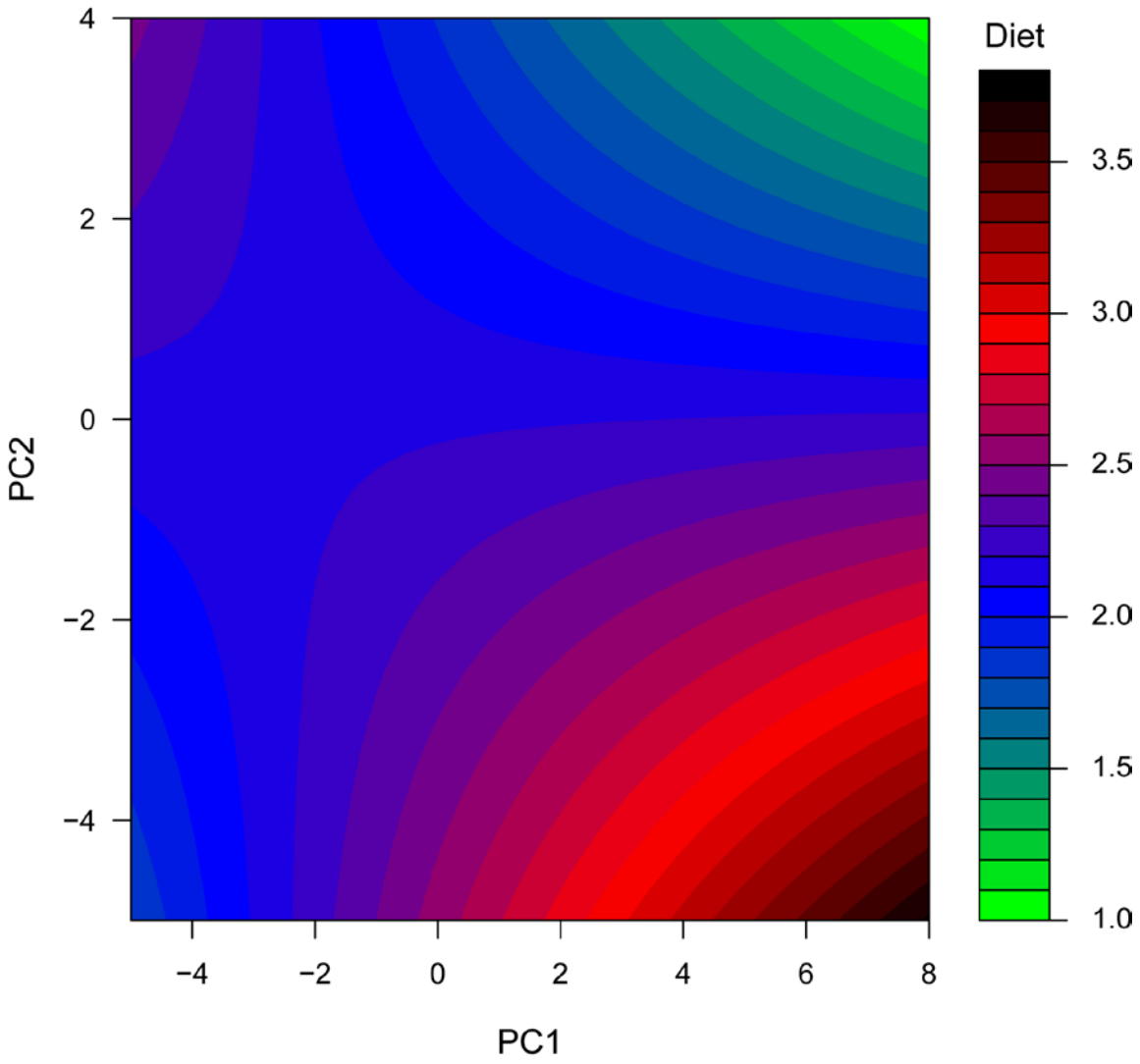

Figure 2.8. Relationship between PC1, PC2, and diet according to a PGLS analysis. Algae and detritus are represented in green, zooplankton is blue, macroinvertebrates are red, and mollusks are black. PC1 is most strongly associated negatively with measures related to gill raker surface area. PC2 is most strongly associated positively with gill raker density and negatively with space between gill rakers.

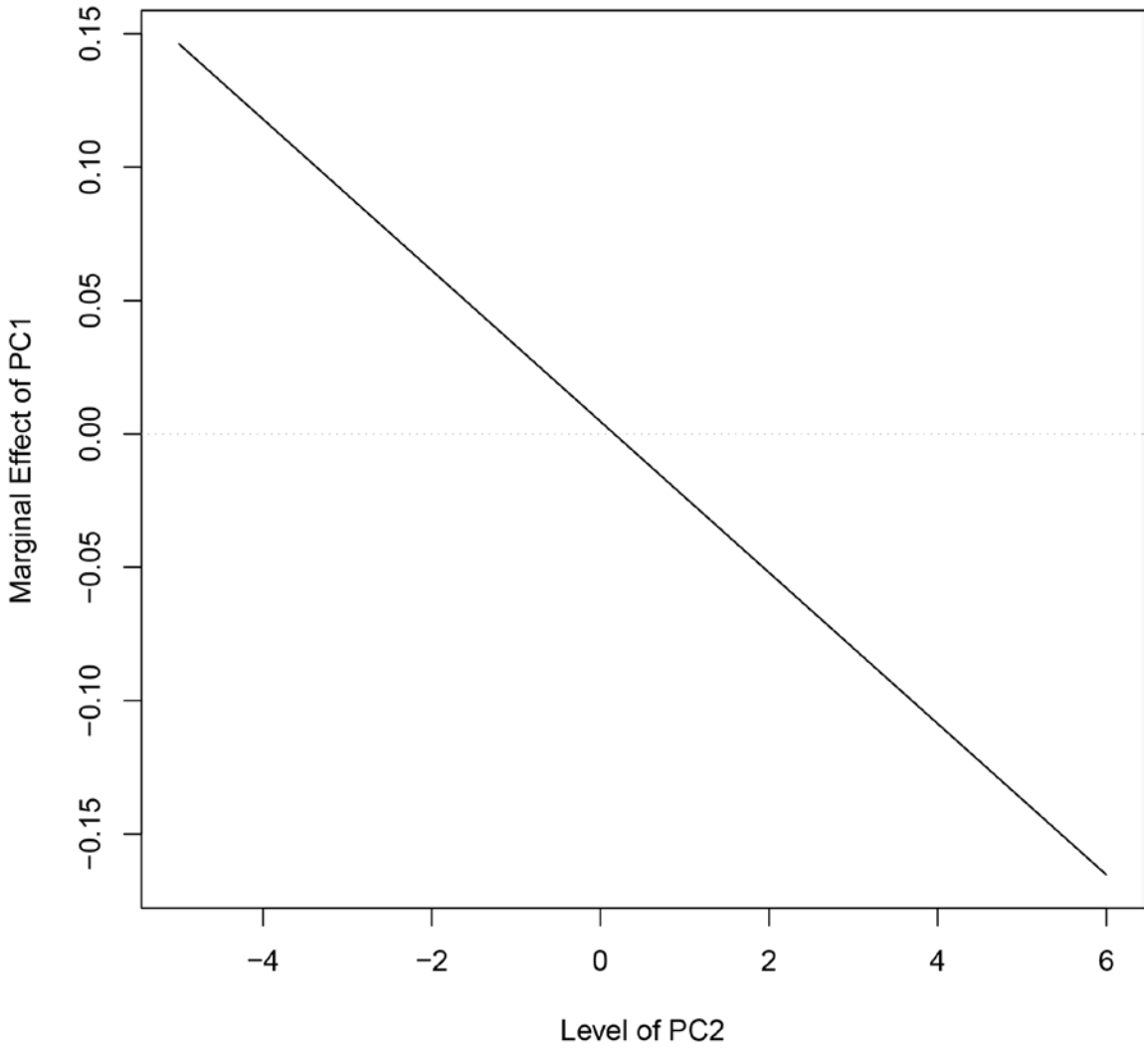

Figure 2.9. Relationship between PC2 and marginal effect of PC1 according to a PGLS analysis of PC1, PC2, and diet. When PC2 has a low value the relationship between PC1 and diet is positive but when PC2 has a high value the relationship between PC1 and diet is negative.

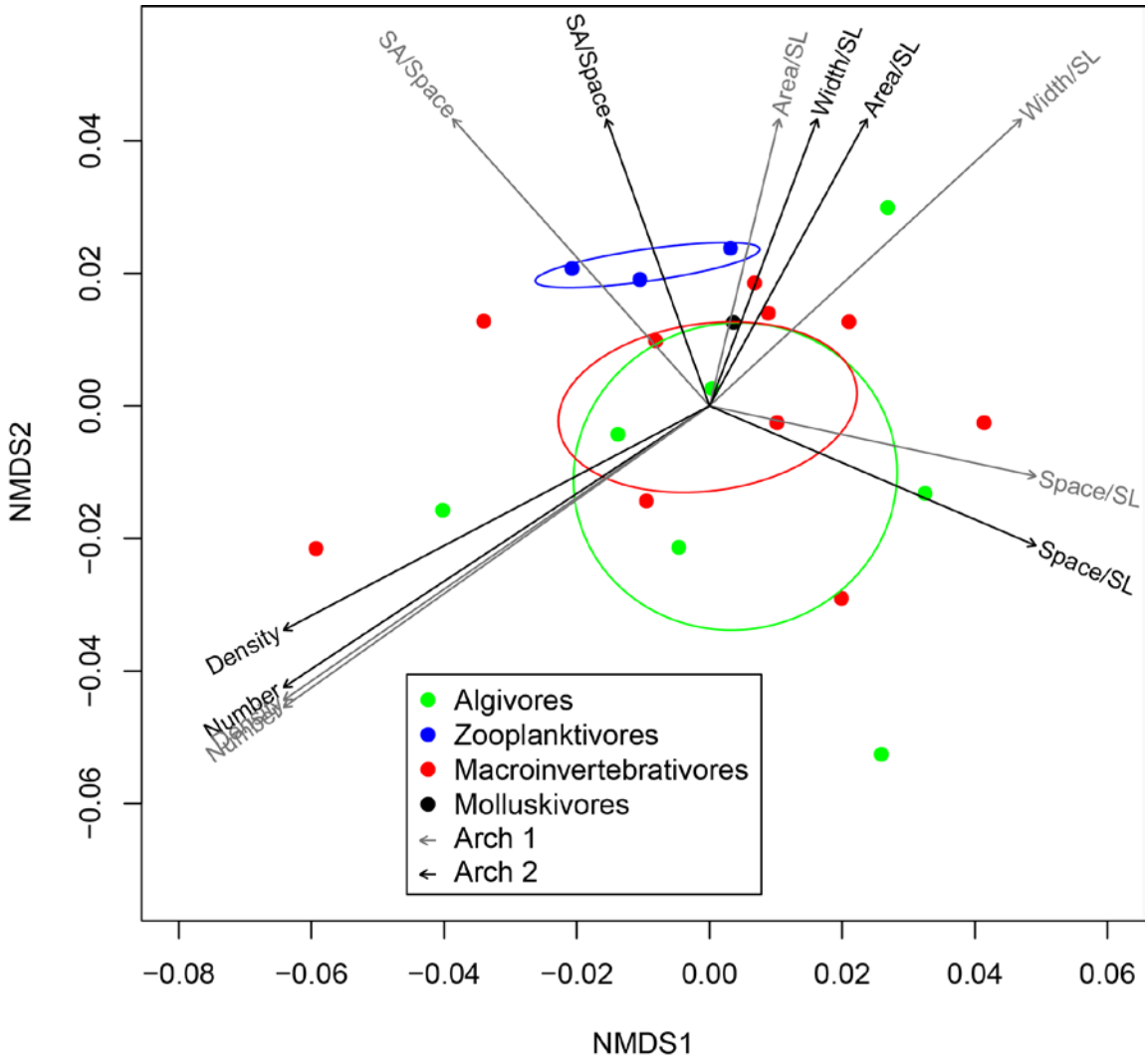

Figure 2.10. Non-metric multidimensional scaling analysis of diet and gill raker morphology of twenty-one sucker species. Points represent species and are colored according to discrete diet score. Ellipses are 95% confidence intervals for diet drawn around point scores based on standard errors. The significant predictors of differences in diet among species are shown as arrows. Gray arrows are gill raker measures from arch 1 that are significant predictors of diet and black arrows are measures from arch 2 that are significant predictors of diet.

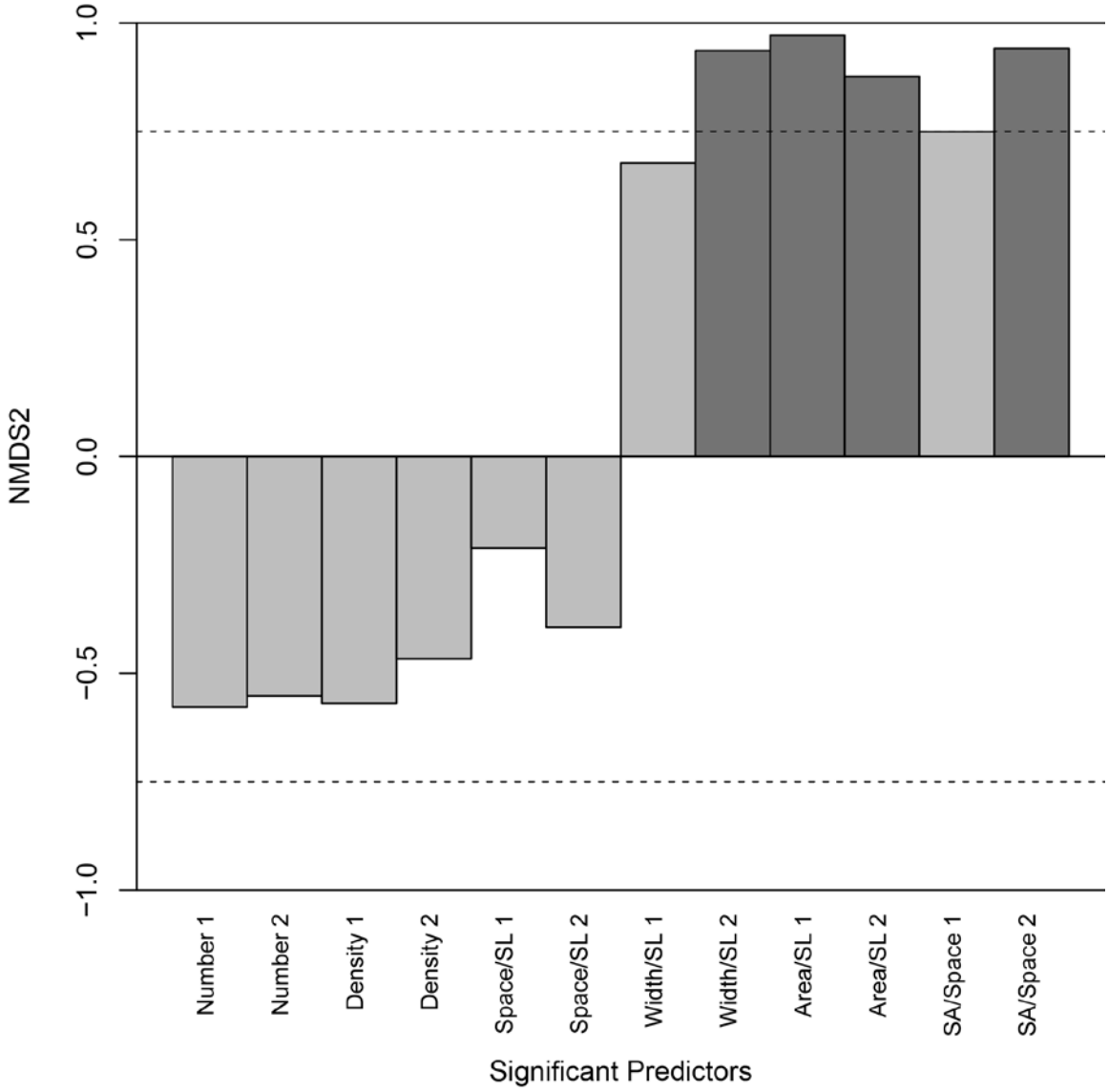

Figure 2.11. Vertical component of the vector for each significant predictor of diet as determined from an NMDS analysis. Feeding guilds most strongly separated along NMDS2, the vertical axis in the NMDS analysis. Gill raker measures with vertical components of their predictive vector greater than 0.75 are shown in dark gray.

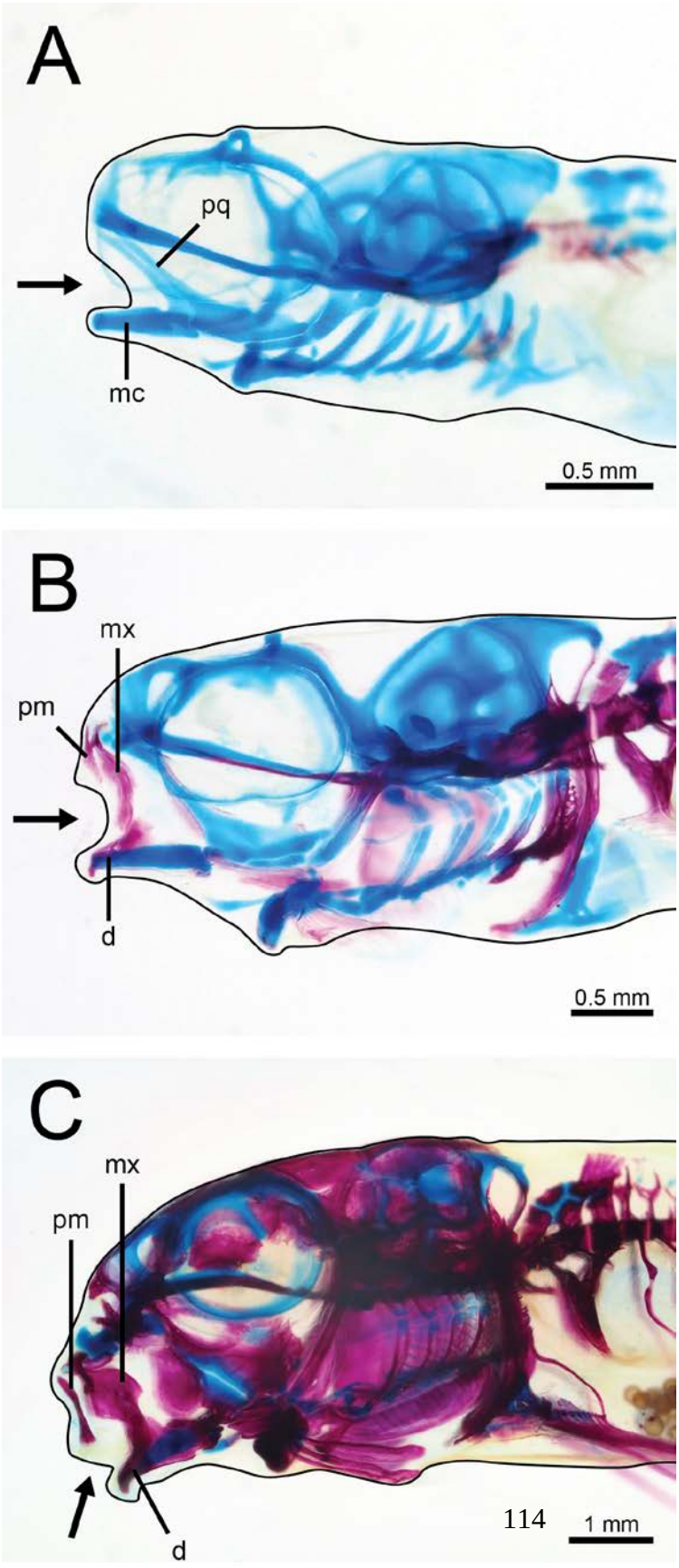
A
pq
mc
0.5 mm
B
mx
pm
d
0.5 mm
C
mx
pm
d
1 mm

Figure 3.1. Mouth transformation in *Hypentelium nigricans* from a terminal orientation (**A**) to a subterminal orientation (**C**) with an intermediate specimen shown (**B**). Lateral views with anterior to the left. The body is outlined and the direction of mouth opening is indicated with arrows. **A**: 10.35 mm, **B**: 12.80 mm, **C**: 20.78 mm. d, dentary; mc, Meckel's cartilage; mx, maxilla; pm, premaxilla; pq, palatoquadrate.

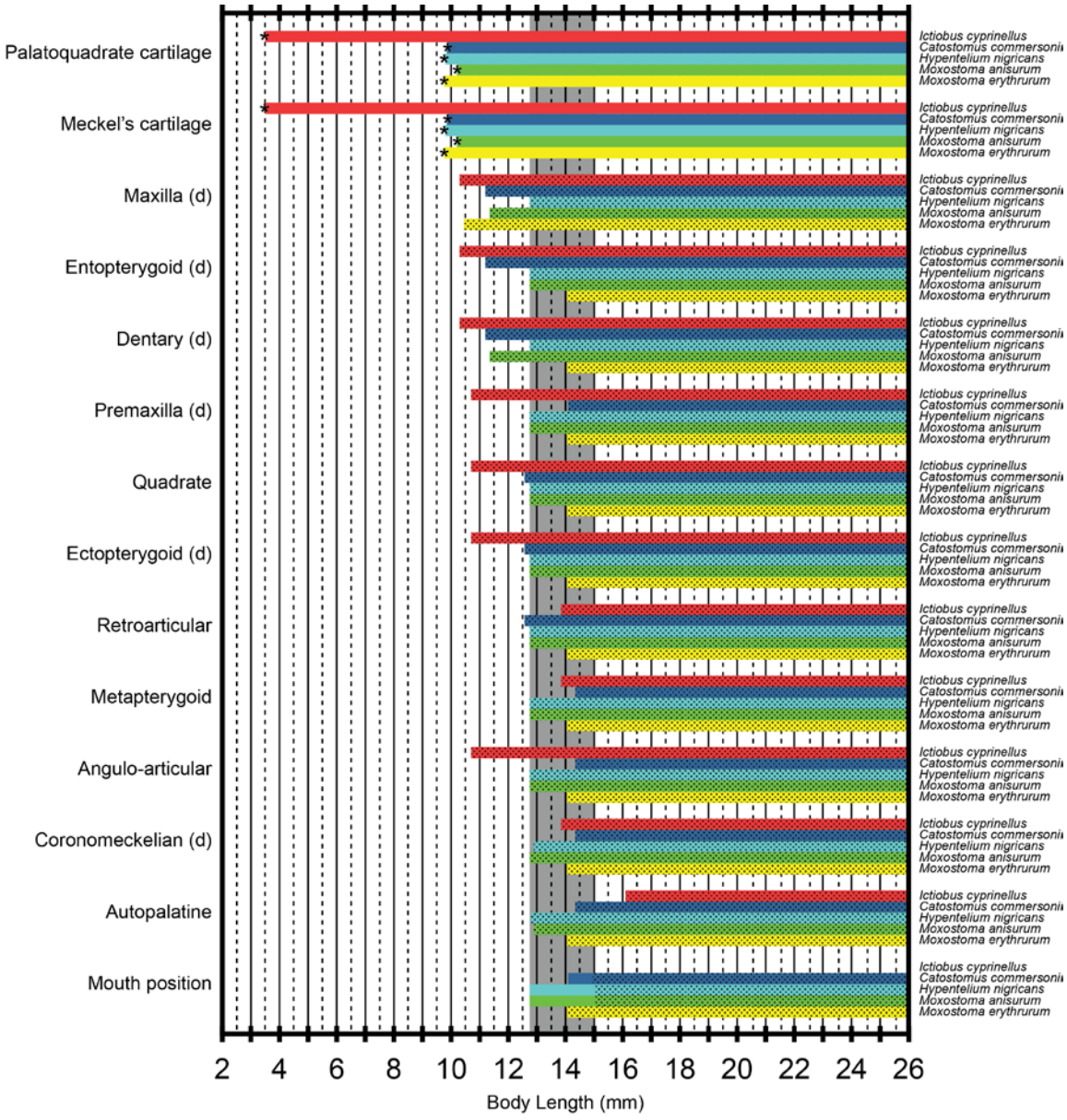

Figure 3.2. Sequence of chondrification and ossification of the mandibular arch and associated dermal bones. Bones of dermal origin are indicated with a (d) following their names. Cartilage development is indicated with solid bars and bone development is indicated with stippled bars except for mouth position where solid bars indicate where the mouth is intermediate to terminal and subterminal and stippled bars indicate a fully

subterminal orientation. Asterisks indicate that the structure was present in the smallest specimen examined. The vertical gray box indicates the transition from a terminal mouth orientation to a subterminal orientation.

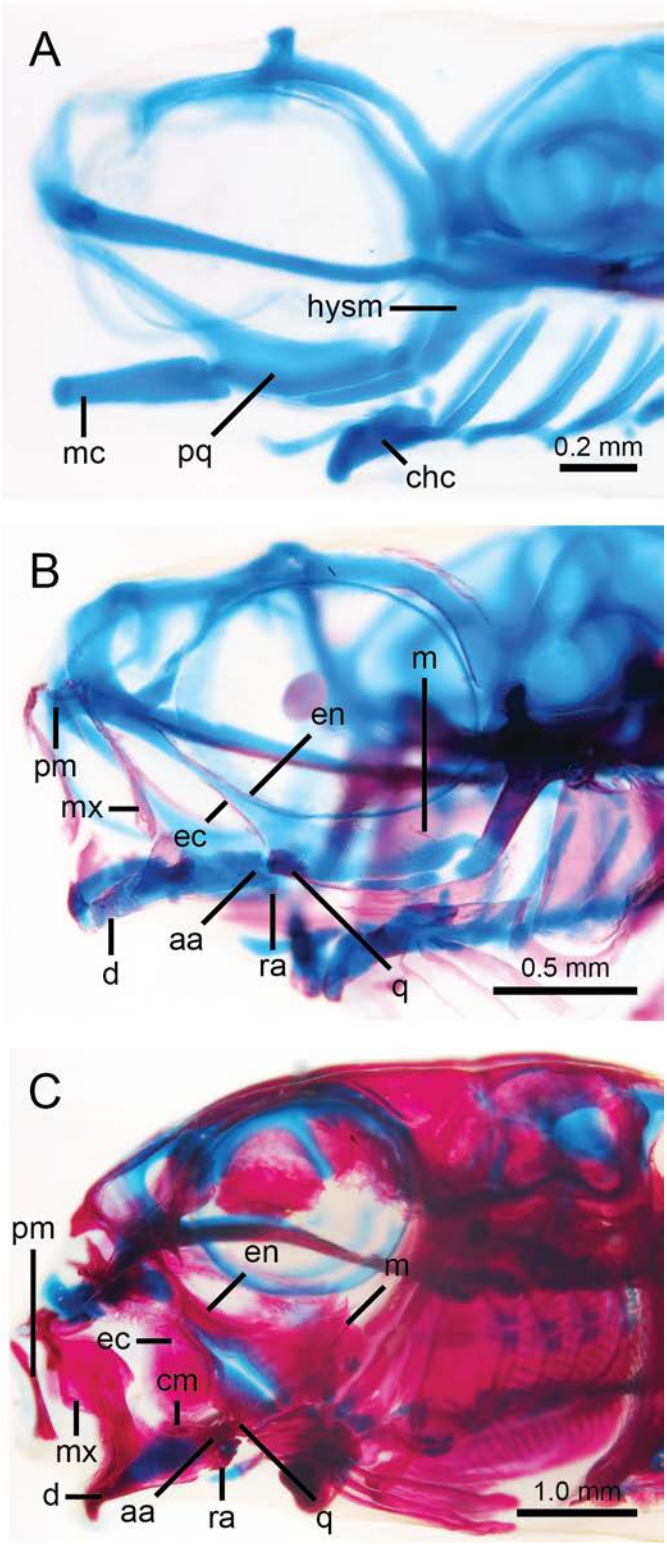
A
hysm
mc
pq
chc
0.2 mm
B
m
en
pm
mx
ec
aa
d
ra
q
0.5 mm
C
pm
en
m
ec
cm
mx
d
aa
ra
q
1.0 mm

Figure 3.3. Development of the mandibular arch and associated dermal bones in *Hypentelium nigricans*. Lateral views with anterior to the left. **A**: 11.00 mm, **B**: 12.35 mm, **C**: 21.80 mm. aa, angulo-articular; chc, ceratohyal cartilage; cm, coronomeckelian; d, dentary; ec, ectopterygoid; en, entopterygoid; hysm, hyosymplectic cartilage; m, metapterygoid; mc, Meckel's cartilage; mx, maxilla; pm, premaxilla; pq, palatoquadrate; q, quadrate; ra, retroarticular.

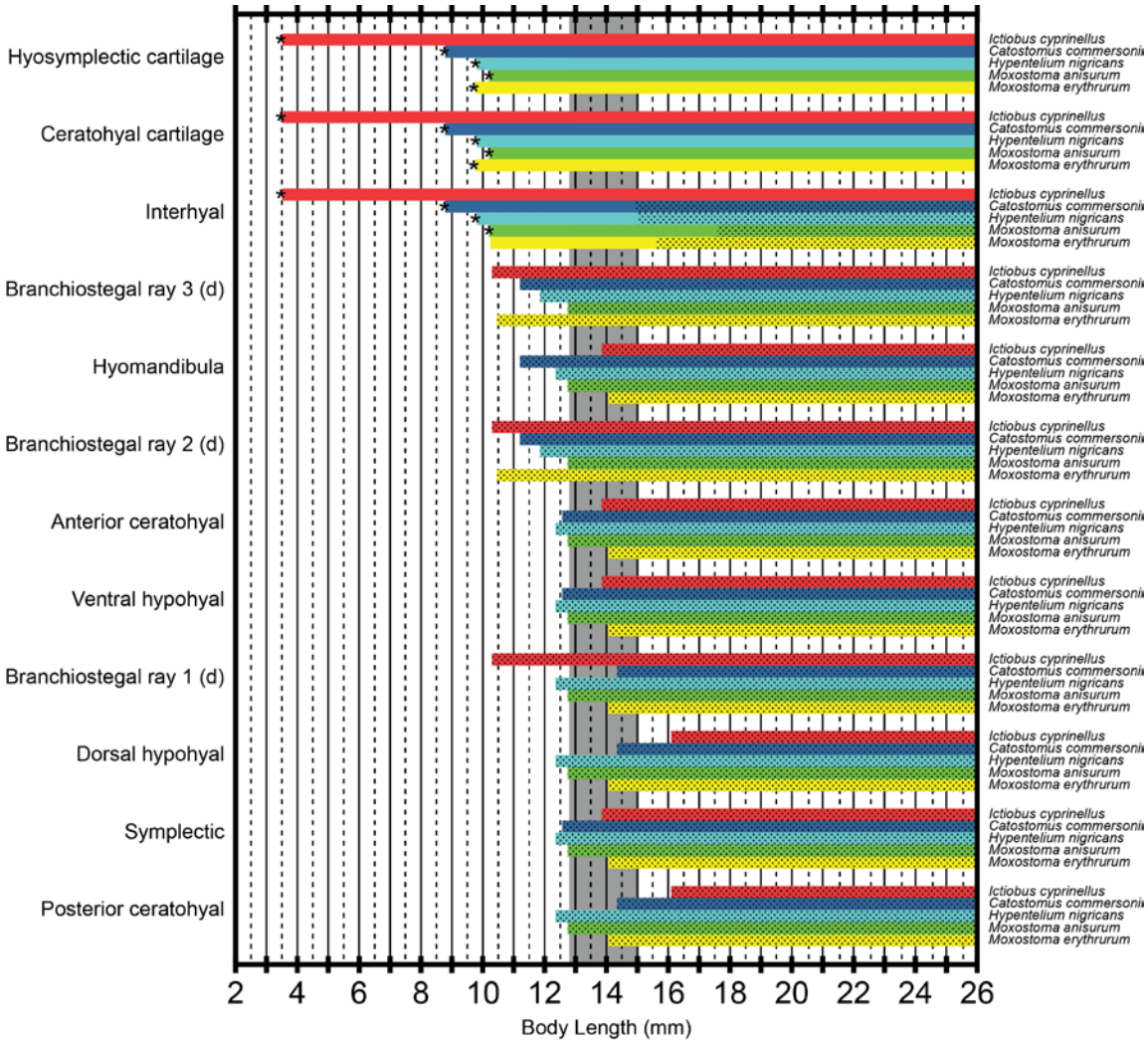

Figure 3.4. Sequence of chondrification and ossification of the hyoid arch. Cartilage development is indicated with solid bars and bone development is indicated with stippled bars. Asterisks indicate that the structure was present in the smallest specimen examined. The vertical gray box indicates the transition from a terminal mouth orientation to a subterminal orientation. Bones of dermal origin are indicated with a (d) following their names.

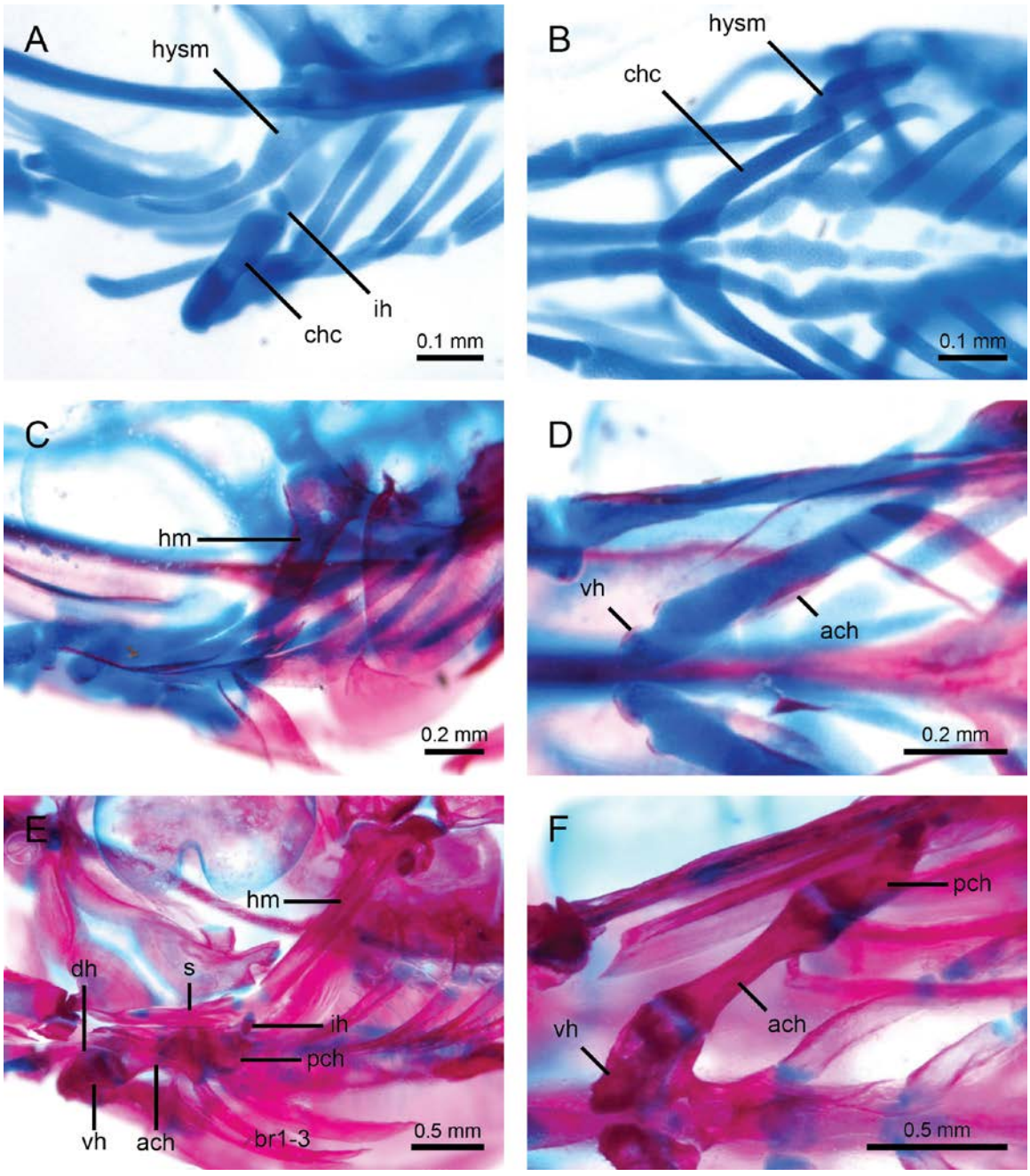

Figure 5.5. Hyoid arch development in *Catostomus commersonii*. **A**: 10.00 mm, lateral view. **B**: 10.00 mm, ventral view. **C**: 12.57 mm, lateral view. **D**: 12.57 mm, ventral view. **E**: 18.45 mm, lateral view. **F**: 18.45 mm, ventral view. Anterior to the left. ach, anterior

ceratohyal; br1, br2, br3, branchiostegal rays 1-3; chc, ceratohyal cartilage; dh, dorsal hypohyal; hm, hyomandibular; hysm, hyosymplectic cartilage; ih, interhyal; pch, posterior ceratohyal; s, symplectic; vh, ventral hypohyal.

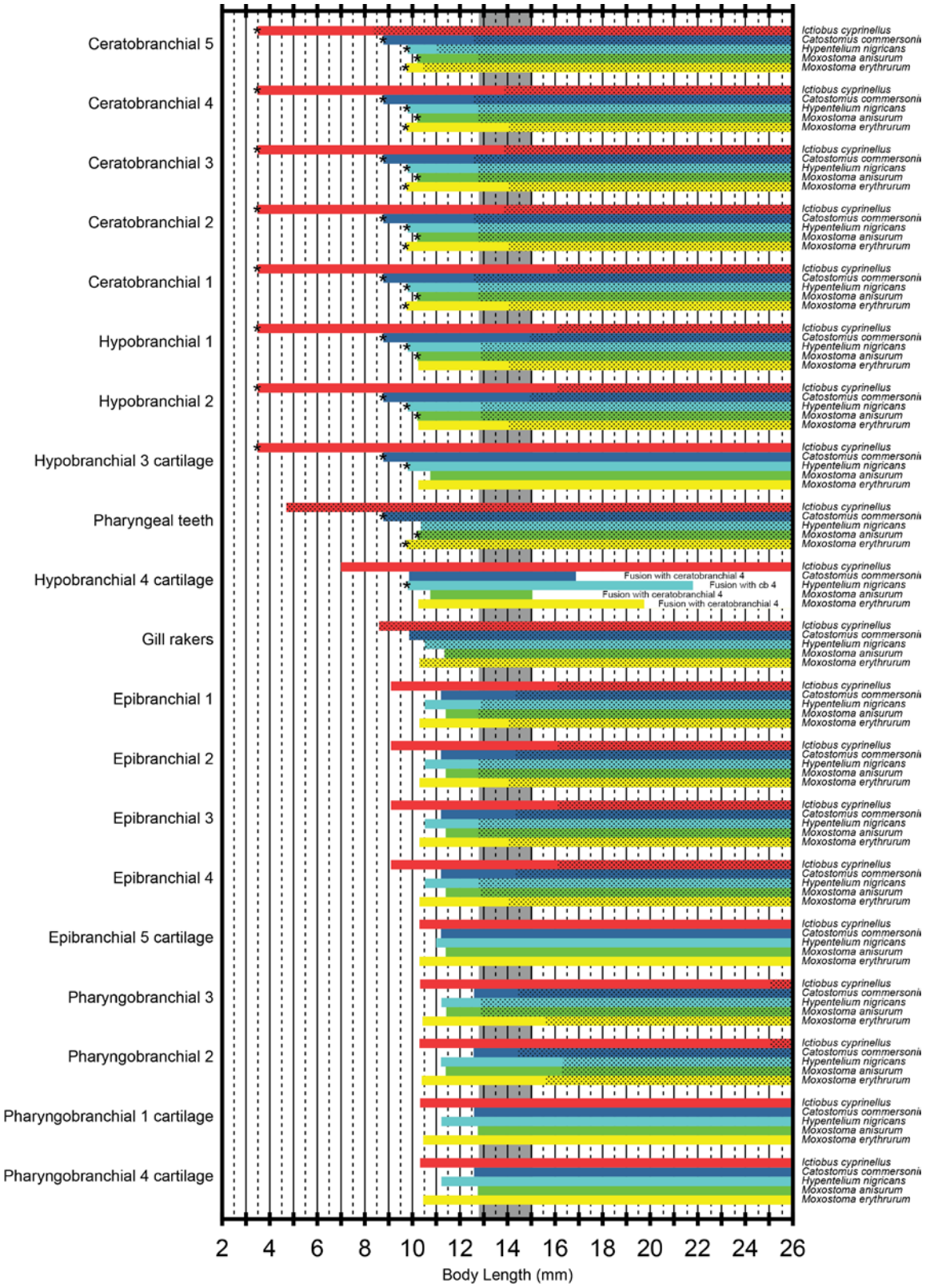
Ceratobranchial 5
Ceratobranchial 4
Ceratobranchial 3
Ceratobranchial 2
Ceratobranchial 1
Hypobranchial 1
Hypobranchial 2
Hypobranchial 3 cartilage
Pharyngeal teeth
Hypobranchial 4 cartilage
Gill rakers
Epibranchial 1
Epibranchial 2
Epibranchial 3
Epibranchial 4
Epibranchial 5 cartilage
Pharyngobranchial 3
Pharyngobranchial 2
Pharyngobranchial 1 cartilage
Pharyngobranchial 4 cartilage
Ictiobus cyprinellus
Catostomus commersonii
Hypentelium nigricans
Moxostoma anisurum
Moxostoma erythrurum
Fusion with ceratobranchial 4
Fusion with cb 4
Fusion with ceratobranchial 4
Fusion with ceratobranchial 4
2
4
6
8
10
12
14
16
18
20
22
24
26
Body Length (mm)

Figure 3.6. Sequence of chondrification and ossification of the branchial arches. Cartilage development is indicated with solid bars and bone development is indicated with stippled bars. Asterisks indicate that the structure was present in the smallest specimen examined. The vertical gray box indicates the transition from a terminal mouth orientation to a subterminal orientation.

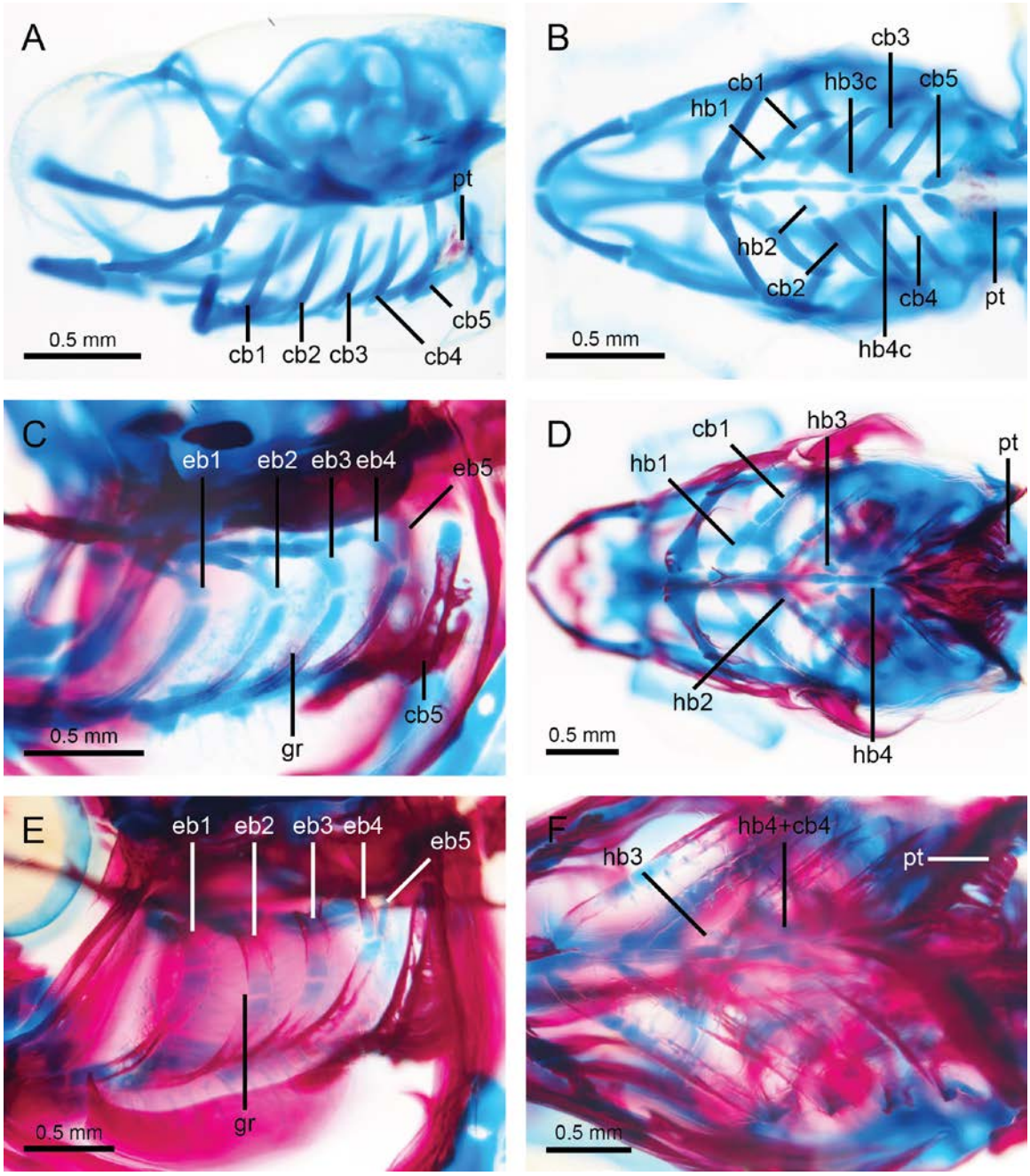

Figure 3.7. Development of the five branchial arches in *Moxostoma anisurum*. **A**: 11.35 mm, lateral view. **B**: 11.35 mm, ventral view. **C**: 12.75 mm, lateral view. **D**: 12.75 mm, ventral view. **E**: 16.30 mm, lateral view. **F**: 16.30 mm, ventral view. Anterior to the left.

cb1, cb2, cb3, cb4, cb5, ceratobranchials 1-5; eb1, eb2, eb3, eb4, eb5, epibranchials 1-5; gr, gill raker; hb1, hb2, hb3, hb4, hypobranchials 1-4; hb3c, hypobranchial 3 cartilage; hb4c, hypobranchial 4 cartilage; pt, pharyngeal tooth.

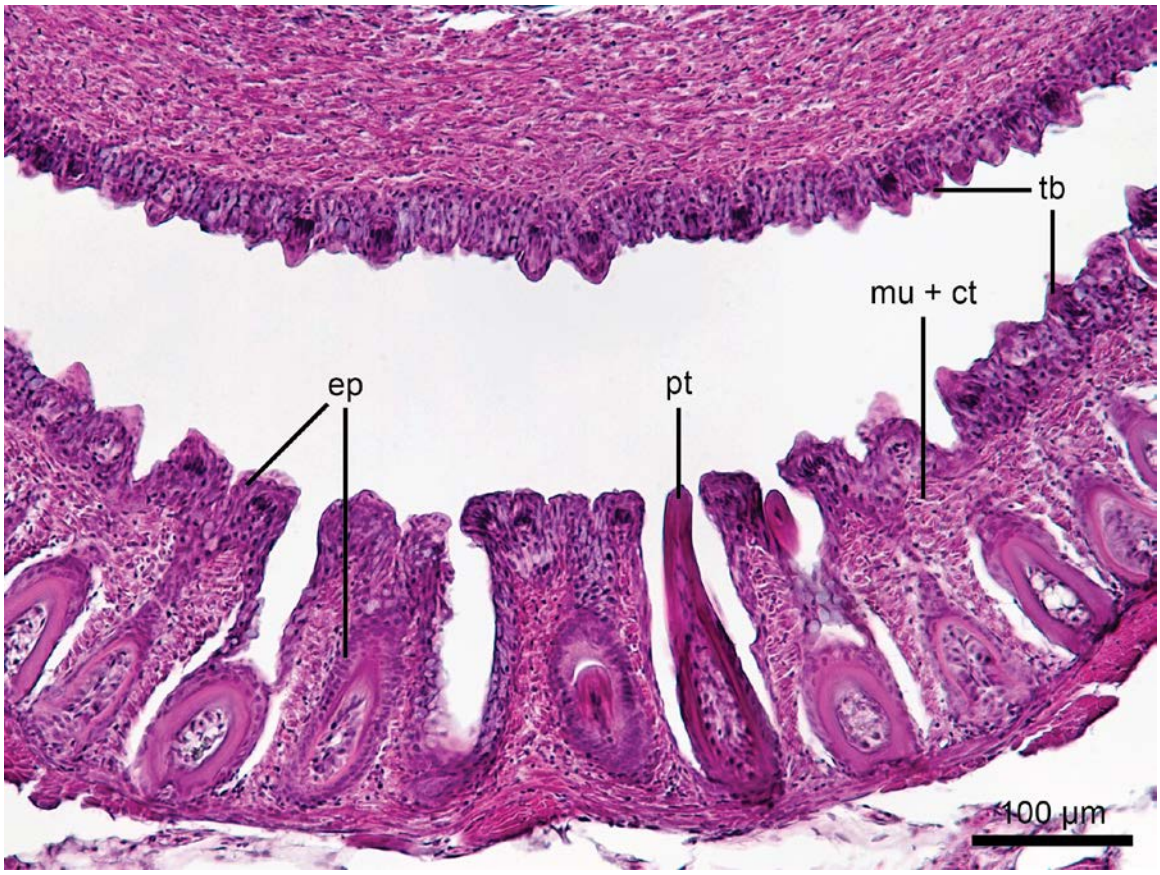

Figure 3.8. Transverse section through the pharyngeal teeth of a 15.39 mm *Hypentelium nigricans*, hematoxylin and eosin stained, 10 µm thick. ct, connective tissue; ep, epithelium; mu, muscle; pt, pharyngeal tooth; tb, taste bud.

Figure 3.9. Transverse section through ceratobranchial 2 of a 24.06 mm *Moxostoma erythrurum*, hematoxylin and eosin stained, 10 µm thick. cb2, ceratobranchial 2; ct, connective tissue; ep, epithelium; gr, gill raker; mu, muscle; tb, taste bud.

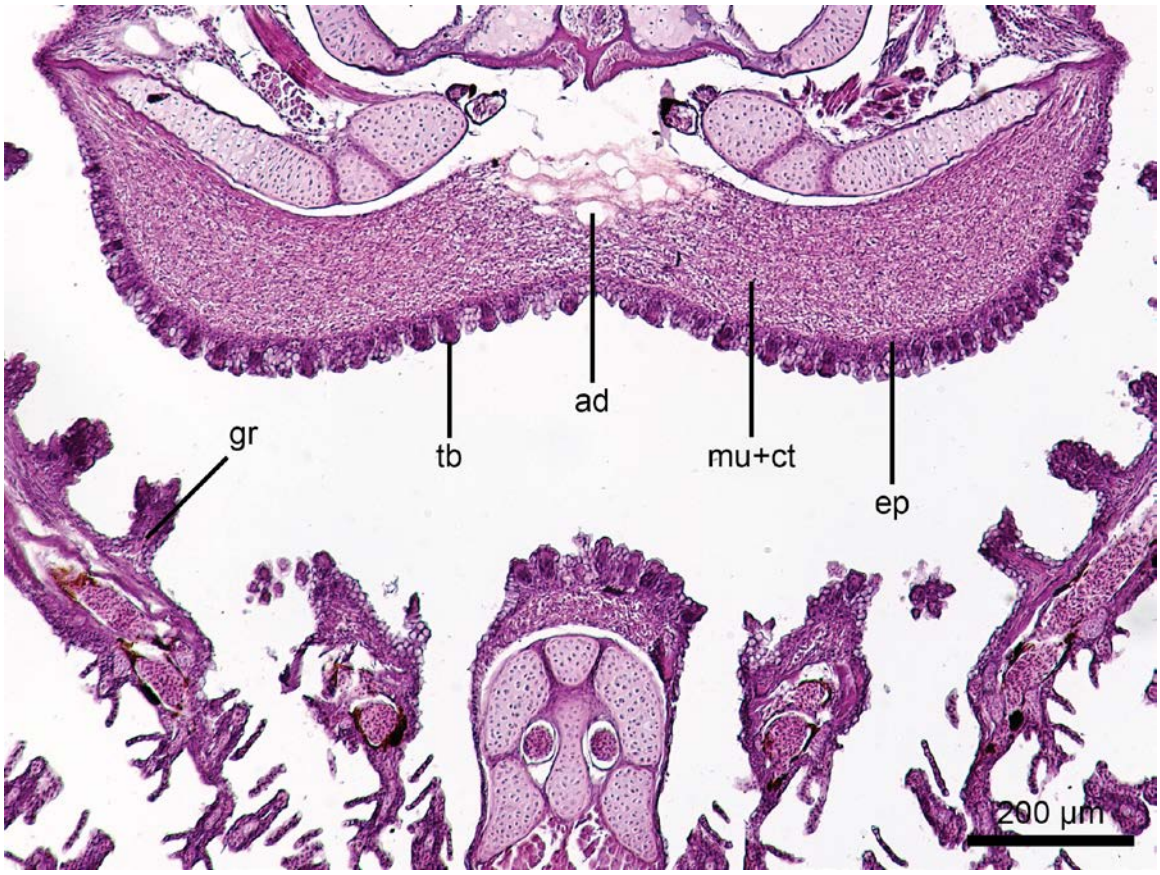

Figure 3.10. Transverse section through ceratobranchials 2 and 3 of a 16.17 mm *Hypentelium nigricans*, hematoxylin and eosin stained, 10 µm thick. ad, adipose; ct, connective tissue; ep, epithelium; gr, gill raker; mu, muscle; tb, taste bud.

Figure 3.11. Transverse section through the chewing pad of a 12.36 mm *Ictiobus cyprinellus*, hematoxylin and eosin stained, 10 µm thick. ct, connective tissue; kep, keratinized epithelium; mu, muscle; pt, pharyngeal tooth.

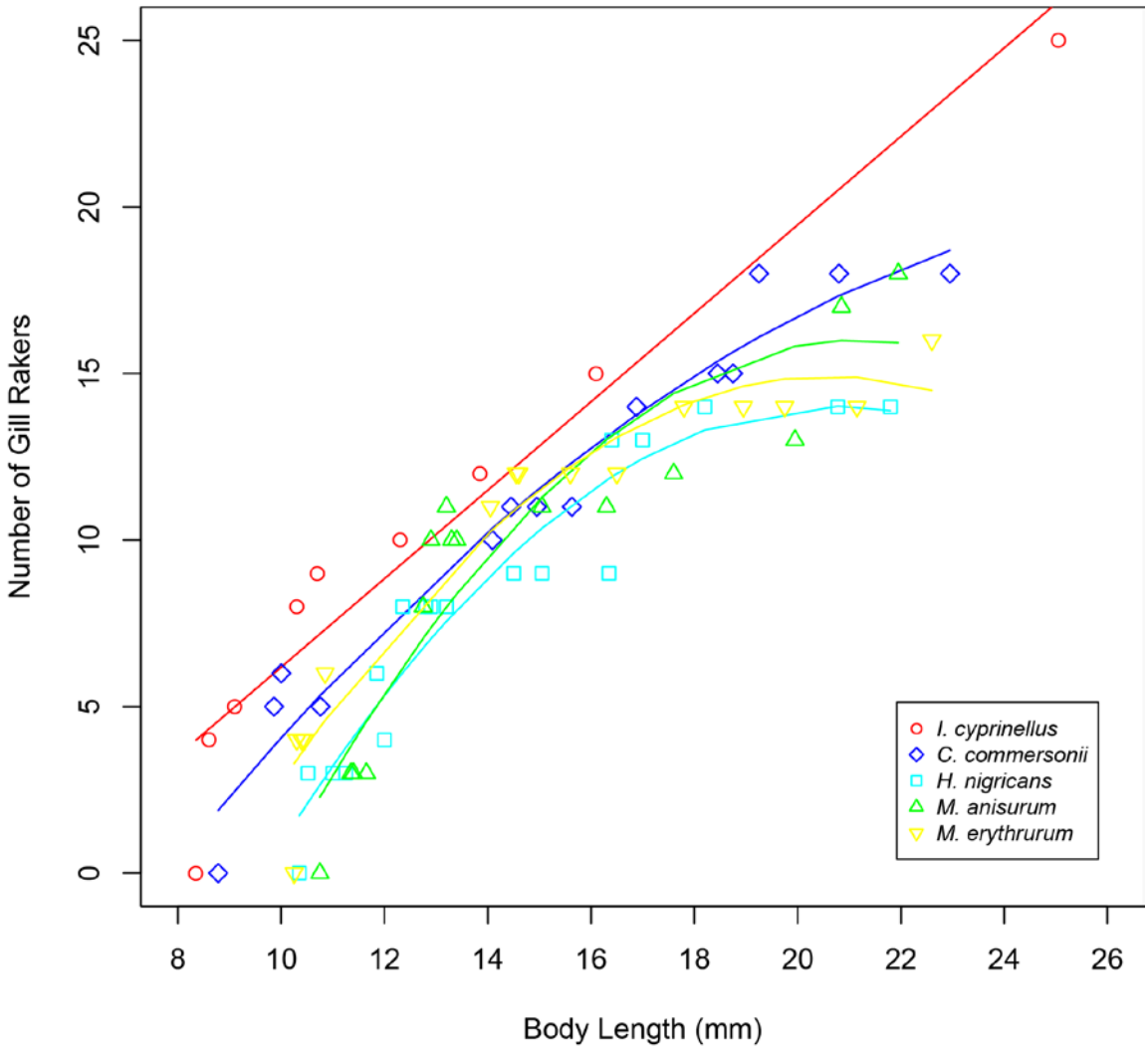

Figure 3.12. Number of gill rakers in larval and early juveniles of five species of freshwater suckers. Significant linear regressions are shown as straight lines and significant quadratic regressions are shown as curved lines. Body length is notochord length for preflexion larvae and standard length for larger specimens.

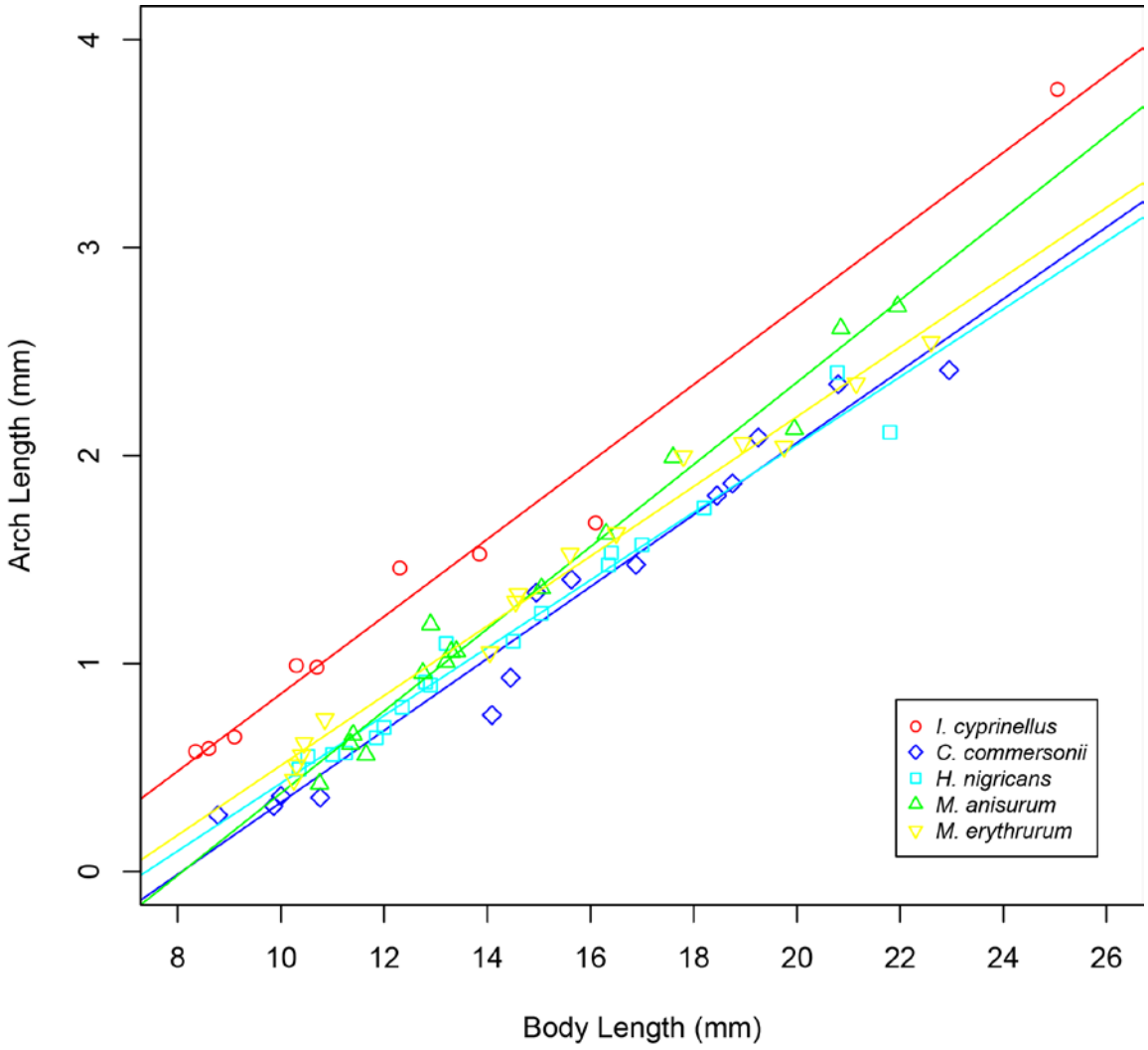

Figure 3.13. Length of the second branchial arch in larval and early juveniles of five species of freshwater suckers. Lines are linear regressions for each species. Body length is notochord length for preflexion larvae and standard length for larger specimens.

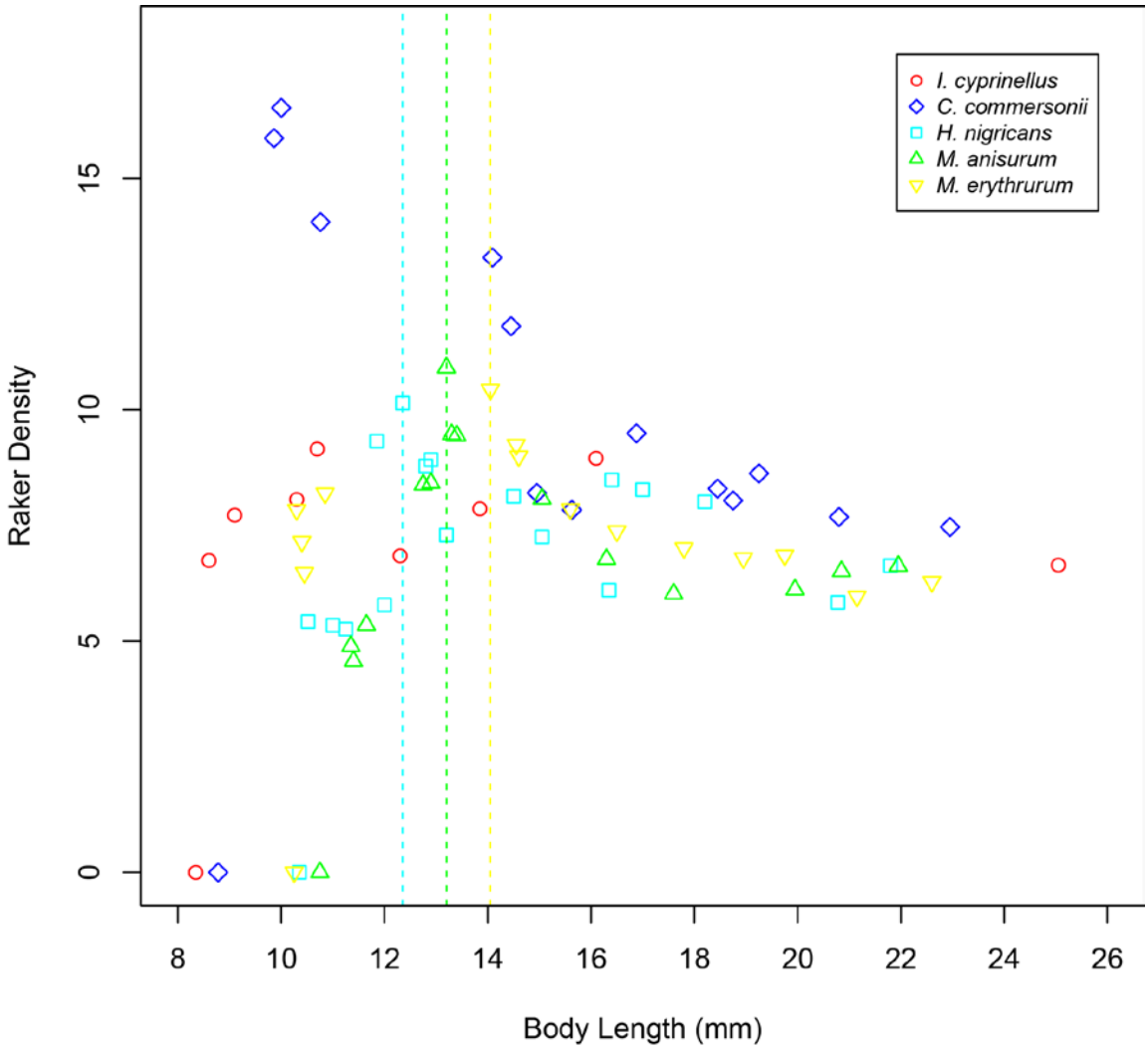

Figure 3.14. Density of gill rakers in larval and early juveniles of five species of freshwater suckers. Density was calculated as the number of gill rakers on the second branchial arch divided by the length of that arch. Maximum values for *Hypentelium nigricans*, *Moxostoma anisurum*, and *Moxostoma erythrurum* are indicated as dashed vertical lines. Body length is notochord length for preflexion larvae and standard length for larger specimens.

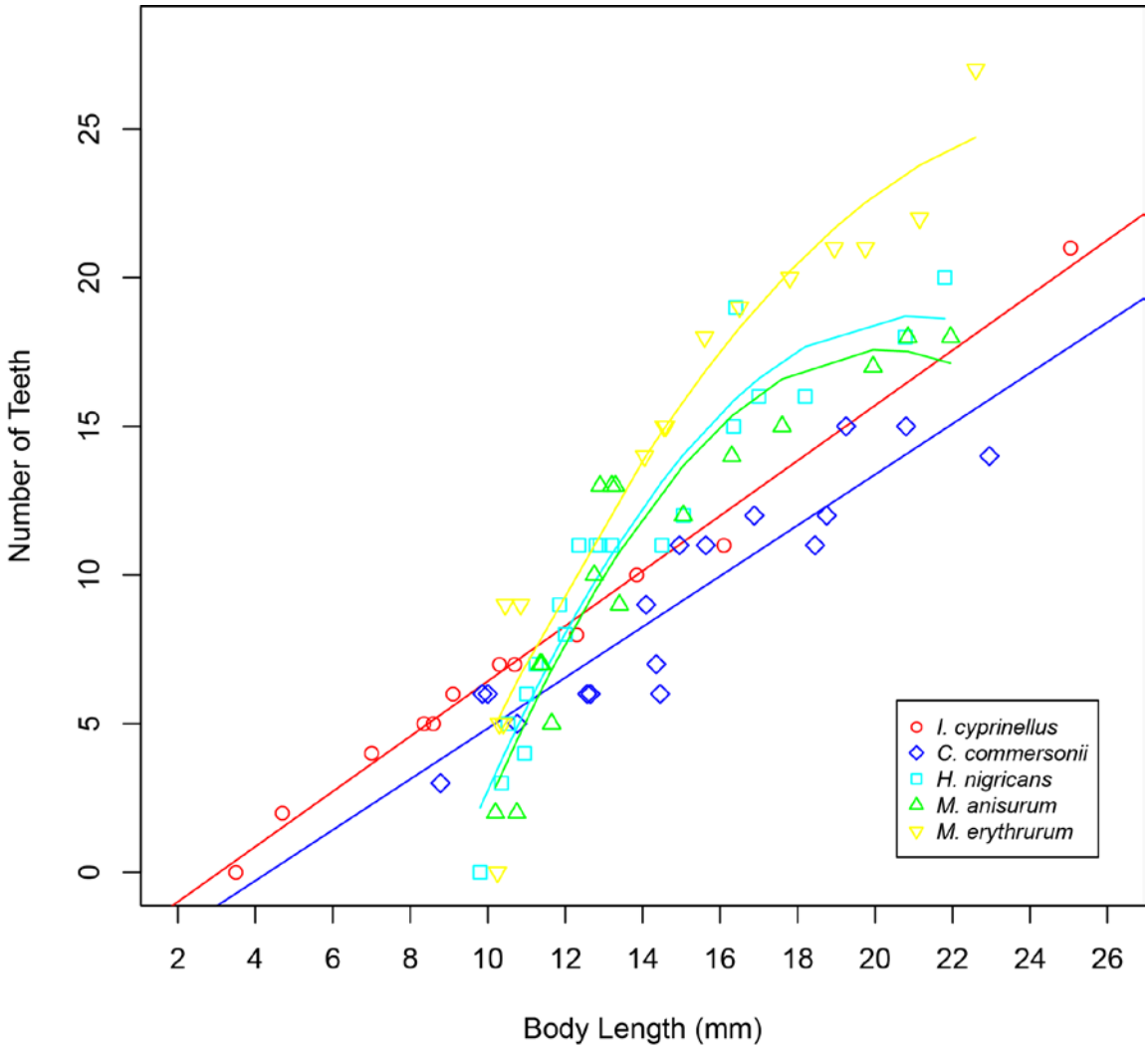

Figure 3.15. Number of pharyngeal teeth in larval and early juveniles of five species of freshwater suckers. Significant linear regressions are shown as straight lines and significant quadratic regressions are shown as curved lines. Body length is notochord length for preflexion larvae and standard length for larger specimens.

Bibliography

Alberch P, Gould SJ, Oster GF, Wake DB. 1979. Size and shape in ontogeny and phylogeny. *Paleobiology* 5: 296-317.

Alexander RM. 1967. *Functional Design in Fishes*. London: Hutchinson University Library.

Barrowclough, GF, Groth JG, Mertz LA. 2006. The RAG-1 exon in the avian order Caprimulgiformes: Phylogeny, heterozygosity, and base composition. *Molecular Phylogenetics and Evolution* 41: 238-248.

Becker GC. 1983. *Fishes of Wisconsin.* Madison, WI: The University of Wisconsin Press.

Betancur-R. R, Broughton RE, Wiley EO, Carpenter K, López JA, Li C, Holcroft NI, Arcila D, Sanciangco M, Cureton II JC, Zhang F, Buser T, Campbell MA, Ballesteros JA, Roa-Varon A, Willis S, Borden WC, Rowley T, Reneau PC, Hough DJ, Lu G, Grande T, Arratia G, Ortí G. 2013. The tree of life and a new classification of bony fishes. *PLOS Currents Tree of Life* 2013 Apr 18 Edition 1.

Betancur-R. R, Li C, Munroe TA, Ballesteros JA, Ortí G. 2013. Addressing gene tree discordance and non-stationarity to resolve multi-locus phylogeny of the flatfishes (Teleostei: Pleuronectiformes). *Systematic Biology* 62: 763-785.

Block AJ, Mabee PM. 2012. Development of the mandibular, hyoid arch and gill arch skeleton in the Chinese barb Puntius semifasciolatus: comparisons of ossification sequences among Cypriniformes. *Journal of Fish Biology* 81:54-80.

Blomberg SP, Garland JR T, Ives AR. 2003. Testing for phylogenetic signal in comparative data: Behavioral traits are more labile. *Evolution* 57: 717-745.

Böhme M. 2007. Revision of the cyprinids from the Early Oligocene of the Ceské Stredohori Mountains, and the phylogenetic relationships of *Protothymallus* Laube 1901 (Teleostei, Cyprinidae, Gobioninae). *Acta Musei Nationalis Pragae, Ser. B, Historia Naturalis* 63: 175-194.

Britz R, Conway KW. 2009. Osteology of *Paedocyrpis*, a miniature and highly developmentally truncated fish (Teleostei: Ostariophysi: Cyprinidae). *Journal of Morphology* 270: 389-412.

Britz R., Conway KW. 2011. The Cypriniformes tree of confusion. *Zootaxa* 2946: 73-78.

Broughton RE, Betancur-R. R, Li C, Arratia G, Ortí G. 2013. Multi-locus phylogenetic analysis reveals the pattern and tempo of bony fish evolution. *PLOS Currents* 2013.

Callan WT, Sanderson SL. 2003. Feeding mechanisms in carp: cross flow filtration, palatal protrusions and flow reversals. *Journal of Experimental Biology* 206: 883-892.

Cavender TM. 1986. Review of the fossil history of North American freshwater fishes. In: Hocutt CH, Wiley EO, editors. *Zoogeography of North American Freshwater Fishes*. New York: John Wiley & Sons. pp. 699-724.

Cavender TM. 1991. The fossil record of the Cyprinidae. In: Winfield IJ, Nelson JS, editors. *Cyprinid Fishes: Systematics, Biology and Exploitation*. New York: Chapman & Hall. pp. 34-54.

Cavender TM, Coburn MM. 1992. Phylogenetic relationships of North American Cyprinidae. In: Mayden RL, editor. *Systematics, Historical Ecology, and North American Freshwater Fishes*. Stanford: Stanford University Press. pp. 293–327.

Chen GJ, Chang M-M, Wang Q. 2010. Redescription of *Cobitis longipectoralis* Zhou, 1992 (Cypriniformes: Cobitidae) from late early Miocene of East China. *Science China Series D* 53: 945-955.

Chen G, Fang F, Chang M-M. 2005. A new cyprinid closely related to cultrins + xenocyprinins from the mid-Tertiary of South China. *Journal of Vertebrate Paleontology* 25: 492-501.

Chen W-J, Lavoué S, Mayden RL. 2013. Evolutionary origin and early biogeography of otophysan fishes (Ostariophysi: Teleostei). *Evolution* 67: 2218-2239.

Chen W-J, Mayden RL. 2009. Molecular systematics of the Cyprinoidea (Teleostei: Cypriniformes), the world's largest clade of freshwater fishes: further evidence from six nuclear genes. *Molecular Phylogenetics and Evolution* 52: 544-549.

Chen W-J, Miya M, Saitoh K, Mayden RL. 2008. Phylogenetic utility of two existing and four novel nuclear gene loci in reconstructing Tree of Life of ray-finned fishes: The order Cypriniformes (Ostariophysi) as a case study. *Gene* 423: 125-134.

Conway KW. 2011. Osteology of the South Asian Genus *Psilorhynchus* McClelland, 1839 (Teleostei: Ostariophysi: Psilorhynchidae), with investigation of its phylogenetic relationships within the order Cypriniformes. *Journal of the Linnean Society - London* 163: 50-154.

Conway KW, Hirt MV, Yang L, Mayden RL, Simons AM. 2010. Cypriniformes: systematics and paleontology. In: Nelson JS, Schultze H-P, Wilson MVH, editors. *Origin and Phylogenetic Interrelationships of Teleosts*. Munich: Verlag Dr. Freidrich Pfeil. pp. 295-316.

Conway KW, Mayden RL. 2007. The gill arches of *Psilorhynchus*. *Copeia* 2007: 267–280.

Cubbage CC, Mabee PM. 1996. Development of the cranium and paired fins in the Zebrafish Danio rerio (Ostariophysi, Cyprinidae). *Journal of Morphology* 229:121-160.

de Beer GR. 1930. *Embryos and Evolution*. Oxford: Clarendon Press.

de Beer GR. 1940. *Embryos and Ancestors*. Oxford: Oxford University Press.

Dingerkus G, Uhler D. 1977. Enzyme clearing of alcian blue stained whole small vertebrates for demonstration of cartilage. Stain Technol 52:229-232.
Doosey MH, Bart HL. 2011. Morphological variation of the palatal organ and chewing pad of Catostomidae (Teleostei: Cypriniformes). *Journal of Morpholology* 272: 1092-1108.

Doosey MH, Bart HL, Saitoh K, Miya M. 2010. Phylogenetic relationships of catostomid fishes (Actinopterygii: Cypriniformes) base on mitochondrial ND4/ND5 gene sequences. *Molecular Phylogenetics and Evolution* 54: 1028-1034.

Drenner RW, Vinyard VL, Hambright KD, Gophen M. 1987. Particle ingestion by *Tilapia galilaea* is not affected by removal of gill rakers and microbranchiospines. *Transactions of the American Fisheries Society* 116: 272-276.

Drummond AJ, Rambaut A. 2007. BEAST: Bayesian evolutionary analysis by sampling trees. *BMC Evolutionary Biology* 7: 214.

Drummond AJ, Suchard MA, Xie D, Rambaut A. 2012. Bayesian phylogenetics with BEAUti and BEAST 1.7. *Molecular Biology and Evolution* 29: 1969-1973.

Eastman JT. 1977. The pharyngeal bones and teeth of catostomid fishes. *American Midland Naturalist* 97: 68-88.

Edgar RC. 2004. MUSCLE: multiple sequence alignment with high accuracy and high throughput. *Nucleic Acids Research* 32: 1792-1797.

Engeman JM, Aspinwall N, Mabee PM. 2009. Development of the pharyngeal arch skeleton in Catostomus commersonii (Teleostei: Cypriniformes). *Journal of Morphology* 270:291-305.

Fang F, Norén M, Liao T-Y, Källersjö M, Kullander SO. 2009. Molecular phylogenetic interrelationships of the south Asian cyprinid genera *Danio*, *Devario* and *Microrasbora* (Teleostei, Cyprinidae, Danioninae). *Zoologica Scripta* 38: 237–156.

Fontana W, Schuster P. 1998. Shaping space: The possible and the attainable in RNA genotype-phenotype mapping. *Journal of Theoretical Biology* 194: 491–515.

Fink WL. 1982. The conceptual relationship between ontogeny and phylogeny. *Paleobiology* 8: 254-264.

Fink WL. 1988. Phylogenetic analysis and the detection of ontogenetic patterns. In: McKinney ML, editor. *Heterochrony in Evolution*. New York: Plenum Publishing Corporation. pp. 71-91.

Fink SV, Fink WL. 1981. Interrelationships of the ostariophysans fishes (Teleostei). *Zoological Journal of the Linnean Society - London* 72: 297-353.

Foster PG, Hickey DA. 1999. Compositional bias may affect both DNA-based and protein-based phylogenetic reconstructions. *Journal of Molecular Evolution* 48: 284-290.

Friedman M, Keck BP, Dornburg A, Eytan RI, Martin CH, Hulsey D, Wainwright PC, Near TJ. 2013. Molecular and fossil evidence place the origin of cichlid fishes long after Gondwanan rifting. *Proceeding of the Royal Society B* 280: 1775 20132648.

Frickhinger KA. 1994. *The Fossils of Solnhofen*. Korb, Germany: Goldschneck Verlag.

Froese R, Pauly D, editors. 2013. FishBase. World Wide Web electronic publication. www.fishbase.org, version (12/2013).

Gradstein FM, Ogg JG, Schmitz MD, Ogg GM. 2012. *The Geologic Time Scale 2012*. Oxford, U.K.: Elsevier. Available from http://works.bepress.com/mark_schmitz/15/.

Grande T. 1999. Distribution patterns and historical biogeography of gonorynchiform fishes (Teleostei: Ostariophysi). In: Arratia G, Schultze H-P, editors. *Mesozoic Fishes 2 – Systematics and Fossil Record*. München, Germany: Verlag Dr. Friedrich Pfeil. pp. 425-444.

Gould SJ. 1977. Ontogeny and Phylogeny. Cambridge, MA: Harvard University Press.
Hasegawa M, Hashimoto T. 1993. Basal divergences in birds and the phylogenetic utility of the nuclear RAG-1 gene. *Molecular Phylogenetics and Evolution* 12: 115-123.

Hall BK. 1992. *Evolutionary Developmental Biology*. London: Chapman and Hall.

Hall BK, Miyake T. 1995. How do embryos measure time? In: McNamara KJ, editor. *Evolutionary Change and Heterochrony*. New York: John Wiley & Sons. pp. 3-20.

Ho SYW, Phillips MJ. 2009. Accounting for calibration uncertainty in phylogenetic estimation of evolutionary divergence times. *Systematic Biology* 58: 367-380.

Hora SL. 1920. Revision of the Indian Homalopteridae and of the genus *Psilorhynchus* (Cyprinidae). *Records of the Indian Museum* 19: 195–215.

Hoogenboezem W, van den Boogaart JGM, Sibbing FA, Lammens EHRR, Terlouw A, Osse JWM. 1991. A new model of particle retention and branchial sieve adjustment in filter-feeding bream (*Abramis brama*) (Cyprinidae). *Canadian Journal of Fish Aquaculture Science* 48: 7-18.

Hundt PJ, Iglésias SP, Hoey AS, Simons AM. 2014. A multilocus molecular phylogeny of combtooth blennies (Percomorpha: Blennioidei: Blenniidae): multiple invasions of intertidal habitats. *Molecular Phylogenetics and Evolution* 70: 47-56.

Iwai T. 1964. A comparative study of the taste buds in gill rakers and gill arches of teleostean fishes. *Bulletin of the Misaki Marine Biological Institute, Kyoto University* 7: 19-34.

Javier P. 2004. Early specializations in the branchial apparatus of jawless vertebrates: a consideration of gill number and size. In: Arratia G, Wilson MVH, Cloutier R, editors. *Recent Advances in the Origin and Early Radiation of Vertebrates*. Munich: Verlag Dr. Freidrich Pfeil. pp. 29-52.

Jeffroy O, Brinkmann H, Delsuc F, Philippe H. 2006. Phylogenomics: The beginning of incongruence? *Trends in Genetics* 22: 225-231.

Jenkins RE, Burkhead NM. 1993. *Freshwater Fishes of Virginia.* Bethesda, MD: American Fisheries Society.

Kimball S, Mattis P. 2012. *GIMP v2.8: GNU Image Manipulation Program.* Available from http://www.gimp.org.

Klingenberg CP, Spence JR. 1993. Heterochrony and allometry: lessons from the water strider genus *Limnoporus*. *Evolution* 47: 1834-1853.

Kottelat M, Britz R, Tan HH, Witte KE. 2006. *Paedocypris*, a new genus of Southeast Asian cyprinid fish with a remarkable sexual dimorphism, comprises the world's smallest vertebrate. *Proceedings of the Royal Society B - Biological Sciences* 273: 895–899.

Lake JA. 1994. Reconstructing evolutionary trees from DNA and protein sequences: Paralinear distances. *Proceedings of the National Academy of Sciences USA* 91: 1155–1159.

Lanfear R, Calcott B, Ho SYW, Guindon S. 2012. PartitionFinder: Combined selection of partitioning schemes and substitution models for phylogenetic analyses. *Molecular Biology and Evolution* 29: 1695-1701.

Lockhart PJ, Steel MA, Hendy MD, Penny D. 1994. Recovering evolutionary trees under a more realistic model of sequence evolution. *Molecular Biology and Evolution* 11: 605-612.

Loomis WF, Smith DW. 1990. Molecular phylogeny of *Dictyostelium discoideum* by protein sequence comparison. *Proceedings of the National Academy of Sciences USA* 87: 9093-9097.

López JA, Chen W-J, Guillermo O, Wood RM. 2004. Esociform phylogeny. *Copeia* 2004: 449-464.

Liu J, Chang M-M. 2009. A new Eocene catostomid (Teleostei: Cypriniformes) from northeastern China and early divergence of Catostomidae. *Science in China Series D* 52: 189-202.

Maddison DR, Maddison WP. 2005. *MacClade 4: Analysis of phylogeny and character evolution*. Version 4.08a. Available from http://macclade.org.

Marshall CR. 2008. A simple method for bracketing absolute divergence times on molecular phylogenies using multiple fossil calibration points. *American Naturalist* 171: 726-742.

Mayden RL, Tang KL, Conway KW, Freyhof J, Chamberlain SJ, Haskins M, Schneider LM, Sudkamp M, Wood RM, Agnew MK, Bufalino A, Sulaiman Z, Miya M, Saitoh K, He S. 2007. Phylogenetic relationships of *Danio* within the order Cypriniformes: a framework for comparative and evolutionary studies of a model species. *Journal of Experimental Zoolology Part B* 308B: 642–654.

Mayden RL, Tang KL, Wood RM, Chen W-J, Agnew MK, Conway KW, Yang L, Simons AM, Bart H., Harris PM, Li J, Wang X, Saitoh K, He S, Liu H, Chen Y, Nishida M, Miya M. 2008. Inferring the tree of life of the order Cypriniformes, the earth's most diverse clade of freshwater fishes: Implications of varied taxon and character sampling. *Journal of Sysematics and Evolution* 46: 424-438.

Mayden RL, Chen W-J. 2010. The world's smallest vertebrate species of the genus *Paedocypris*: A new family of freshwater fishes and the sister group to the world's most diverse clade of freshwater fishes (Teleostei: Cypriniformes). *Molecular Phylogenetics and Evolution* 57: 152-175.

McNamara KJ. 1988. The abundance of heterochrony in the fossil record. In: McKinney ML, editor. *Heterochrony in Evolution*. New York: Plenum Publishing Corporation. pp. 287-325.

Miller MA, Pfeiffer W, Schwartz T. 2010. “Creating the CIPRES Science Gateway for inference of large phylogenetic trees" in *Proceedings of the Gateway Computing Environments Workshop (GCE)*, 14 Nov. 2010, New Orleans, LA. pp. 1-8.

Mooers AO, Holmes EC. 2000. The evolution of base composition and phylogenetic inference. *Trends in Ecology and Evolution* 15: 365-369.

Nakatani M, Miya M, Mabuchi K, Saitoh K, Nishida M. 2011. Evolutionary history of Otophysi (Teleostei), a major clade of the modern freshwater fishes: Pangaean origin and Mesozoic radiation. *BMC Evolutionary Biology* 11.

Near TJ, Bossu CM, Bradburd GS, Carlson RL, Harrington RC, Hollingsworth PR, Keck BP, Etnier DA. 2011. Phylogeny and temporal diversification of darters (Percidae: Etheostomatinae). *Systematic Biology* 60: 565-595.

Near TJ, Dornburg A, Eytan RI, Keck BP, Smith WL, Kuhn KL, Moore JA, Price SA, Burbrink FT, Friedman M, Wainwright PC. 2013. Phylogeny and tempo of diversification in the superradiation of spiny-rayed fishes. *Proceedings of the National Academy of Sciences USA* 110: 12738-12743.

Near TJ, Eytan RI, Dornburg A, Kuhn KL, Moore JA, Davis MP, Wainwright PC, Friedman M, Smith WL. 2012. Resolution of ray-finned fish phylogeny and timing of diversification. *Proceedings of the National Academy of Sciences USA* 109: 13698-13703.

Nelson JS. 2006. *Fishes of the World.* New York: John Wiley & Sons Inc.

Nikolsky GV. 1963. *The Ecology of Fishes*. New York: Academic Press.

Oliveira C, Avelino GS, Abe KT, Mariguela TC, Benine RC, Ortí G, Vari RP, Corrêa e Castro RM. 2011. Phylogenetic relationships within the speciose family Characidae (Teleostei: Ostariophysi: Characiformes) based on multilocus analysis and extensive ingroup sampling. *BMC Evolutionary Biology* 11.

Pagel M. 1999. Inferring the historical patterns of biological evolution. *Nature* 401: 877-884.

Paradis E, Claude J, Strimmer K. 2004. APE: analyses of phylogenetics and evolution in R language. *Bioinformatics* 20: 289-290.

Potthoff T. 1984. Clearing and staining techniques. In: Moser HG, editor. *Ontongeny and Systematics of Fishes*. Lawrence, KS: Allen Press. pp. 35-37.

Poyato-Ariza FJ. 1994. A new Early Cretaceous gonorynchiform fish (Teleostei: Ostariophysi) from Las Hoyas (Cuenca, Spain). *Occasional Publications of the Museum of Natural History, University of Kansas* 164: 1-37.

Poyato-Ariza FJ. 1996. A revision of *Rubiesichthys gregalis* WENZ 1984 (Ostariophysi, Gonorynchiformes), from the Early Cretaceous of Spain. In: Arratia G, Viohl G, editors. *Mesozoic Fishes – Systematics and Paleoecology*. München, Germany: Verlag Dr. Friedrich Pfeil. pp. 319-328.

Presnell JK, Schreibman MP. 1997. *Humason's Animal Tissue Techniques*. Baltimore: The John Hopkins University Press.

Prokofiev AM. 2007. Redescription of a fossil loach *Triplophysa opinata* (Yakowlew, 1959) from the Miocene of Kirgizia (Balitoridae: Nemacheilinae). *Journal of Ichthyology* 47: 26-31. [in Russian].

R Core Team. 2013. *R: A language and environment for statistical computing*. R Foundation for Statistical Computing, Vienna, Austria. Available from http://www.R-project.org/.

R Core Team. 2014. *R: A language and environment for statistical computing*. R Foundation for Statistical Computing, Vienna, Austria. Available from http://www.R-project.org/.

Rambaut A, Drummond AJ. 2007. *Tracer v1.4*. Available from http://beast.bio.ed.ac.uk/Tracer.

Reilly SM. 1997. An integrative approach to heterochrony: the distinction between interspecific and intraspecific phenomena. *Biological Journal of the Linnean Society* 60: 119-143.

Revell LJ. 2012. phytools: An R package for phylogenetic comparative biology (and other things). *Methods in Ecology and Evolution* 3: 217-223.

Rüber L, Kottelat M, Tan HH, Ng PKL, Britz R. 2007. Evolution of miniaturization and the phylogenetic position of *Paedocypris*, comprising the world's smallest vertebrate. *BMC Evolutionary Biology* 7: 1–10.

Saitoh K, Sado T, Doosey MH, Bart Jr HL, Inoue JG, Nishida M, Mayden RL, Miya M. 2011. Evidence from mitochondrial genomics supports the lower Mesozoic of South Asia

as the time and place of basal divergence of cypriniform fishes (Actinopterygii: Ostariophysi). *Zoological Journal of the Linnean Society* 161: 633-662.

Saitoh K, Sado T, Mayden RL, Hanzawa N, Nakamura K, Nishida M, Miya M. 2006. Mitogenomic evolution and interrelationships of the Cypriniformes (Actinopterygii. Ostariophysi): The first evidence toward resolution of higher-level relationships of the world's largest freshwater fish clade based on 59 whole mitogenome sequences. *Journal of Molecular Evolution* 63: 826-841.

Sanderson MJ. 2003. r8s: inferring absolute rates of evolution and divergence times in the absence of a molecular clock. *Bioinformatics* 19: 301-302.

Sanderson SL, Cheer AY, Goodrich JS, Grazlano JD, Callan WT. 2001. Crossflow filtration in suspension-feeding fishes. *Nature* 412: 439-441.

Sawada Y. 1981. Phylogeny and zoogeography of superfamily Cobitoidea (Cyprinoidei. Cypriniformes). *Memoirs of the Faculty of Fisheries Hokkaido University* 28:65-223.

Schuster P. 2000. Taming combinatorial explosion. *Proceedings of the National Academy of Sciences of the United States of America* 97: 7678–7680.

Sibbing FA, Osseand WM, Terlou A. 1986. Food handling in the carp (*Cyprus carpio*): its movement patterns, mechanisms and limitations. *Journal of Zoology* 210: 161-203.

Siebert DJ. 1987. *Interrelationships among families of the order Cypriniformes (Teleostei).* Ph.D. Dissertation. New York: City University of New York.

Šlechtová V, Bohlen J, Tan HH. 2007. Families of Cobitoidea (Teleostei. Cypriniformes) as revealed from nuclear genetic data and the position of the mysterious genera *Barbucca, Psilorhynchus, Serpenticobitis* and *Vaillantella*. *Molecular Phylogenetics and Evolution* 44: 1358-1365.

Smith GR. 1992. Phylogeny and biogeography of the Catostomidae, freshwater fishes of North America and Asia. In: Mayden, RL, editor. *Systematics, Historical Ecology, and North American Freshwater Fishes*. Standford: Standford Universiy Press. pp. 778-826.

Smith KK. 2002. Sequence heterochrony and the evolution of development. *Journal of Morphology* 252: 82-97.

Speigel JR, Quist MC, Morris JE. 2011. Trophic ecology and gill raker morphology of seven catostomid species in Iowa rivers. *Journal of Applied Ichthyology* 27: 1159-1164.

Stamatakis A. 2014. RAxML version 8: A tool for phylogenetic analysis and post-analysis of large phylogenies. *Bioinformatics* 2014: 1-2.

Swofford DL. 2003. PAUP*: phylogenetic analysis using parsimony (*and other methods). Version 4. Sinauer Associates, Sunderland, MA.

Systchevskaya EK. 1986. Paleogene freshwater fish fauna of the USSR and Mongolia. *The Joint Soviet-Mongolian paleontological expedition, Transactions* 29: 5-157.

Tang KL, Agnew MK, Chen W-J, Hirt MV, Sado T, Schneider LM, Freyhof J, Sulaiman Z, Swartz E, Vidthayanon C, Miya M, Saitoh K, Simons AM, Wood RM, Mayden RL. 2010. Systematics of the subfamily Danioninae (Teleostei: Cypriniformes: Cyprinidae). *Molecular Phylogenetics and Evolution* 57: 189–214.

Tarrío R, Rodríguez-Trelles R, Ayala FJ. 2000. Tree rooting with outgroups when they differ in their nucleotide composition from the ingroup: The *Drosophila saltans* and *willistoni* groups, a case study. *Molecular Phylogenetics and Evolution* 16: 344-349.

Toro E, Herrel A, Irschick D. 2004. The evolution of jumping performance in Caribbean Anolis lizards. *American Naturalist* 163: 844–856.

Unmack PJ, Allen GR, Johnson JB. 2013. Phylogeny and biogeography of rainbowfishes (Melanotaeniidae) from Australia and New Guinea. *Molecular Phylogenetics and Evolution* 67: 15-27.

Vandewalle P, Gluckmann I, Wagemans F. 1998. A critical assessment of the Alcian Blue/alizarine double staining in fish larvae and fry. *Belgian Journal of Zoology* 128:93-95.

Wainwright PC, Alfaro ME, Bolnick DI, Hulsey CD. 2005. Many-to-one mapping of form to function: A general principle in organismal design? *Integrative Comparative Biology* 45: 256-262.

Webster M, Zelditch ML. 2005. Evolutionary modifications of ontogeny: heterochrony and beyond. *Paleobiology* 31: 354-372.

Wilson MVH. 1980. Oldest known *Esox* (Pisces: Esocidae), part of a new Paleocene teleost fauna from western Canada. *Canadian Journal of Earth Sciences* 17: 307-312.

Yasuda F. 1960. The relationship of the gill structure and food habits of some coastal fishes in Japan. *Record of Oceanographic Works Japan* 5:139-152.

Yakovlev VN. 1959. Fish from the Miocene deposits of Kirgizia. *Paleontologicheskii Zhurnal* 3: 107-111.

Zheng Y, Peng R, Kuro-o M, Zeng X. 2011. Exploring patterns and extent of bias in estimating divergence time from mitochondrial DNA sequence data in a particular lineage: A case study of salamanders (Order Caudata). *Molecular Biology and Evolution* 28: 2521-2535.

Zhou JJ. 1990. The Cyprinidae fossils from Middle Miocene of Shanwang Basin. *Vertebrata PalAsiatica* 28: 95-127. [in Chinese with English summary].

Zhou JJ. 1992. A new cobitid from the middle Miocene of Shanwang, Shandong. *Vertebrata PalAsiatica* 30: 71-76. [in Chinese with English summary].